Investigating annealing twin formation mechanisms in face-centered cubic nickel

Submitted in partial fulfillment of the requirements for the degree of
Doctor of Philosophy
in
Materials Science and Engineering

Brian Lin

B.S., Dept. of Materials Sci. & Eng., University of Illinois at Urbana-Champaign, 2010
M.S., Dept. of Materials Sci. & Eng., Carnegie Mellon University, 2013

Carnegie Mellon University
Pittsburgh, PA
July 2015

ACKNOWLEDGEMENTS

I would like to thank my advisors, Dr. Gregory Rohrer and Dr. Anthony Rollett, for their support, guidance, and most importantly, patience throughout the course of my graduate research. It has been an honor to be your student and my pleasure to work under both of your supervisions. I would also like to thank Dr. Nathalie Bozzolo and Dr. Marc Bernacki for being accommodating research hosts during my stay in France. Their advice and discussions always opened new outlets to my research with each visit.

In addition thank you to my Dr. Paul Salvador and Dr. Elizabeth Holm, my internal committee members. Their time spent reading, challenging, guiding, and providing feedback on my ideas is much appreciated. To my entire committee, Greg, Tony, Nathalie, Paul, Liz, thank you not only being honest and harshest critics, but ensuring that I strive for the highest level of scientific excellence.

Especially thank you to Dr. Yuan Jin, who was not only my research colleague in this joint-collaboration, but also a friend. The weeks spent together were incredibly frustrating and tiring in the rush for results, but also incredibly rewarding.

There are a number of faculty members and colleagues to thank at CMU as well, all of whom have provided insightful advice and support throughout my graduate career. This also includes the staff, students, and group members, who have helped me with various aspects of my research career. Whether it was training to learn a new equipment, administrative and financial issues, or editing documents and critiquing presentations, thank you.

Thank you to my family and friends for their patience and guidance as well, especially when research was not easy. To my parents for allowing me to pursue graduate school and pushing the boundaries of science and to my friends for ensuring my well being outside of the academic environment, thank you.

Finally, I would like to acknowledge my funding sources. My time at CMU has been supported by the Materials World Network of the National Science Foundation (NSF) under Award No. DMR-1107896. Without their funding, the research behind this dissertation would not have been possible to begin with.

Brian Lin

ABSTRACT

The origins and formation mechanism of annealing twin boundaries in face centered cubic (FCC) materials has remained unclear for over a century in the material science community. Although these interfaces are readily observable through simple means such as optical microscopy, the appearance of these highly faceted, straight boundaries remains an open scientific question. Annealing twins play important roles in material properties, where the low energy structure of the unique boundary provides improved integranular properties in materials achieved through grain boundary engineering (GBE). This enables metals exhibiting higher corrosion resistance, higher strength, more fatigue resistance, crack propagation resistance, and other superior properties for use in pressure vessels, turbine blades, and so forth.

Annealing twin boundaries arise with the heat treatment of low-to-medium stacking fault energy FCC metals in both the recrystallization and grain growth regimes. While a number of formation theories have been proposed in the past, such as the growth accident model, grain encounter model, grain boundary dissociation model, and stacking fault packets, none have fully satisfied the scientific community due to a lack of direct observation of a twin boundary formation event. However, by performing *ex-situ* annealing experiments over a single recrystallization cycle as well as grain growth, new data has been generated to directly identify the formation of a twin boundary and to better understand annealing twin formation mechanisms.

Two techniques were utilized to obtain the *ex-situ* information on annealing twin formation in high purity (99.999%) FCC nickel. The first was scanning electron microscopy coupled with an electron backscatter detector to obtain individual crystal orientations necessary for misorientation studies. Ex-situ heat treatments were performed to monitor the growth of grains in the same area during the recrystallization of nickel specimen cold-rolled to 25% and annealed at 490°C. The second set of data analyzed came from high-energy x-ray diffraction microscopy performed at a synchrotron x-ray source on a high purity nickel microstructure undergoing grain growth at 800°C. This non-destructive technique provided the three-dimensional crystallographic characterization of a microstructural volume and enabled the ex-situ monitoring of the same volume with applied thermal treatments. The microstructure evolution during both recrystallization and grain growth was observed and the formation of new annealing twins was detected in both regimes.

The role of the crystallographic interface(s) in the microstructure that resulted in annealing twin formation was studied. Previous work did not have the extensive crystallographic orientation data available nor were the stereological 2D and 3D techniques available to obtain the full description of a grain boundary character of a material. The orientation of the grain boundary plane that resulted in the formation of an annealing twin event was investigated, as each proposed annealing twin formation mechanism would promote annealing twin formation on different planes, namely {111} and non-{111}.

It was found that the processes of twin formation during recrystallization and grain growth were different from one another. During recrystallization, annealing twins are readily formed at the recrystallization interface and are left behind within recrystallizing grains, where the driving force is presumably the stored energy of the deformed matrix. However, during grain growth, annealing twins formed exclusively at triple junctions. Furthermore, the driving force for annealing twin was the replacement of higher energy grain boundaries with lower energy grain boundaries.

During recrystallization, annealing twin boundaries formed from migrating planes that are close to {111}. In contrast, during grain growth, there were no unique relationships found for the grain boundaries at the triple junction. However, the triple line was found to lie close to the {111} plane of the parent grain that exhibits the twin. Furthermore, the effect of temperature on annealing twin formation was studied for recrystallization at temperatures from 350 to 550 °C and for grain growth at temperatures from 550 to 950 °C. Here it was found that temperature had little effect on the twin content in either regime, provided the same change in grain size was achieved. Although the crystallographic findings support the growth accident mechanism of annealing twin formation, the absence of a temperature dependence runs counter to this idea.

The results in this dissertation are the first to show the role of crystallography in annealing twin formation in a bulk, annealed microstructure. It is proposed that annealing twin formation is primarily dependent on the number of appropriate grain boundaries and triple lines for nucleation in the microstructure. More specifically, to maximize the population of annealing boundaries in the microstructure, the focus should be on maximizing the number of {111} planes on the recrystallization front during recrystallization and triple lines that lie in the {111} plane of a grain during grain growth.

Table of Contents

List of Figures

List of Tables

1 Introduction

Metals are structural materials present in everyday products and materials in modern society. Even as research in the material science community focuses on next generation materials of thin films, polymers, and carbon fiber composites, metals still and will continue to retain a dominant presence in society. The development of new diffraction techniques to understand texture and anisotropy in metals has opened new outlets into metallurgical research. As almost all everyday structural materials are polycrystalline microstructures, a structure made up of many grains, it is of the utmost importance to understand how these grains behave together as a whole and how they influence one another on the microscopic level to macroscopic responses.

1.1 Motivation

While the field of texture, i.e. the aggregate orientation of all the grains in a material, has matured significantly in the last few decades [1], understanding the aggregate role of grain boundary misorientation population has undergone less development. The grain boundary refers to the interface between two grains in a polycrystalline microstructure and is dependent on the orientation of the two neighboring grains. As a defect, grain boundaries provide diffusional pathways in the microstructure, thereby influencing intergranular properties such as electrical or thermal conductivity, but grain boundaries can also influence mechanical properties like creep and strength, because they act as barriers to dislocation motion [2][3].

The energy, strength, and mobility of a grain boundary are all dependent on its structure. For example, generally boundaries that are lower in excess volume per atom and energy have lower diffusivity rates that can help arrest corrosion [2][4][5][6]. In the field of grain boundary engineering (GBE) it was found that, by increasing the population of special boundaries over other random boundaries, one can improve the intergranular properties of a material by altering the grain boundary populations and network [7][8][9][10]. The thermo-mechanical processing

(TMP) steps in GBE have been successful in face centered cubic (FCC) metals in terms of, e.g., improving the strength of the material by increasing the annealing twin boundary population and connectivity [11][12][13][14][15]. While the phrase “special boundaries” is commonly used, for all practical purposes it is only annealing twin and twin-related boundaries that are special for GBE.

Although the success of grain boundary engineering has been well documented, finding the optimal thermo-mechanical processing parameters has been largely a trial and error process. Since the introduction of the field of grain boundary engineering in the 1980s, only a few GBE products [16][17] have been successfully introduced into the market [18]. The success in finding optimal processing parameters has been limited by the lack of scientific understanding behind how these special boundaries form. Studies have generally focused on whether the TMP resulted in a favorable grain boundary population distribution that would lead to improved intergranular properties, represented by the large black arrow connecting thermo-mechanical processing to improved intergranular properties in Fig. 1.1, with a secondary focus on the microstructure development. However, understanding the formation mechanism behind the annealing twins, shown in arrow Fig. 1.1 connecting thermo-mechanical processing to microstructure properties, would enable the control and design of materials with enhanced properties. While additional information is still needed on how the special boundaries alter the grain boundary network connectivity, the arrow connecting microstructure properties to improved intergranular properties, this is not the focus of this thesis.

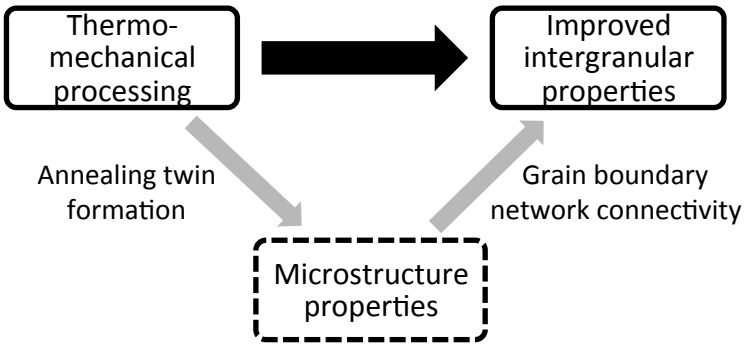

Figure 1.1. A schematic illustrating the traditional approach to grain boundary engineering, which has focused on whether thermo-mechanical processes bring about improved intergranular properties. The work presented here focuses on how thermo-mechanical processing drives annealing twin formation

While the first mechanism for the origin of annealing twins was proposed as early as 1926 [19], to date there is no definitive explanation for the formation of annealing twins. A number of theories have been presented, such as the accidental formation of a stacking fault along a migrating boundary [19][20][21][22], the decomposition of grain boundaries to lower energy boundaries [23][24], the random encounter of prior existing grains that have a twin misorientation relationship [25][26], or the accumulation and extension of stacking faults [27]. These will be reviewed more in detail in the Background (Chapter 2). However, what is lacking in the literature are observations of annealing twin formation during processing. Here, ex-situ crystallographic studies have been performed to examine the process of annealing twin formation within the microstructure during annealing in recrystallization and grain growth.

This work was a joint collaboration with Mines-Paristech CEMEF under a Materials World Network grant and also with the Department of Physics at Carnegie Mellon University. From the multiple collaborations, ex-situ studies at the mesosopic-scale were examined to understand the conditions that promote annealing twin formation within the microstructure. The

findings from this work will provide new knowledge leading to improved microstructure control and engineering of favorable grain boundaries, and thus provide the information necessary to better manipulate the grain boundary network for specific intergranular properties.

1.2 Hypothesis

Annealing twins are formed as the microstructure reduces its excess energy, whether in recrystallization by reducing the overall stored energy or in grain growth by reducing the overall interfacial energy. During this process, it is hypothesized that certain microstructural geometries will promote annealing twin formation. More specifically, it is hypothesized that the migration of {111} interfaces during recrystallization and grain growth creates the favorable conditions for twin formation. As a test of this hypothesis, microstructures are characterized crystallographically at different stage of microstructural evolution so that the annealing twin formation can be correlated to specific interface planes.

1.3 Objectives

The primary objective of this thesis in the study of annealing twin formation in nickel (Ni) is to measure the crystallography of the grain boundaries that form annealing twins during recrystallization and grain growth. A second objective is to determine whether the overall interfacial energy is lowered in the course of formation of an annealing twin.

To achieve this objectives, ex-situ heat treatment experiments coupled with microscopy are utilized to investigate the evolution of the microstructure with annealing. Electron backscatter diffraction (EBSD) coupled with scanning electron microscopy (SEM) is primarily used to investigate the grain boundary character resulting in annealing twin formation in recrystallization and grain growth. However because EBSD is a surface characterization technique, near-field high energy x-ray diffraction (nf-HEDM) is also used to study the evolution

of a 3D Ni microstructure undergoing grain growth. The details of these two techniques are presented in the Experimental Background (Chapter 3).

The results are divided into four chapters. The first chapter presents the ex-situ observations of Ni undergoing recrystallization and determines a relationship between the migrating recrystallization front and the formation of a twin. The second chapter presents the characterization of twin-related domains in the 3D microstructure and concludes that the twin variant selection from recrystallization is a random process. The third chapter presents the ex-situ observations of the 3D Ni microstructure undergoing grain growth and identifies the nucleation of annealing twins as a result of reducing the overall interfacial energy. Finally the last chapter addresses the (lack of) effect of temperature on the annealing twin content in both recrystallization and grain growth for the same change in grain size.

The hypothesis is revisited in the discussion, with an examination of how the {111} plane could influence annealing twin formation at the atomistic level. Additionally, the implications of the {111} plane for annealing twin formation are analyzed for potential directions for the grain boundary engineering of new, improved materials.

2 Background

2.1 Grain Boundaries in Microstructures

The microstructure contains the arrangement of differently orientated crystals of varying sizes and shape, referred to as grains. The interfaces between these different crystals are known as grain boundaries and are important for intergranular properties. Where three grain boundaries come together, they form a triple line, which is part of the grain boundary network. Finally the intersection of triple lines forms a quadruple point. Each microstructure feature plays an important role in material properties; for example, size plays a critical role in material hardness [28][29].

2.1.1 Grain Boundary Characterization

The grain boundary is defined by a total of five macroscopic parameters [30] and three microscopic parameters. Three of the five macroscopic parameters define the orientation relationship, or the misorientation, between the two grains, which is often defined by an axis-angle pair or a misorientation matrix. Two additional macroscopic parameters define the grain boundary inclination, which describes the spatial orientation of the grain boundary plane by a normal unit vector in one of the grains. The three microscopic parameters define the translation of atoms from one crystal to another, but in the length-scales studied in this thesis is neither observable nor quantifiable.

The identification of a grain boundary is achieved by identifying the orientation of the two neighboring grains. The misorientation is determined by the calculating the transformation necessary to transform one crystal frame back into the reference frame, and then into the crystal frame of the second grain of interest. Mathematically, this is shown in Eq. 2.1, where g_A and g_B

are the orientation matrices of the two grains and Δg_{AB} is the misorientation matrix. The graphic visualization of the math is shown in Fig. 2.1.

$$\Delta g_{AB} = g_B g_A^{-1} \qquad \text{(Eq. 2.1)}$$

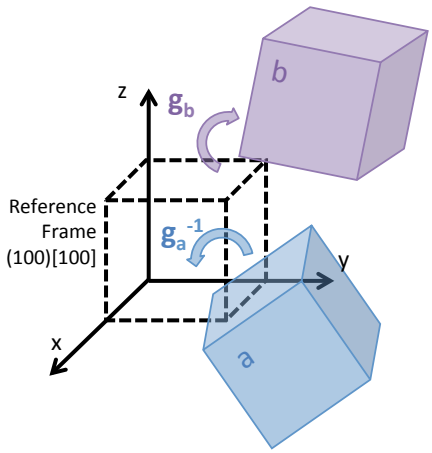

Figure 2.1. Illustration of the transformation from grain A to the reference frame and then into grain B. This overall transformation describes the misorientation between two grains.

However the misorientation matrix Δg_{AB} is not easily interpreted. Instead, transforming the misorientation matrix into an axis-angle scheme, calculated from Eq. 2.2 and 2.3, provides a more accessible interpretation of the boundary. A common axis, $\vec{R}$, between the two grains is found, and the angle, θ, describes the rotation about that axis necessary to produce the given misorientation. When the axis is perpendicular to the grain boundary normal, this is known as a tilt boundary. While if the axis is parallel to the grain boundary normal, this is known a twist boundary, shown in Fig. 2.2a and 2.2b respectively. Most grain boundaries however exhibit a mix of twist and tilt characteristics.

$$\vec{R} = \frac{(\Delta g_{23} - \Delta g_{32}), (\Delta g_{31} - \Delta g_{13}), (\Delta g_{12} - \Delta g_{21})}{\sqrt{(\Delta g_{23} - \Delta g_{32})^2 + (\Delta g_{31} - \Delta g_{13})^2 + (\Delta g_{12} - \Delta g_{21})^2}} \qquad \text{(Eq. 2.2)}$$

$$\cos\theta = \frac{1}{2}(trace(\Delta g) - 1) \qquad \text{(Eq. 2.3)}$$

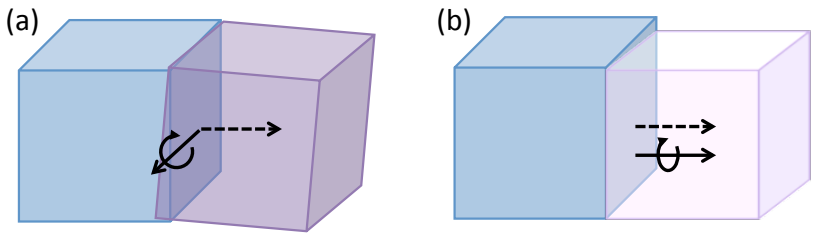

Figure 2.2. Illustration of a (a) tilt boundary and (b) twist boundary. The dashed arrow refers the grain boundary normal and the solid arrow is the rotation axis with an associated rotation to transform one grain to the other. In the tilt boundary, the grain boundary normal is perpendicular to the rotation axis and in the twist boundary the two are parallel.

To simplify, however, grain boundaries are often categorized by more general means. For example, when the misorientation angle in the axis-angle definition of the grain boundary is less than 15°, a grain boundary will often be referred to as a low angle grain boundary (LAGB). By contrast, grain boundaries with a misorientation angle greater than 15° are considered to be high angle grain boundaries (HAGB). In LAGBs the misorientation can be accommodated by describing the grain boundary as an array of dislocation. Past a misorientation angle of 15°, the dislocation density increases such that the dislocations must overlap and this simple model no longer applies for HAGBs. Although not invariably the case, high angle grain boundaries usually will have a higher energy than LAGBs. However the properties of all grain boundaries vary and can depend on the structure, which can be defined by the coincident site lattice model.

One of the early definitions for relating the crystallographic lattice of two different grains was the coincident site lattice (CSL) model [31]. This model describes the number of overlapping crystal lattice sites between the two grains. Lower CSL numbers (or "sigma" values) correspond to higher degrees of overlap of the crystal lattices (a reciprocal relationship). Under this model, one might therefore expect that low CSL boundaries correspond to low energy boundaries and high CSL boundaries correspond to high energy boundaries, however these

relationships have been proven to not be true [32]. Nonetheless, the CSL theory is a useful method to classify grain boundaries and in particular is frequently used as a means to quantify the degree of grain boundary engineering in a microstructure.

2.1.2 Grain Boundary Energy

The grain boundary is a planar defect that separates two differently orientated crystalline lattices. In the simplest idea, the grain boundary energy, γ_{GB}, has an energy based on the number of bonds (B) required to join the two free surface, γ_s^1 and γ_s^2. This is given by Eq. 2.4. and is applicable for all grain boundaries.

$$\gamma_{GB} = (\gamma_s^1 + \gamma_s^2) - B \qquad \text{Eq. 2.4}$$

A LAGB, however, can be modeled by a discrete dislocation array, which considers the density of dislocations necessary to introduce the given misorientation. The grain boundary energy for this tilt or twist LAGB is dependent on the sum of dislocation energies necessary. This is the Read and Shockley approach [33], but is limited to botundaries in which the dislocations do not overlap. For general grain boundaries and CSL boundaries this approach is non-applicable.

The relative grain boundary energy can be experimentally measured by considering the geometry of grain boundaries at a triple junction. Assuming thermodynamic equilibrium is achieved at the triple junction, then the Herring equation [34], Eq. 2.5, describes the balance of forces.

$$\gamma_i \vec{t}_i + \frac{\partial \gamma_i}{\partial \beta} \vec{n}_i = 0 \qquad \text{Eq. 2.5}$$

Where γ_i is the grain boundary energy, $\vec{t}_i$ is the tangential force, and $\vec{n}_i$ is the normal force of the i^{th} grain boundary, and β the rotational force. The illustration of each component with its respective grain boundary is shown in Fig. 2.3a. The Herring equation is often simplified by

assuming that the torque terms, the energy differential with respect to the rotation angle, $\frac{\partial \gamma_i}{\partial \beta}$, are small and can be neglected. By only considering the tensile forces, this results in the simplified relationship of Young's equation [34], given in Eq. 2.6.

$$\frac{\gamma_1}{\sin \theta_{2,3}} = \frac{\gamma_2}{\sin \theta_{1,3}} = \frac{\gamma_3}{\sin \theta_{1,2}} \qquad \text{Eq. 2.6}$$

The relative grain boundary energies $(\gamma_1, \gamma_2, \gamma_3)$ are calculated based on the geometry of the triple junction depicted in Fig. 2.3b, by knowing the dihedral angles $(\theta_{2,3}, \theta_{1,3}, \theta_{1,2})$. This requires a 3D microstructure in order to have a full description of the grain boundary to obtain the correct dihedral angle. By calculating this across a given number of grain boundaries, one obtains the grain boundary energy distribution (GBED) of a material, where the units of the given distribution are in arbitrary units of multiples of a random (or uniform) density (MRD or MUD). The GBED describes the energy of each boundary in 5-parameter space, where it has been found that the population is inversely related to the energy [35][36]. That is, low energy boundaries have higher populations than high energy boundaries, thus creating an anisotropic distribution due to the anisotropic energy properties.

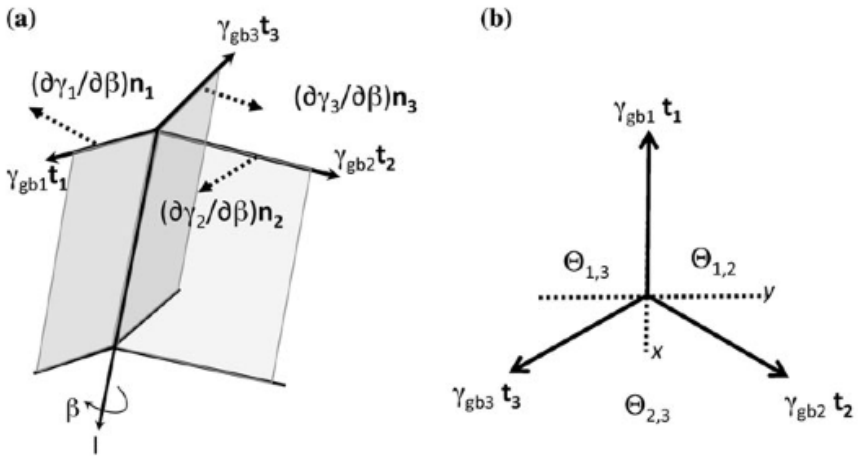

Figure 2.3. Illustrations to show the balance of interfacial energies at a triple junction (a) according to the Herring equation and (b) according to Young's equation. The variables shown correspond to Eq. 2.5 and 2.6 respectively. Figure reproduced from [Rohrer 2011]

Other methods of calculating the relative grain boundary energy involve thermal grooving according to the Mullin's equation [37]. Additionally, by using atomistic simulations, grain boundary energies can also be determined synthetically. Simulations of static grain boundaries (kT = 0) have provided an absolute measurement of 388 grain boundary enthalpies [38] across a range of FCC metals that agree reasonably with experimental observations [39][40]. From these simulation results, more recent work has been made to fit the grain boundary enthalpy distribution as a function of the five degrees of macroscopic freedom in grain boundaries [41].

2.2 Microstructure Evolution during Deformation, Recrystallization, and Grain Growth

As a material may undergo a bulk change, such as a reduction in thickness during rolling, the microstructure undergoes a change with mechanical treatment. Similarly, as increasing temperatures increase thermal vibrations of atoms, this leads to changes in the microstructure

often to reduce the overall free energy. Understanding how the microstructure responds to thermo-mechanical processing is key for controlling microstructural properties such as grain size, orientation, or misorientation, which may influence material's macroscopic properties.

2.2.1 Deformation

Cold-working of a metal either by compression or rolling not only permanently deforms the material, but also introduces dislocations into the microstructure. The increasing plastic deformation corresponds to an increasing population of dislocations and an increase in the stored energy of the material [42][43][44]. The stored energy reflects the amount of energy that would be released if the same volume of material was dislocation free. In the simplest assumption, the deformation is assumed to be uniform and stored energy is assumed to be homogenous throughout the material [45][46].

This is in fact not the case as deformation is often heterogeneous in a microstructure, with more dislocations accumulating in particular grain orientations [47][48][49] or near grain boundaries [50] like shown in Fig. 2.4. Here the color is "inverse pole figure" (IPFz) in relation to the surface normal, which means that surfaces near {111} are blue, {110} are green} and {100} are red with interpolation in the standard stereographic triangle. As deformation increases, the stored energy may be reduced by dislocation annihilation or the formation of lower energy dislocation arrays and sub-grain structures. During annealing the rearrangement of dislocations is known as recovery, sometimes polygonization, which follows deformation but precedes recrystallization [51][52][53]. The coarsening of these sub-grains are also believed to be the origin of the recrystallization nuclei [54][55], thereby linking deformation and recrystallization, at least in high stacking fault energy metals.

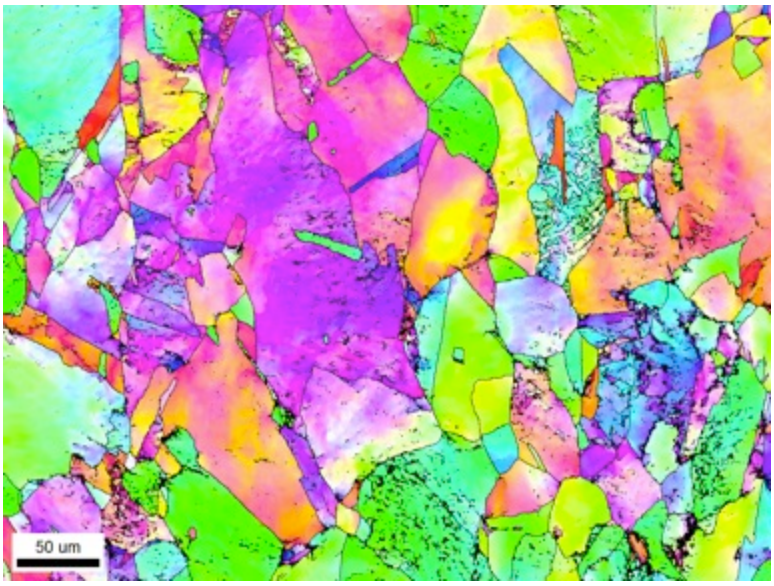

Figure 2.4. EBSD-IPFz image of a Ni microstructure deformed to 25% with HAGB from 15-65° colored black. In certain grains there is a lack of boundaries found in the interior of grains while others contain a high abundance, revealing the heterogeneity of deformation in the microstructure.

2.2.2 Recrystallization

Recrystallization is the process of forming new grains in a deformed microstructure [56]. The deformed microstructure (whether by rolling, compression, or torsion), contains a certain amount of stored energy. The deformation breaks up the grains of the original microstructure into smaller cells, which lead to the nuclei for recrystallization. Recrystallization usually initiates at the areas of highest deformation first, where there are the most dislocations and re-ordering into sub-grains as well as the highest stored energy in the material [57][58]. Locally strong orientation gradients play a role by allowing high-angle, high-mobility boundaries to form, which are required around a nucleus in order for it to be able to grow [59]. The process of recrystallization then introduces new defect-free grains in a strained microstructure, reducing the overall stored energy of the microstructure.

The progress of recrystallization can be measured by the rate at which the stored energy is removed. Experimentally however, this is taken be the volume fraction of the strain-free

regions in the microstructure relative to the original deformed matrix. An example of a mostly recrystallized microstructure is shown in Fig. 2.5, where the new grains have a single color indicating one uniform orientation, whereas deformed regions, circled, show a spread due to the dislocations causing slight crystallographic rotations.

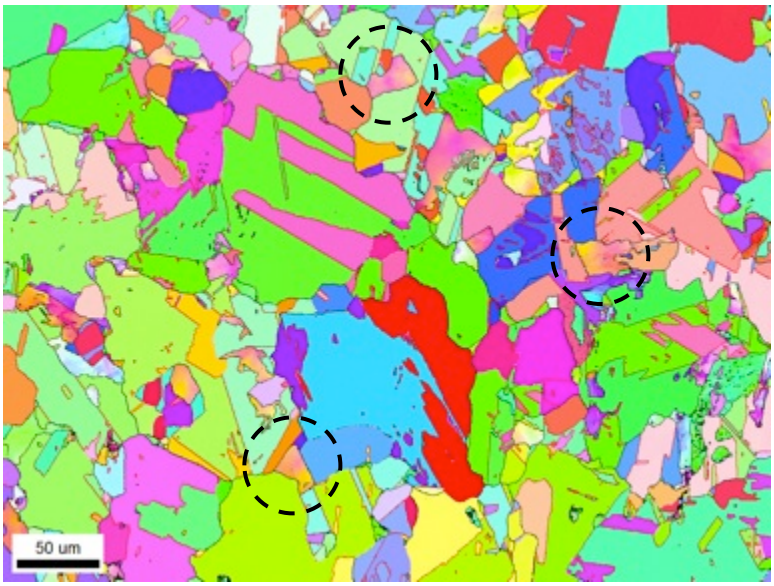

Figure 2.5. EBSD-IPFz image of a Ni microstructure of the same region as Fig. 2.1 and partially recrystallized with HAGB colored black and special boundaries colored red. The original deformed microstructure has been replaced by the recrystallized regions of strain free (single color) grains. Regions circled show the remnants of the deformed microstructure.

2.2.3 Grain Growth

Grain growth is the coarsening of individual grains in the microstructure. The larger grains grow at the expense of the smaller ones, thereby reducing both the number of grains in the system and increasing the average grain size. Grain growth is driven by the curvature of the grain boundaries, where boundaries migrate towards their center of curvature to reduce their area [60][61][62]. This reduces the overall interfacial energy in the microstructure, such that theoretically a microstructure undergoing grain growth should ultimately end with one grain. Because grain growth depends on the grain boundaries being mobile via atom transfer, it is

highly temperature dependent. For most pure metals, a temperature of $0.4T_m$ is necessary to achieve grain growth.

2.3 Annealing Twin Formation

In face centered cubic materials, annealing twin boundaries are unique in their appearance and occurrence as long, faceted boundaries within the microstructure. For the purposes of this document, an annealing twin refers to any grain that shares a twin misorientation relationship with another grain. The term twin boundary will be used to refer to grain boundary featuring a 60°<111> misorientation. The term coherent twin boundary will be used to refer to a twin boundary where the interface plane is (111) on both sides of the boundary, where as the incoherent twin boundary fails this condition. In the EBSD image of a microstructure in Fig. 2.6, the coherent twin boundaries, labeled CTB, and the incoherent twin boundaries, labeled ITB, are shown. A Σ3 boundary, which is a designation that will be used sparingly in the document, has the same definition as the twin boundary.

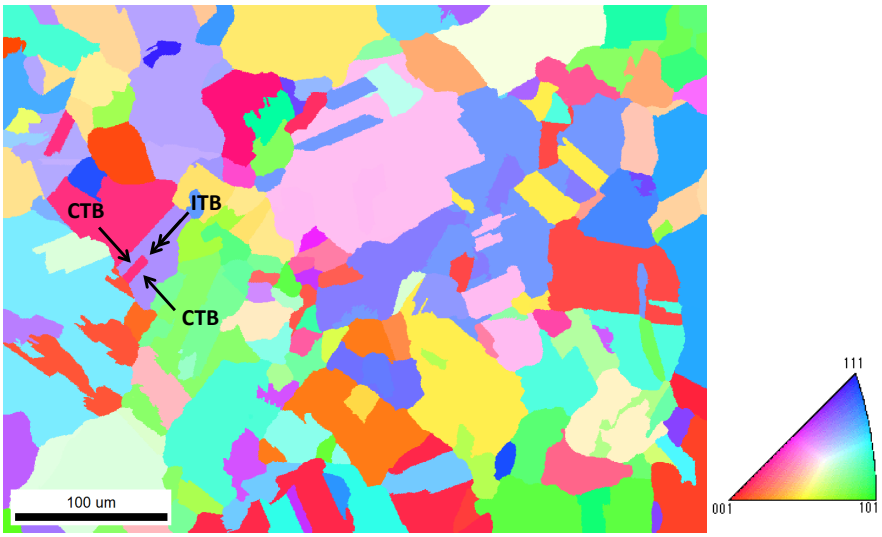

Figure 2.6. EBSD colored by IPFz of a fully recrystallized Ni specimen. The arrows with labeled CTB point to the coherent twin boundaries of the twinned pink grain to its purple neighbor, where the double arrow labeled ITB point to the incoherent twin boundary segment.

2.3.1 General Characteristics

The structure of a coherent annealing twin boundary found in FCC metals is shown in Fig. 2.7. The segment labeled a-b is the twin plane, where either side of the boundary is a (111) plane in the respective grain. In this illustration, to transform from the original to the twinned grain, one can visualize the rotation of the top half by 180° twist from the bottom half, although due to the crystal symmetry, this is equivalent to a 60° rotation about <111>.

Annealing twins form primarily in FCC materials that have a low to intermediate (<100 mJ/m^2) stacking fault energy and have undergone heat treatment in either recrystallization or grain growth. This includes copper, nickel, and stainless steel, all of which have also been shown to be successfully grain boundary engineered [63][64][65]. At the twin boundary, the original stacking sequence of the FCC crystal:

ABC ABC ABC

is mirrored at the coherent twin plane of B, as shown in Figure 2.7, changing the stacking sequence to:

ABC **ABA** CBA

In the ABA region, the structure exhibits a hexagonal close packed (HCP) structure. Doing so, the twin boundary energy can be roughly approximated by taking the difference in energy between HCP and FCC structure, which is half of the stacking fault energy. In comparison to the general grain boundary energy, roughly 1.0 J/m^2, the coherent twin boundary energy in Ni is two orders of magnitude less (~0.06 J/m^2) based on molecular statics [38]. However the energy of incoherent twin boundaries features a wide range of energy values from 0.2 up to 1.0 J/m^2 [Olmsted 2009].

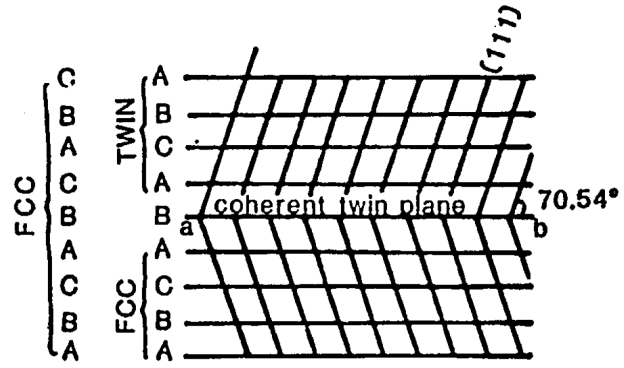

Figure 2.7. Illustration of the change in stacking sequence found at the coherent twin plane annealing twin boundary from a perfect FCC stacking sequence. Figure reproduced from [23].

2.3.2 Annealing twin formation theories

Carpenter and Tamura provided the earliest explanation on the nature of annealing twins. They suggested that annealing twins form as a result of atomic rearrangements during grain growth [19]. Atoms would slip into the "wrong" position onto the closest packed plane, and the following atoms take up the necessary positions to produce the twinned crystal in order to minimize energy. While there has been no direct proof of such an event occurring, this concept is the foundation for the idea of "growth accidents". Other theories for annealing twin formation that have also been proposed include the grain boundary dissociation model [23][24][66], the grain encounter model [25][26][67], and the formation of stacking fault packets on migrating grain boundaries [27]. The chronological order and contributors to the overall framework of these models are summarized in Table 2.1.

Table 2.1. Timeline of Theoretical Models for Twin Mechanisms

Growth Accident	Carpenter and Tamura (1926), Burke (1950), Fisher and Fullman (1951), Gleiter (1969), Pande (1996)
Grain Boundary Dissociation	Meyers and Murr (1978), Goodhew (1979) Kopezky (1983)
Grain Encounter	Burgers (1953), Nielsen (1967), Kurzydlowski (1991)
Stacking Fault Packets on Migrating Boundaries	Dash and Brown (1963)

Gleiter provided a further framework into the growth accident model by providing an atomistic model behind the formation of annealing twins [22]. Grain boundaries are treated to have {111} facets or steps of favorable orientations that are responsible for migration. As one grain shrinks and the other grows, the atoms that are transferred will impinge upon the close packed plane, or the {111} plane in a FCC material. The impinging atoms have two sites of possible nucleation, based on the stacking previously sequence shown in Figure 2.8.

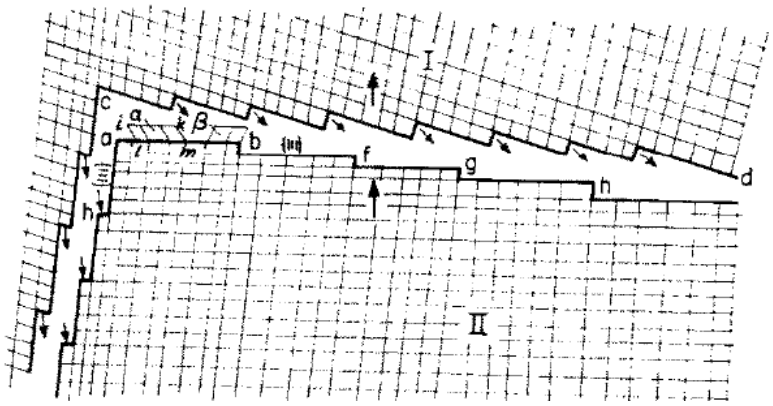

Figure 2.8. Schematic of Gleiter's growth accident model. Grain II grows into Grain I designated by the arrows. Atoms migrating from grain I to II can go to either the improper stacking sequence or proper sequence on a (111) ledge. This results in either the formation of a twinned cluster at the interface,α, or a continuation of the original grain, β. Figure reproduced from [22]

The nucleation of these impinging clusters result in an increase in the free energy up until a critical size, which will then decrease in free energy again. While retaining the original stacking sequence provides the lowest overall energy, a twinned plane provides the next possible lowest energy configuration. By considering the geometry of the initial cluster, Gleiter proposed Eqn. 2.7. for determining the probability of a twin forming:

$$\mathbf{p = exp\left\{\frac{-Q}{\left(\frac{\pi\varepsilon^2 h^2}{Q\sigma_z}-1\right)kT}\right\} exp\left\{\frac{\ln\frac{\Delta G^\circ}{kT}}{\frac{\pi\varepsilon^2 h^2}{Q\sigma_z}-1}\right\}} \qquad \textbf{Eq. 2.7}$$

The probability, p, of a twin forming is based on the absolute temperature, T, in Kelvins, as well twin boundary energy, σ_z, in J / m^2. Other variables related to the formation of a twin nucleus are h, the height of the nucleating cluster in meters, and ε, the energy per step height of the nucleating cluster in J / m^2. While Q is the activation enthalpy for grain boundary migration in J / atom, and ΔG° is the Gibbs free energy per volume of atoms in the grain boundary in J / m^2.

The growth accident model treats the formation of a twin grain using a classical nucleation model coupled with the kinetics necessary for grain boundary migration. The effect of temperature on the probability of annealing twin formation is plotted in Fig. 2.9. The values used are: σ_z = 0.0336 J / m^2, h = 2.0344 x10^{-10} , ε = 0.497 J / m^2, Q = 2 x10^{-19} J / atom, and ΔG°/k to be 0.2. The values are taken from [68]. The observed effect of increasing the temperature is increasing the probability of forming an annealing twin in the microstructure. This implies that more twins should be observed in the microstructure with increasing temperature, which the previous findings will be discussed later in 2.3.3.1 and further studied in Chapter 7.

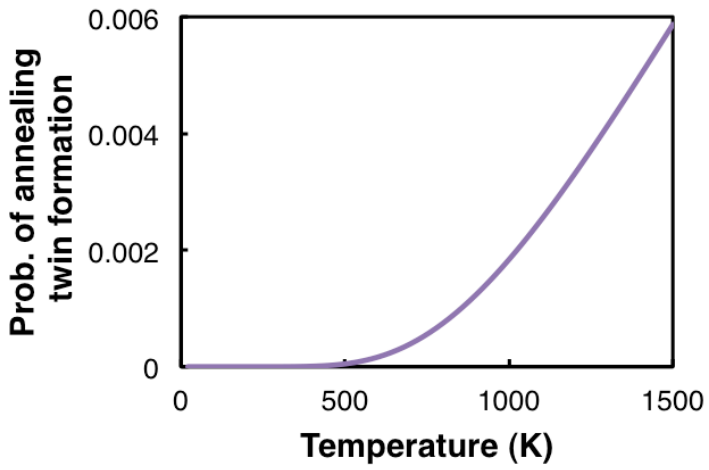

Figure 2.9. The effect of temperature on the probability of forming an annealing twin from Gleiter's growth accident model. Probability of formation increases with increasing temperature.

Meyers and Murr provided a model that did not require migration of the grain boundary, however annealing twins needed to decrease the overall interfacial free energy of the system [23]. The grain boundary decomposition model simply follows that high angle grain boundaries, which are usually higher in energy, can decompose into lower energy grain boundaries [24]. The coherent boundary of the twin is immobile, while the incoherent boundary of the twin is free to migrate and extend the twin into the original grain shown in Fig, 2.8. This should only occur if the overall interfacial energy is reduced in the system despite the addition of an extra twin boundary, as suggested by Eqn. 2.8:

$$\gamma_{TB}A_{TB} + \gamma_{tb}A_{tb} + \gamma_{gb'}A_{gb'} < \gamma_{gb}A_{gb} \qquad \textbf{Eq. 2.8}$$

Here γ_{TB}, γ_{tb}, γ_{gb}, and $\gamma_{gb'}$ correspond to the surface energy of the coherent twin boundary, incoherent twin boundary, new random boundary, and the old random boundary respectively. Similarly A_{TB}, A_{tb}, A_{gb}, and $A_{gb'}$ correspond to the areas of each boundary. Although this equation is applicable for any two randomly orientated grains, boundaries that are close to the

coherent twin misorientation are favored as the area of the formed coherent twin boundary is maximized and therefore costs the least amount of energy. Additionally, it has been noted that particular configurations can give rise to the grain boundary decomposition of a twin boundary [24][69]

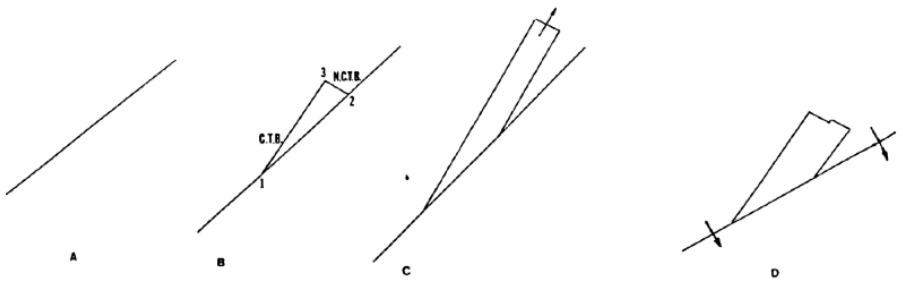

Figure 2.10. Schematic for the grain boundary decomposition model. The annealing twin forms from by replacing the original grain boundary with three new grain boundaries, which must all be lower in energy. The glissile nature of the incoherent twin boundary that is formed is responsible for elongating the twin in the grain, without the need for any migration from the original boundary.

In the grain encounter model, within a given volume of material, there is a simply probability that two spatially separated, growing grains have a twin misorientation relationship [25]. When these two grains impinge, a twin boundary is formed and assumed to take its lower energy configuration as shown in Fig. 2.9. In a completely randomly textured material, the probability of finding such a relationship is only approximately 2 %. However the consideration of texture (i.e. from cold-rolling) can alter and increase probabilities in which two grains may be twin related [67]. However, in this model, it is generally hard to explain how more than one twin boundary of the same misorientation can be formed.

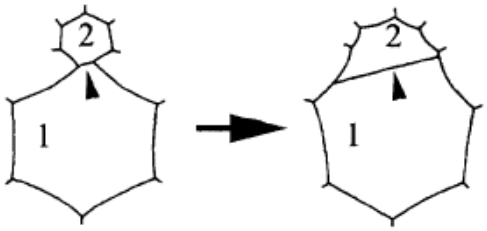

Figure 2.11. Schematic for the growth encounter model. Two growing grains share a twin misorientation relationship. When the two grains impinge, the low-mobility twin boundary is formed and the low-energy twin boundary is elongated.

In the stacking fault packet model presented by Dash and Brown, they noted the presence of stacking faults at migrating grain boundaries with the use of transmission electron microscopy (TEM) [27]. The accumulation of these stacking faults causes an increase of localized residual strain, but the nucleation of a twin alleviates this. The twin grows by glide of the stacking fault packets into the recrystallized, strain-free grain, where the additional layers of stacking fault packets dictate the thickness of the twin shown in Fig. 2.10. Although so far, these observations have been limited to the TEM and to the author's knowledge have not been observed in in a bulk sample.

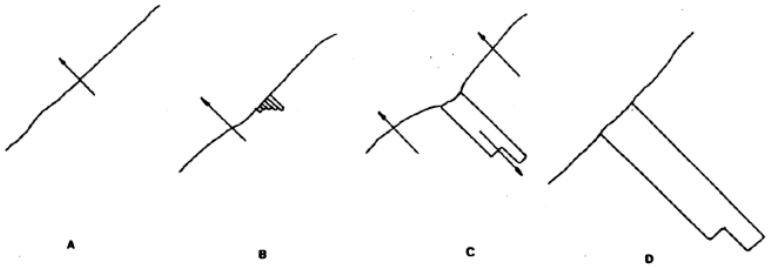

Figure 2.12. Schematic for the stacking fault packets at the migrating grain boundary. The accumulation of the stacking faults results in the formation of a twin behind and perpendicular to the migration front, which helps relieve the in the microstructure from the excess stacking faults.

Mahajan *et al.* presented the most recent proposal for annealing twin formation mechanism in FCC materials with the objective of unifying the growth accident model and generation of stacking fault packets [70]. Based on the previous observations by Pande *et al.*, temperature was observed to play no role on the twin density, p, contrary to Gleiter's model. Instead, only the change in grain size, D_0 to D, played a role in the annealing twin density [71]. This produced Eq. 2.9, in which the twin density could be directly calculated from the change in grain size, agreeing with the experimental data of [72][73][74].

$$\frac{p}{p_0} = \frac{D_0}{D} \log \frac{D}{D_0} \qquad \text{Eq. 2.9}$$

In Mahajan's model, the following assumptions are made: the annealing twin forms from a migrating boundary, the boundaries can be described with {111} steps or facets, where the driving force is dependent on the grain boundary curvature [70]. In the schematic shown in Fig. 2.11, the migrating grain boundaries of grain I and II force the {111} step to move upwards, depositing new {111} planes underneath each step via partial Shockley loops. This event still depends on the grain growth accident model, where the width of the annealing twins depend on the migration rate of the {111} step.

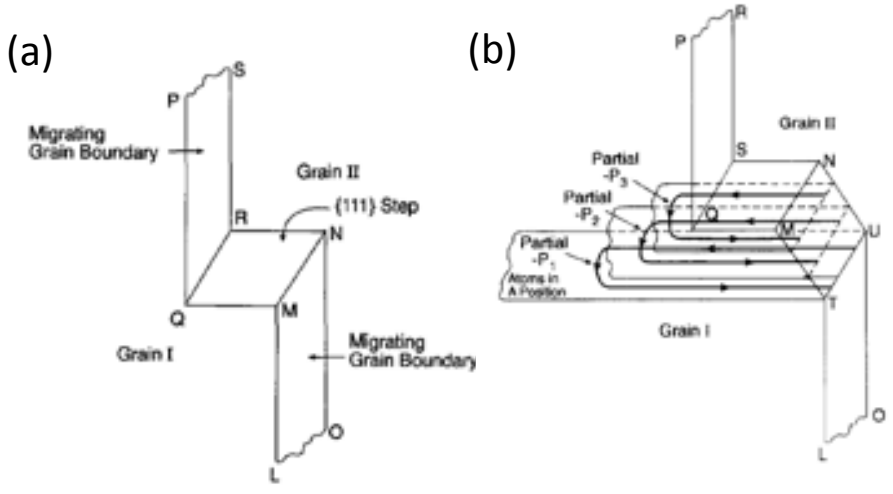

Figure 2.13. Schematic of moving {111} step during grain boundary migration and creating Shockley partials to nucleate a twin. Figure reproduced from reference [Mahajan 1997].

2.3.3 Developments in understanding annealing twin formation

2.3.3.1 Factors influencing annealing twin formation

Modifying the stacking fault energy has been shown to influence the twin content in the microstructure. This was directly observed in Charnock and Nutting's observations in adding carbon and nickel to austenitic iron [75], as well as in the work by Rath *et al.* with boron-doped Ni [76][77], and indirectly by comparing the twin content between Cu and brass microstructures. The general trend observed, independent of material, is that increasing stacking fault energy reduces the twin content in the microstructure. This is explained by the increasing twin boundary energy that is directly related to the stacking fault energy. As each reviewed model is dependent on the cost to create a twin boundary, then the increased twin boundary energy works against the mechanisms promoting annealing twin formation.

The other factors that have been examined in detail that influence annealing twin content are TMP parameters for recrystallization and grain growth. Various authors have tested the influence of prior strain on the twin content of different purity nickel undergoing recrystallization. Increasing strains from 2.5 to 7.5% [78], 30% and 60% [79], 40%, 60%, and 80% [80] for a given starting microstructure and annealed until full recrystallization (at varying temperatures) all showed the same trend that increasing stored energy increased the twin density of a given grain size in each experiment respectively.

The role of temperature during annealing twin formation, in either recrystallization or grain growth, is not clear. The growth accident model assumes the formation of a nucleus at a heterogeneous site in the microstructure. In Gleiter's equation [22], it is expected that changing temperature will change the nucleation rate of new twins in the microstructure. However, only a weak trend is observed between temperature and the twin density [71]. While the same work in

Ni has shown that twin content does not change as a function of temperature for a given deformation [78][79], Field *et al.*'s work shows the opposite trend where decreasing the temperature led to more twins per grain in Cu [81]! However all studies agreed with the general trend that the twin content was dependent on the grain size as proposed by Pande [71]. Furthermore, Pande's equation has been consistently shown to provide a good fit between different material systems [68],

2.3.3.2 Observations of annealing twin formation

Two previous groups have directly observed the formation of annealing twins. Gastaldi *et al.* observed the formation of annealing twins in aluminum undergoing growth utilizing x-ray synchrotron topography [82], while Song *et al.* observed the formation of annealing twins in a Pb-based alloy by in-situ heating stage in EBSD [83]. The results of both experiments supported the growth accident model, where the migration of high angle boundaries was required for the formation of a twin boundary. This introduces an interesting question of why are the direct observations indicative of the growth accident model, even though the trends in temperature are not?

Viswanathan and Bauer performed a study of twin formations in annealed copper bicrystal samples with [100] tilt boundaries [84]. Their observations agreed with the former two in that single twins can form as a result of growth accidents on the {111} plane on a HAGB, replacing the original boundary with an immobile coherent twin and mobile incoherent twin boundary. While varying temperature was tested, the data was too meager to draw any definitive conclusions even though at increased temperatures HAGBs did twin. Furthermore, their work also showed that twins never formed from LAGB configuration, which was presumably energetically limited.

2.3.3.3 Recent work investigating annealing twin formation

Recent work by Jin *et al.* had shown that annealing twins primarily occurred during recrystallization, where the twin density increased during recrystallization and consequently decreased as the microstructure underwent grain growth [85]. The justification behind this difference was the geometric requirement of annealing twin formation, where using the growth accident model, the authors proposed only convex boundaries migrating away from their center of mass can be responsible for the formation of long, straight twin boundary, as shown in Fig. 2.12. Where as concave boundaries migrating towards their center of mass forming a twin would require the formation of partial dislocations, designated by the red x's, and is therefore energetically costly. Due of the lack of convex fronts migrating away from their center of mass in the microstructure during grain growth, then it is proposed there are no twinning events during grain growth (with the possible exception of triple junctions).

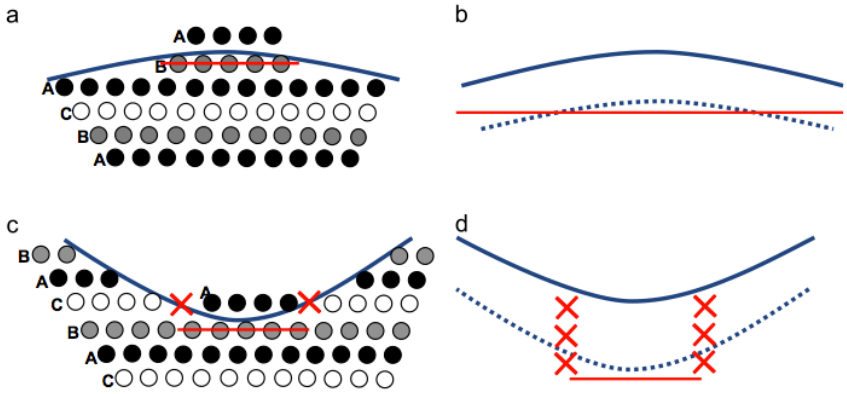

Figure 2.14. Annealing twin formation at a convex (a) or at concave (c) migrating boundary. The stacking sequence of the compact planes for the growing grain is shown along a <110> direction and the orientation of the consumed crystal is random. The twin occurs by forming a cluster of atoms in the wrong position (A instead of C) on a {111} facet. (b) and (d) show how the twin boundary can evolve following the migration based on the curvature. The red lines represent coherent twin boundaries and the red crosses represent the Shockley partial dislocations that are necessary in the case of the concave boundary. Figure reproduced from [85]

The twin density was recently shown to correlate strongly with the tortuosity of the microstructure front by the same group of authors [79]. A higher tortuosity resulted in a higher twin density, where the authors argued that this was also due to the increased number of convex fronts. The increased number of convex segments on the recrystallization front, as illustrated by the arrows in Fig. 2.13, provided an increased number of potential twin nucleation sites in the microstructure, hence increasing the twin density. These two studies emphasize that there must be a geometric relationship between the grain boundary front and the crystal plane that exhibits twinning.

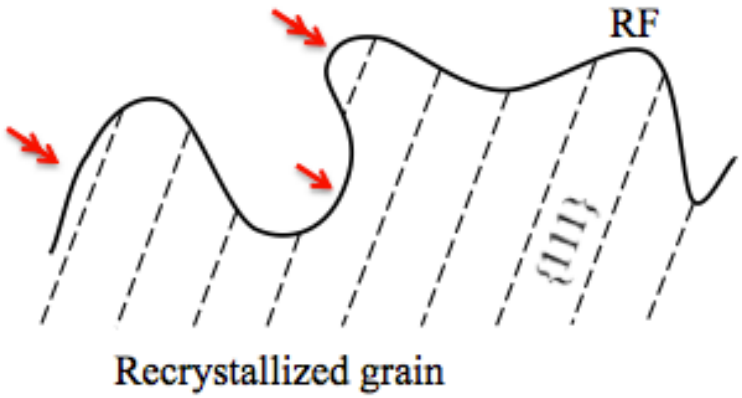

Figure 2.15. Schematic of a tortuous, recrystallization front (RF) with portions of the front that close to being parallel to {111} (arrowed). The tortuosity provides additional nucleation sites for annealing twin formation in comparison to a flat front. Figure reproduced from [79].

Beyond these two recent papers by Jin *et al.* and Viswanathan's work on Cu bicystal pairs that exhibit annealing, little work has been done to consider the crystallographic role of the interface that results in annealing twin formation. While twins have been assumed to nucleate from the grain boundary, whether from stacking fault packets that extend into the grain, Shockley partials that repel and elongate the twin boundary, or the dissociation of grain boundaries, it might expected that different boundaries will have different responses for these mechanisms to occur.

2.3.4 Investigating the role of crystallographic orientation

In Ashby and Harper's experiment, an indentation was made on a copper single crystal and annealed to form new recrystallizing grains [86]. Annealing twins were noted to form with the migration of the recrystallizing grain boundary as shown in Fig. 2.14. What was not highlighted was that one of the recrystallizing grains has more annealing twins than the others. The different contrast in the optical micrograph indicates the grains are of different orientations, which implies here that orientation plays a role. From a typical micrograph, one can observe that grains have a range of twin content. While some of this can be attributable to taking the cross-section of a 3D microstructure, it could also imply that texture, or more specifically the orientation of the grain boundary, may play a role. However the techniques available in the past did not allow for feasible, direct measurements of the grain orientations.

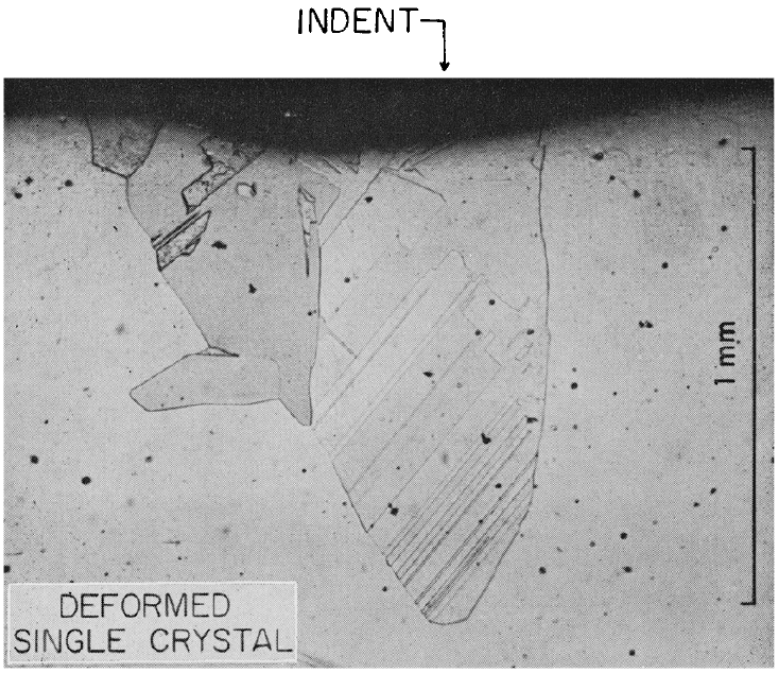

Figure 2.16. Stimulated recrystallizing grains at an indent in a deformed Cu single crystal that feature annealing twins. The grain on the right has considerably more twins than the grain on the right, which is presumably due to the difference in orientation and migration direction. Figure reproduced from [86].

Each annealing twin formation model presents a different relationship for the migrating grain boundary plane that would exhibit the formation of a twin boundary. In Mahajan's model, annealing twins are formed on planes that are perpendicular to the {111}. In the grain boundary dissociation model, annealing twins are formed off planes that are close to the {111} plane, but not exactly the {111}. The grain encounter model would show no relationship between the grain boundary migration direction and the formation of the twin. While Gleiter's growth accident model is associated to have twins nucleate from planes that are close to {111}.

To summarize, we expect higher counts of certain migrating grain boundary planes that exhibit twinning at distinct locations in the cubic fundamental zone in the grain boundary plane distribution depending on the twinning mechanism, as illustrated in Fig. 2.15. The growth accident model would feature a high number of planes at the {111}. Whereas the grain boundary dissociation model would feature a broader distribution of planes around {111}. In contrast, Mahajan's model would exhibit planes that lie on the trace band of the {111}, or directions perpendicular to the {111} normal. Thus from studying the crystallographic orientation of the migrating grain boundaries that exhibit twinning from electron backscatter diffraction and near-field high-energy x-ray diffraction, this relationship is yet to be determined.

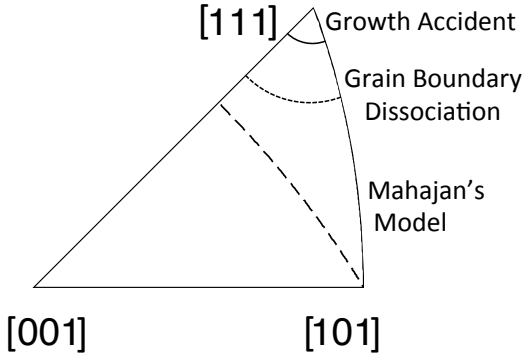

Figure 2.17. Illustration of expected peaks of grain boundary planes that exhibit twinning in an FCC structure should be according to three different FCC annealing twin formation mechanisms.

3 Experimental Background

This chapter introduces the material to be studied and summarizes the two different microscopy techniques utilized to observe the evolution of the microstructure. The first technique is electron backscatter diffraction, which determines the orientation of the grains in the microstructure of a polished sample surface in scanning electron microscopy. The second technique is near-field high energy x-ray diffraction, which utilizes x-rays to determine the orientation of grains within the volume of a given material based on diffraction. These provide a general overview for readers unfamiliar with either technique, while specific experimental details are provided in the results chapters.

3.1 Material Selection and Sample Preparation

High purity nickel has been selected as the material of study for several reasons. As an FCC metal with a medium stacking fault energy, it is a material that exhibits annealing twin formation and is well documented [87][88]. In additional, its success as a GBE material has been well reported [89][90][91][92]. The previous works include an extensive reports on how the final twin fraction of the microstructure varies with TMP parameters, which will be useful for comparing whether the evolving state of the microstructure agrees with what has been observed in literature. For example, with each TMP iteration, the length fraction of Σ3 boundaries has been reported to increase while the length fraction of the random boundaries decreases [93].

A second purpose of studying nickel is that it also serves as a model material for all other nickel-based super alloys, which too have shown success for GBE and has more important industrial usages [94][95]. Furthermore, the majority of GBE candidates are FCC materials, and it has been previously been shown that different FCC materials exhibit similar grain boundary character [96].

One last advantage of using nickel is that its high symmetry and relatively heavy atomic mass provides strong diffraction patterns for indexing orientations in both electron backscatter diffraction and near-field high energy x-ray diffraction.

A high purity nickel rod (with a diameter of 5 mm) of 99.999% purity was obtained from Alfa Aesar. The samples are homogenized by annealing at 410 °C (~0.30 T_m) for 24 hours to eliminate residual strain in the material while minimizing grain growth. For EBSD characterization, nickel samples were mechanically polished starting with SiC 600 grit and progressively finer until 1200 grit, followed by diamond abrasive suspensions of 9 / 3 / 1 μm and finishing with a final polish of colloidal silica of 0.05 μm on a Vibromet™. The specific polishing procedure can be found in Table 3.1.

Table 3.1. Polishing Procedure for FCC Ni

Surface	Polishing	Speed (rpm)	Force (lbs)	Time (min:sec)
SiC Grit Paper	15 μm	120	6	Until Planar
UltraPad	9 μm MetaDi Supreme Diamond Suspension	120	6	3:00
TriDent	3 μm MetaDi Supreme Diamond Suspension	120	6	3:30
TriDent	1 μm MetaDi Supreme Diamond Suspension	120	6	4:00
Microcloth	Collodial silica 0.02 μm MasterMet2	100	4	5:00
Microcloth on VibroMet™		N/A	N/A	1 hour (minimum)

3.2 Electron Backscatter Diffraction

Electron backscatter diffraction is a scanning electron microscope (SEM) based technique used to measure crystallographic orientations. While the SEM uses accelerated electrons from the primary beam as a method of imaging, the same electrons can be used to observe the diffraction patterns from crystals. This is achieved by tilting the sample to 70° with respect to the surface

shown in Fig. 3.1. The diffracted electrons are captured on a phosphor screen to produced visible lines known as Kukuchi bands [97], or electron backscatter patterns, as seen on the camera. The patterns are characteristic of the sample crystal structure and enable indexing the orientation of the crystal they diffracted from [98].

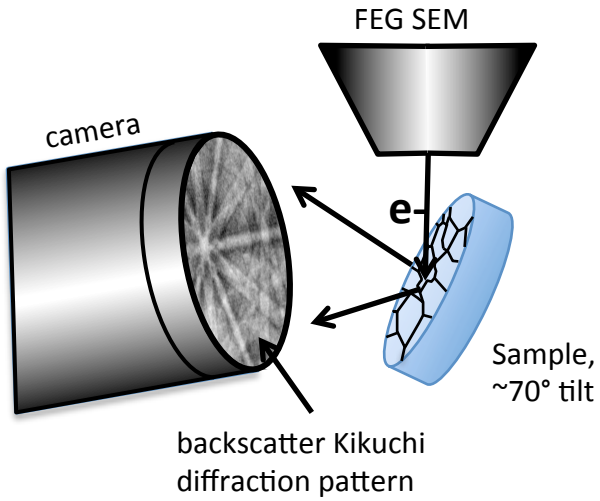

Figure 3.1. Schematic of a typical EBSD setup found inside an SEM. Diffracted electrons are produced from the incident beam against a sample tilted at 70° to produce the backscatter Kikuchi diffraction pattern on the camera. Figure reproduced from [Sutatch 2013]

EBSD systems have become very common for microstructural characterization. These systems provide orientation at a sub-micron resolution. The largest advantage of EBSD systems over other crystallographic orientation tools, such as x-ray diffraction or transmission electron microscopy, is the high throughput of local orientations. However a major limitation is that diffracted electrons come only from the top 10 nm of the samples, and therefore all the obtained maps are only reflective of the surface, which may be not be characteristic of the bulk. Without the use of serial sectioning, EBSD cannot provide full information on the 5-parameter grain boundary character, although this can be approximated with stereology.

The electron backscatter patterns are indexed on either a square or hexagonal grid to produce an orientation map. The hexagonal grid is useful for grain boundary reconstructions of the orientation map to determine appropriate number and length fractions of boundaries. The reconstructed boundaries are created by finding the triple junctions and connecting them with line segments that best outline the grain boundary shape [99]. For segments that deviate a certain number of pixels away, the reconstruction is broken up into several segments to best account for the grain boundary curvature.

The misorientation is found by considering the orientation on both sides of the boundary. This provides three of the five parameters necessary for defining a grain boundary [100]. The trace of the grain boundary in the 2D surface provides one component of the grain boundary normal. Without any information on inclination, the last parameter needed to complete the description of the grain boundary normal is determined stereologically [101]. The last grain boundary normal is the pole from a possible family of boundary planes. By observing several hundreds of similarly orientated bicrystals in the microstructure, it is assumed that the true pole should correspond to the largest population. The information obtained by studying the grain boundary character distribution (GBCD) is useful in determining the distribution of planes at or around a specific misorientation.

3.3 Near-Field High Energy X-ray Diffraction

Near field high energy x-ray diffraction (nf-HEDM) is a technique developed by a collaboration between the Department of Physics at Carnegie Mellon University and Argonne National Lab, and is performed at the 1-ID beamline source at the Advance Photon Source synchrotron [102]. This is relatively new technique and falls under the category of three-dimensional x-ray diffraction microscopy for obtaining information throughout a volume of a

polycrystalline microstructure. The nf-HEDM technique specifically uses high energy x-rays on the order 50-100 keV to penetrate the volume of the material [103].

The incident beam is focused to a planar beam and illuminates a planar slice of the specimen. Diffraction patterns are collected on a near CCD detector at three different distances to track the beams through space shown in Fig. 3.3. The specimen is rotated at one degree intervals to collect all possible diffraction patterns from the microstructure. The diffraction patterns obtained from this technique is shown in Fig. 3.4, where the spots correspond to the diffraction peaks of differently orientated grains in the volume. Hence multiple detector distances and the rotation are necessary to determine the spatial position of the given orientation in space.

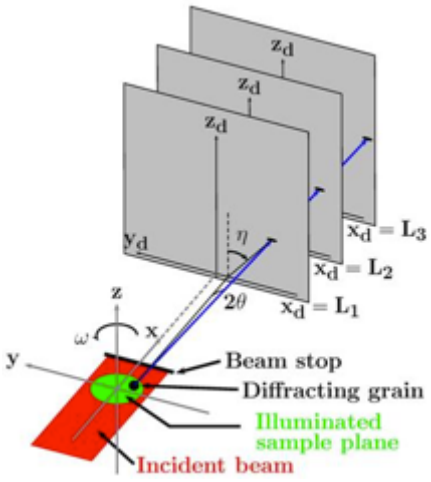

Figure 3.2. Monochromatic high energy x-rays are focused to form a line-focused beam roughly 1 -2 microns high and about 1.3mm wide (red). This beam illuminates a thin planar section of the sample (green). The diffraction spots from individual grains are imaged on a CCD detector; spots have the shape of the illuminated grain cross section projected onto the detector plane at the scattering angles 2θ and ϕ. Figure is reproduced from reference [103].

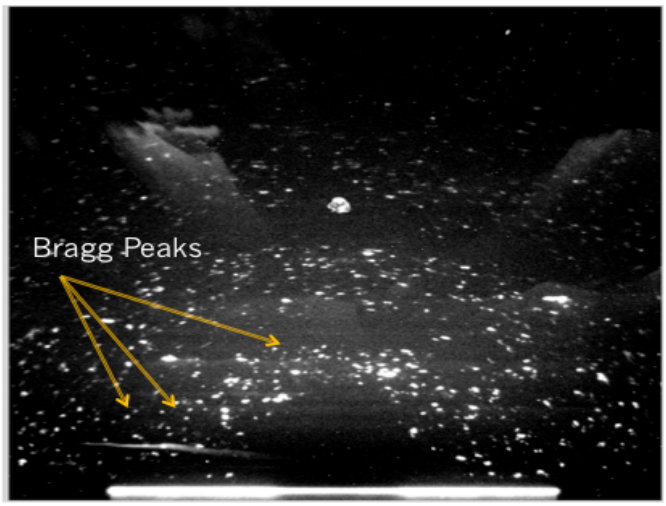

Figure 3.3. Example of captured diffraction peaks from the volume of the microstructure. Bright spots correspond to the Bragg peaks of differently oriented grains in the sample and must be fitted to determine the orientation and spatial location of each grain. Figure reproduced from reference [104]

After capturing all required diffraction patterns for a slice, the specimen is shifted along the z-axis to obtain additional slices each with their own diffraction pattern to capture the 3D details of the microstructure. The resolution of this technique depends on the CCD detectors, which currently provides 1 μm resolution in each x-y slice, and on the thickness of the focused planar beam, which currently provides a 4 μm resolution in the z-dimension.

The raw data is the stack of images containing the diffraction spots and a forward modeling technique is used to reconstruct the microstructure from this data [104]. This is achieved through running a simulation of the experiment and attempting to maximize the overlap of computed, expected diffraction pattern to the experimentally observed patterns as shown in Fig. 3.5. An optimization scheme is utilized to find the best possible match between the experimental peaks and simulated peaks to produce the orientation at the given point in a discrete triangular grid. The discrete triangular grid of each planes are realigned, and by matching similar orientations under a misorientation threshold the data reconstructed into the 3D microstructure.

Because this is a non-destructive technique, samples can be thermally or mechanically treated and the microstructural evolution can be observed [105][106][107][108].

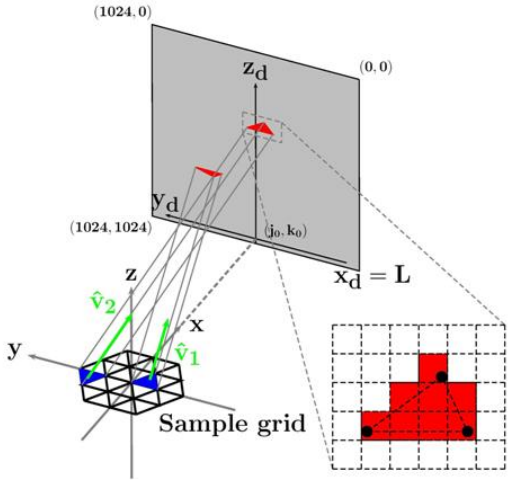

Figure 3.4. The crystallographic orientation in each voxel of the sample grid is adjusted to optimize the overlap of simulated Bragg scattering with the experimental data. Figure is reproduced from reference [103].

4 Annealing twin formation observed during recrystallization

4.1 Introduction

Annealing twin formation in polycrystalline nickel during recrystallization was studied by interrupted anneals over the same area observed by EBSD to monitor the recrystallization progress. Throughout the recrystallization process, the appearance of new twinned grains in the microstructure was identified in the recrystallizing regions of the microstructure. The various crystallographic features of the microstructure were investigated to understand their role on the observations of annealing twin formation. Here it was found that annealing twins nucleate at the recrystallizing interface on planes that are close to the {111} grain boundary plane.

4.2 Experimental Details

4.2.1 Sample Preparation

Cylindrical samples were sectioned using a low-speed saw from the high purity (99.999%) nickel rod (diameter 5 mm) of approximately 2 mm thickness. After homogenization, samples were cold-rolled to 25±0.5% reduction. The samples were mounted in epoxy, mechanically ground, and polished following the metallography procedures for mentioned in Section 3.1.

Crystal orientations of the surface in the rolling and traverse planes after deformation were measured by EBSD using an EDAX/TSL acquisition software with a Hikari EBSD detector on a Quanta 200 FEG SEM for ex-situ observations. Orientation maps with an area of 450 x 450 μm were acquired with a 1.5 μm step size. The samples were repeatedly annealed for 5 minutes at a time at 490°C in a flowing Ar/H_2 atmosphere tube furnace until full recrystallization was achieved at 40 minutes. The recrystallization progress was based on area partitioning by assigning grains as recrystallized if their grain orientation spread (GOS) was <= 1° [109][110]. Error bars for the recrystallized fraction were generated by considering a GOS <= 0.8 ° and <= 1.2 ° for the lower and upper bounds respectively. Further grain growth (although with minimal

change) was also achieved by annealing the samples at 10 minute intervals up to a total time of 60 minutes. The progress of recrystallization based on the grain orientation spread is shown in Fig. 4.1 as well as the change in the average grain diameter. Both the fraction recrystallized and the average grain diameter increased with annealing time.

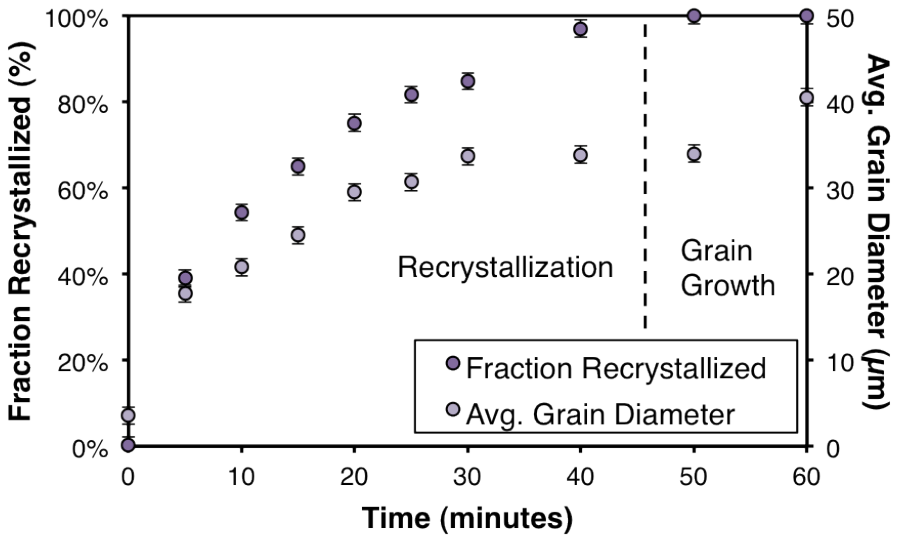

Figure 4.1. The fraction recrystallized with annealing time is shown on the left y-axis and the average grain diameter on the right y-axis . The fraction recrystallized increases with annealing time as does the average grain diameter. Based on the area fraction of grain exhibiting a GOS < 1°, complete recrystallization is taken to occur after 40 minutes, where the increase in the average grain diameter also changes behavior due to the change in driving force.

The microstructure evolution captured by EBSD is shown in the sequence of orientation maps shown in Fig. 4.2 The first column shows the change in the entire area. The second column shows the change in the microstructure based on the grain orientation spread, which reveals the recrystallizing regions. The third column in the microstructure is partitioned to include only grains with a GOS < 1°, showing the recrystallizing grains. The last column in the microstructure is partitioned with a GOS < 1° with twins excluded and colored by grain ID. This shows the recrystallizing nuclei that reveal the multiple twinning occurring during recrystallization.

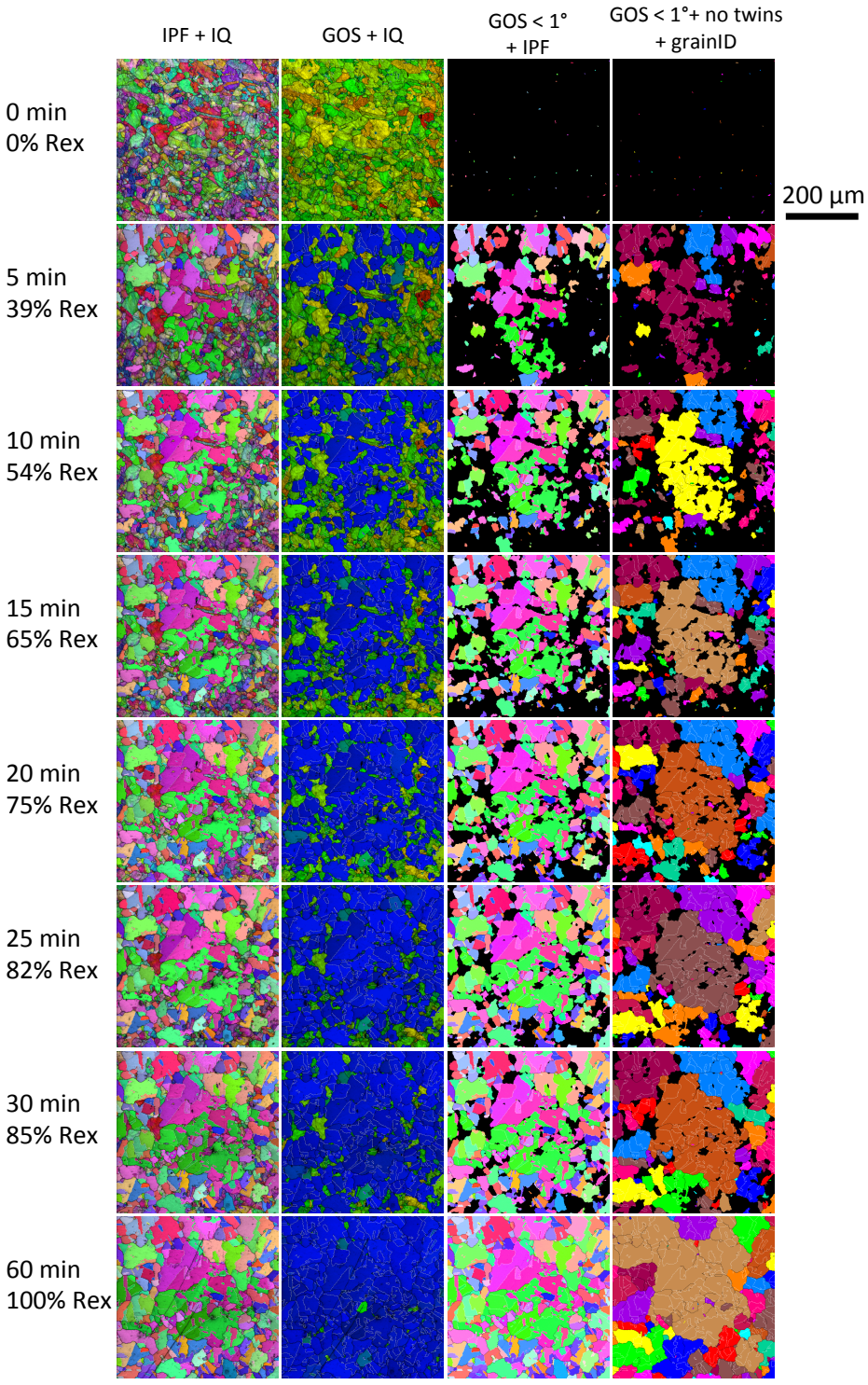

Figure 4.2. 450 x 450 µm EBSD maps capturing the microstructure evolution during annealing at 490 °C across time and fraction recrystallized down the columns, and in each row colored by the IPF and image quality, the GOS and image quality, the IPF of the recrystallizing grains, and the grain IDs identified when twins are excluded.

The number of features in the recrystallized region based on whether annealing twin boundaries are included or ignored was considered and the results are shown in Fig. 4.3. In the case where twin boundaries are included, the number of features corresponds to the number of grains with individual orientations different from its neighbors. The number of features increased steadily throughout the recrystallization process when these twinned grains are counted as individual features. However, when the annealing twin boundaries are excluded, essentially merging the twins and their respective parent recrystallizing nuclei as shown in Fig. 4.2, the total number of features was relatively constant with recrystallization. This indicated that there are a limited number of recrystallizing nuclei that are formed in the deformed matrix [111] and as the growing grains increase in size, they twin. The average number of twins per grain, N_G, was calculated from Eq. 4.1 [80] where the definition of the parameters N_1 refers to the number of features without considering twin boundaries and N_2 is the number of features by considering twin boundaries. The average number of twins per grain exhibited a relatively linear increase with recrystallization, as shown on the left axis in Fig. 4.3. From the observed starting microstructure to the final recrystallized microstructure, the number of twins per grain increase from approximately three to six.

$$N_G = \frac{N_2 - N_1}{N_1} \qquad \text{Eq.4.1}$$

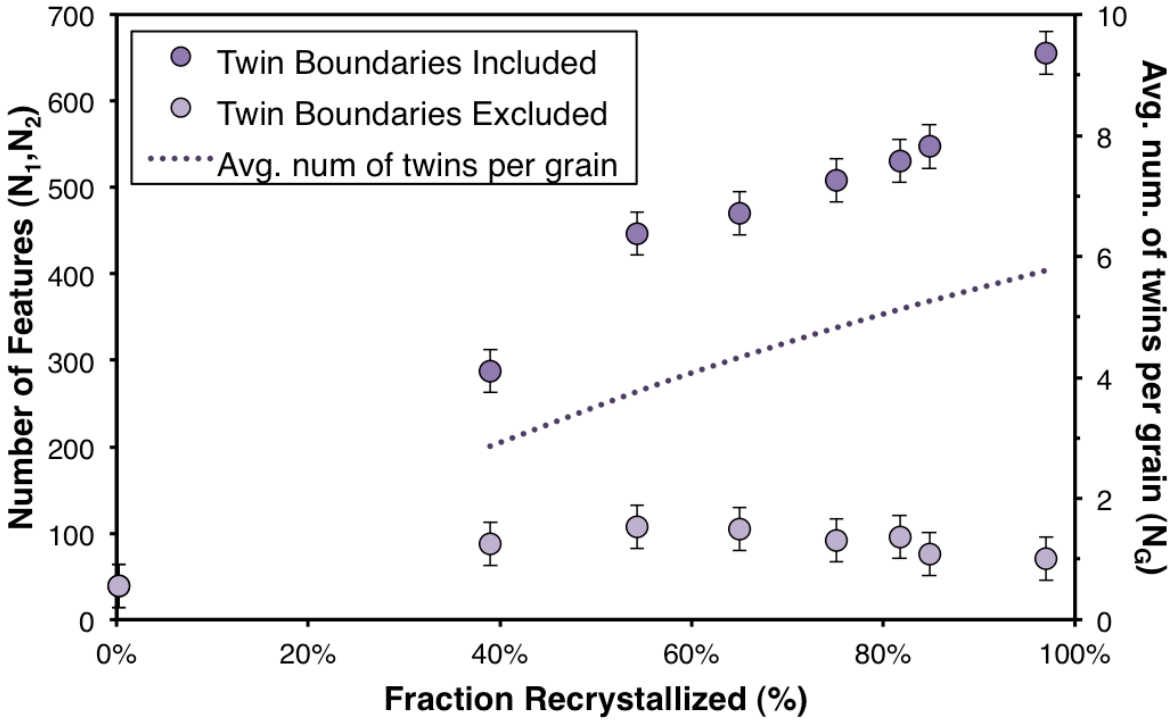

Figure 4.3. Number of grains within the area of interest observed when twins are considered as individual grains and merged to a parent grain on the left y-axis, along with the average number of twins per grain (referenced to the left y-axis).

The twin density, N_L, has been calculated by the Eq. 4.2, presented by Jin *et al.* [Jin 2013], where L_{tb} refers the twin boundary length in a given sample section area, S., The twin density increased with recrystallization from approximately 10 to 50 mm^{-1} as shown in Fig 4.4. and agrees with the similar ex-situ heat treatment experiment performed [85]. The increase in twin density with the fraction recrystallized emphasizes the earlier point that as grains grow during recrystallization, annealing twins are formed, consistent with the increase in the number of twins per grain observed in Fig. 4.2. The question to be answered is where?

$$N_L = \frac{L_{tb}}{S} \times \frac{2}{\pi} \qquad \text{Eq 4.2}$$

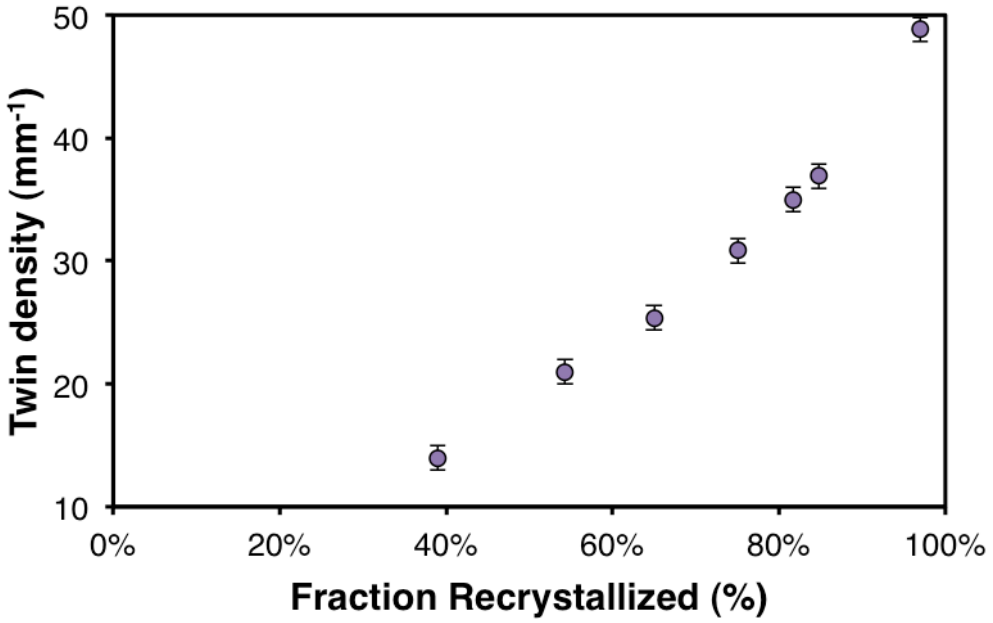

Figure 4.4. Average twin density with the fraction of material recrystallized shows an approximately linear increase with fraction recrystallized.

4.3 Results

4.3.1 Evolution of grain boundary character during recrystallization

The change in the twin boundary length fraction with recrystallization is presented in Fig. 4.5a. Special boundaries, which include twin and high order twin-related boundaries [112], have also been shown on the plot. The length fraction, unsurprisingly, increases over time as new twins are introduced into the system with annealing. However, when only the recrystallized partition of microstructure is considered, then the observed behavior changes drastically as shown in Fig. 4.5b. The recrystallized partition only takes into account the boundaries within recrystallized grains and excludes the interface between the recrystallization front and the deformed matrix. The twin boundaries accounts for the majority of the boundaries in the recrystallized partition. The gradual decrease with the recrystallization process arises from the recrystallizing nuclei

impinging on one another and forming (general) high angle grain boundaries. The independent behavior of the entire microstructure compared to just the recrystallizing partition therefore suggests all the newly formed annealing twins occur on the recrystallizing interface.

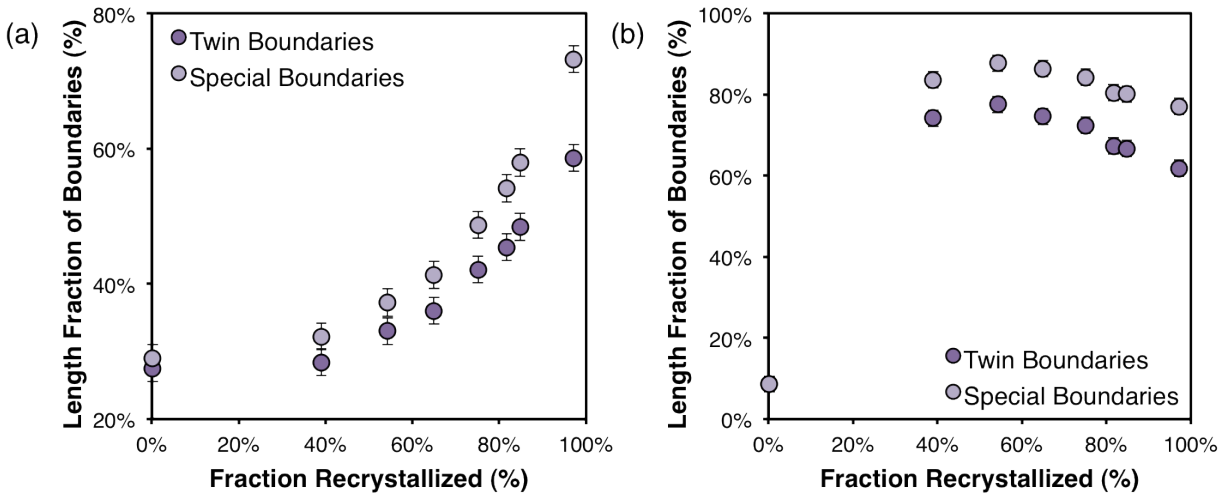

Figure 4.5. Fraction of twin boundaries and special boundaries in the entire area observed as a function of fraction recrystallized in (a), and fraction of twin boundaries and special boundaries in the recrystallized microstructure (not considering the recrystallizing interface) as a function of fraction recrystallized in (b). When considering the entire microstructure the overall length fraction of twins increases but within the recrystallization partition, it is constant.

The trend for the length fraction of special boundaries tracks that of the twin boundaries, which suggests that the twin boundaries accounts for the majority of the special boundaries' behavior. More discussion of the other special boundaries such as the Σ9 and Σ27 and the development in the interconnectivity of the grain boundary network can be found in Appendix 11A.

Furthermore the length fraction of coherent to incoherent twin boundaries over a single recrystallization process was measured and the results are plotted in Fig. 4.6. The coherency is determined by how close the trace of the grain boundary lies to the {111} in the two crystals. Overall there is always a higher length fraction of coherent boundaries than incoherent

boundaries. The ratio of coherent to incoherent twin boundaries shows that during annealing, there are more incoherent boundaries being generated over time.

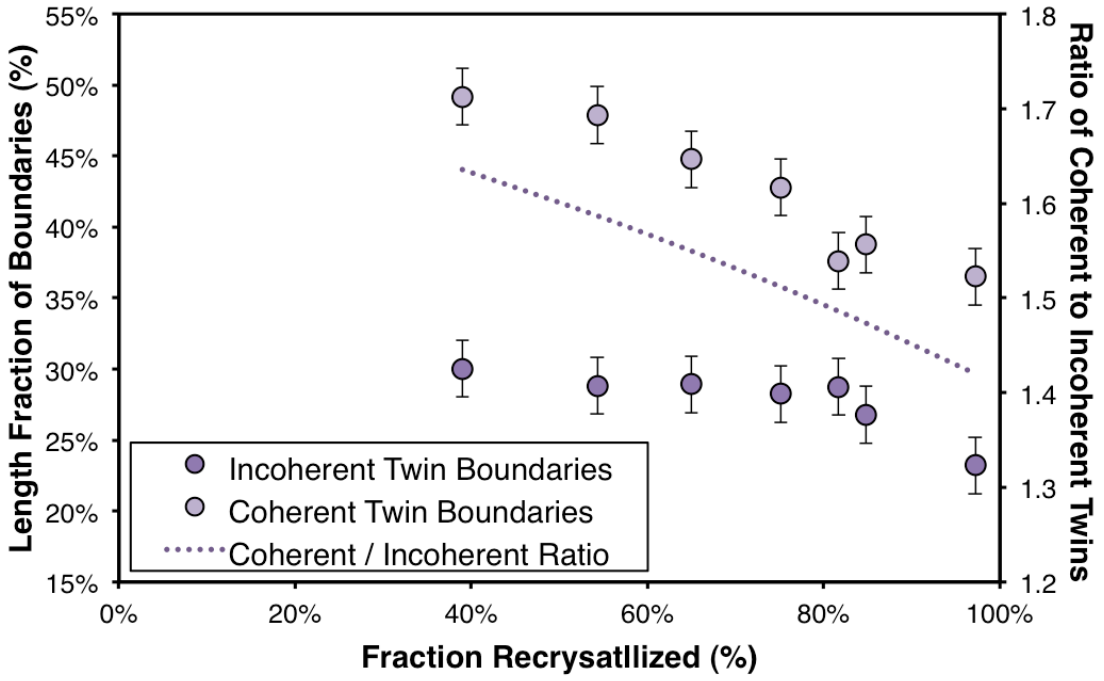

Figure 4.6. The length fraction of coherent and incoherent twin boundaries during recrystallization is shown on the right y-axis. In the left y-axis the ratio of coherent to incoherent twin boundaries is presented, which shows a slight decrease with recrystallization although the length fraction of coherent boundaries is still greater.

The discrepancy between looking at the entire microstructure and the recrystallized fraction motivated examination of the characteristics of the recrystallization interface. The recrystallizing grains are nearly random and show no strong texture component. The 1D misorientation distribution, Fig. 4.7, shows that the overall interface is close to random, but exhibits a slight excess of high angle grain boundaries. The high angle grain boundaries are mostly scatter but can also be high mobility boundaries that are necessary for the growth of grains during recrystallization. The length fraction of twin boundaries are significantly less than the 20-30% usually observed in FCC Ni, but this does not contradict the previous statements.

The twin boundaries are formed at the interface, but are deposited into the recrystallized volume. Therefore, the twin boundaries are connected to the recrystallization front, but not a part of it more than would be expect in a random distribution.

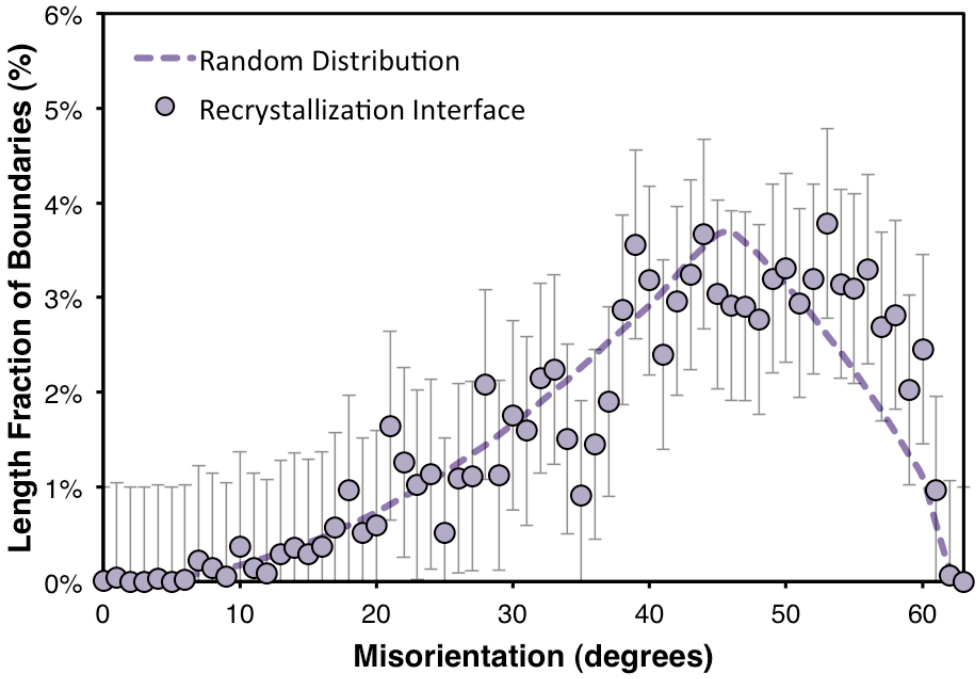

Figure 4.7. The grain boundary misorientation profile of the recrystallization interface is close to a random distribution [Mackenzie] although with an excess of high angle grain boundaries; this reflects the need for growing grains to have high mobility (and thus high angle) boundaries on their surfaces and the twins generated during recrystallization are deposited in the recrystallized volume.

The two-parameter grain boundary plane distribution, which characterizes the grain boundary inclination of all grain boundaries across entire recrystallization front population in the crystal reference frame, showed an interface with a weak bias for {111}, see Fig. 4.8, with a maximum MRD value of 1.25. The region around the (111) is also relatively diffuse based on the MRD values. This was calculated by using a stereological approximation of the reconstructed boundary, as detailed by Kim *et al.* [113], of a recrystallization front that included over 6000 line segments. The peak at (111) is best explained by the {111} being lowest energy plane (based on

the Wulff shape of FCC crystals) and typically shows the highest population as well in FCC metals [35]. Additionally, the {111} plane is also the coherent twin plane. Therefore having a high population of {111} may assist in the formation of annealing twin boundaries. The EBSD observations of these annealing twin formation events are presented in the following section.

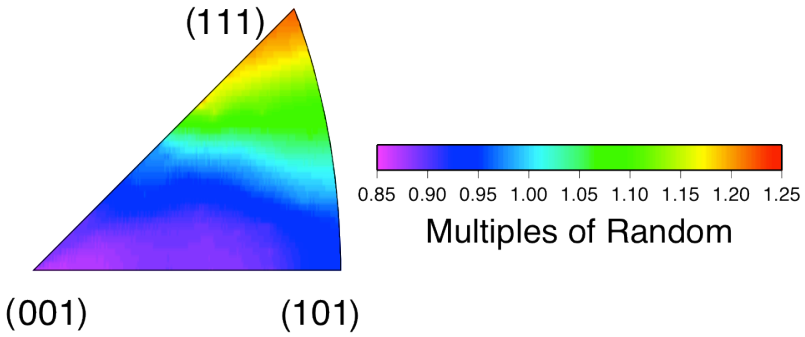

Figure 4.8. Grain boundary plane distribution of the recrystallization interface during annealing shows a peak at {111} with a maximum MRD value of 1.25.

4.3.2 Local observations of annealing twin formation during recrystallization

Twins appeared in the microstructure and occurred on the migrating recrystallizing interfaces, as shown in the sequence of images in Fig. 4.9. In this case, the first twin boundary nucleates and a second twin boundary occurs later to form the twinned grain replacing the deformed region of the microstructure. It was never observed that an annealing twin formed in an already existing region of the recrystallized microstructure. There are however, three apparent mechanisms that lead to the increase of annealing twin boundaries in the microstructure. The first is simply repeated twin formation events trailing the recrystallizing interface as discussed. This type of annealing twin formation was the most frequently observed throughout recrystallization.

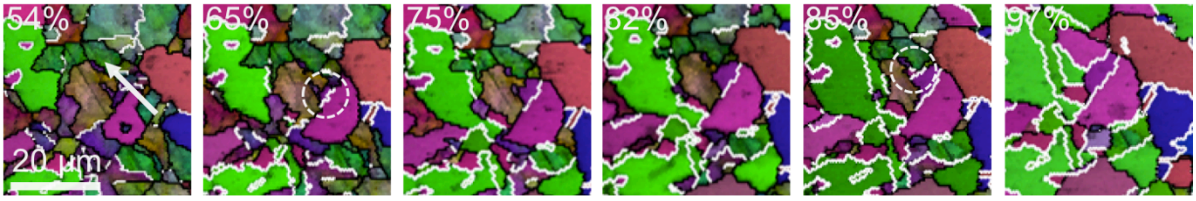

Figure 4.9. The migrating recrystallization front of the purple recrystallizing grain is indicated by the arrow in the first EBSD snapshot. In the next frame, an annealing twin boundary is formed, circled, and later a second twin boundary is formed, again circled. The area fraction recrystallization is shown in the top left corner of each EBSD map.

After formation, annealing twins also increase in size by propagation along the recrystallizing interface. This is clearly observed in the sequence of images presented in Fig. 4.10, where the annealing twin boundary and original parent grain both continue to extend into the deformed matrix. Twin boundaries also form when two spatially separated, twin-related, recrystallizing nuclei grow and impinge on one another shown in Fig 4.11. Given the coherent nature of these twin boundaries and that both grains are ultimately part of a larger twin cluster, it is likely that this twin nucleation event occurred in the bulk of the material and grew towards the surface. As such, this is simply just a more complicated and disjoined process of the second mechanism observed of annealing twin boundary elongation rather than a growth encounter event [25].

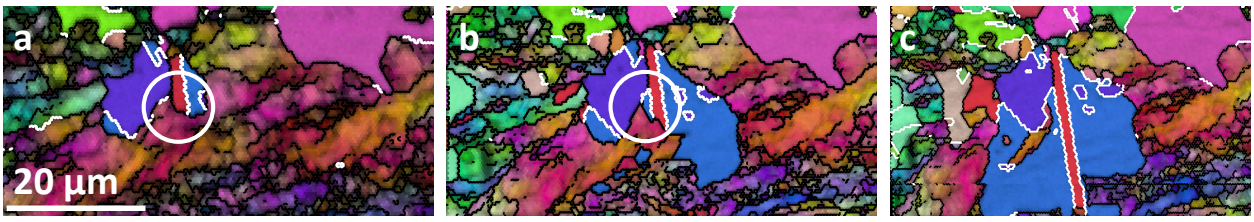

Figure 4.10. The formation of a new twin boundary is observed in the circled region from the EBSD images (a) to (b). The length fraction of the twin boundary increases through rapid elongation of the twin in (b) to (c).

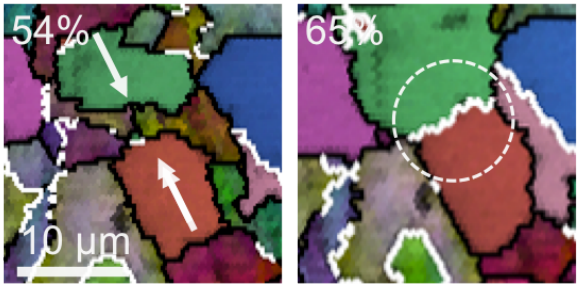

Figure 4.11. In the sequence of EBSD images, the impingement of two spatially separated, twin-related recrystallizing grains growing towards each other, designated by the arrows, result in the formation of a twin boundary, circled. This arises from the elongation of a twin boundary that nucleated in the bulk of the sample, below the section plane.

Within the underlying deformed matrix, no distinct behavior was observed as to when an annealing twin would form. The first new recrystallizing grains typically appeared in the regions of highest deformation, based on GOS, as observed in the sequence of images in Fig. 4.2. The formation of annealing twins occured later, in regions of varying GOS. However, the twin may be forming at a higher deformation region underneath the surface, which is not detectable. Similarly, there do not appear to be microstructure features that specifically promote annealing twin formation. That is, annealing twins do not seem to be forming at prior deformed grain boundaries and triple lines, or the sub-grain structure from the prior plastic deformation, although the latter may require higher resolution to resolve. The lack of correlation could again be due to 2D surface observation that does not capture the true 3D evolution behavior.

4.3.3 Conditions for annealing twin nucleation from recrystallizing interfaces

Twin formation events as identified from the previous section were further analyzed to understand if specific conditions resulted in their formation. The first was a comparison of the migration direction relative to the twin plane. Here an assumption was made that annealing twin formation events does not alter the migration directions of recrystallizing nuclei.

For any coherent annealing twin segment that forms behind the recrystallization growth front, the trace is assumed to be the direction of the {111}. The direction of the grain boundary migration is taken to be the apex point of the convex boundary front from the twin plane trace. The deviation angle is calculated based on the angle between the two vectors as shown in Fig. 4.12. This is a 2D approximation of an event occurring in 3D. Furthermore the underlying assumption here is that the annealing twin formation event does not change the migration behavior of the original grain.

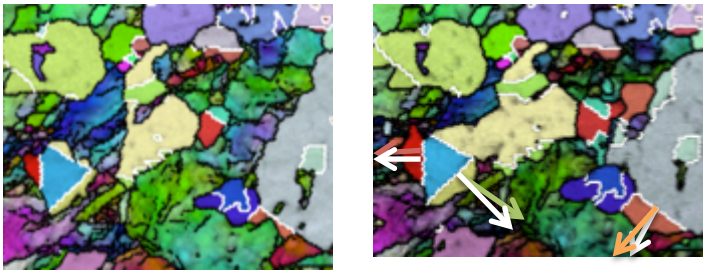

Figure 4.12. EBSD maps showing a selected area between annealing intervals of 5 minutes. The growths of two recrystallizing nuclei are identified in this series and the migration of three portions of recrystallization fronts that have a twin boundary behind them are indicated. The white arrows indicate the approximate direction of the twin plane and the colored arrows the approximate migrating direction.

The result from over 50 recrystallizing interfaces in nickel (at various annealing times) is plotted in the bar chart shown in Fig 4.13. The orientation of the majority of the migrating interfaces that exhibit an annealing twin formation event are within 10° of <111>. This implies that annealing twins form from migrating {111} planes during recrystallization. Qualitatively, the observed frequency is also greater the grain boundary plane distribution obtained from stereology, shown in Fig. 4.8. As a rough estimate, the number of counts in the < 10° fraction is almost twice of that in the 11-20° fraction bin versus the maximum 1.25 MRD peak measured at the (111).

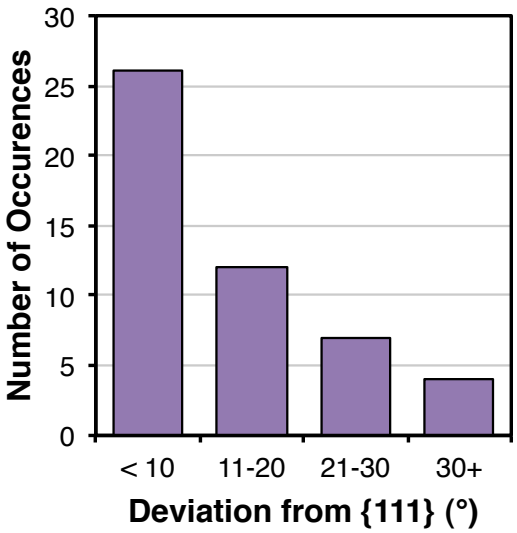

Figure 4.13. Number of occurrences binned by the angle between the observed grain boundary migrations after an annealing twin formation and the {111} twin plane behind the migration front. Formation events mostly belong to the < 10° bin, suggesting that annealing twins nucleate when the recrystallization front is closest to a {111} plane.

Secondly, the evidence indicates annealing twin formation is an event that depends on the migration of the grain boundary [82][83]. As such, the average grain boundary velocity behavior, grain area swept, and change in grain boundary length were examined in the microstructure. The overall grain boundary velocity, taken as the change the average grain size during recrystallization with time, shown in Fig. 4.14a, exhibits a parabolic behavior consistent with other reports [114]. However, the change in annealing twin content, which is found by extracting the change in the number of new twins from Fig. 4.3, as a function of velocity is essentially a scatter plot, Fig. 4.14b.

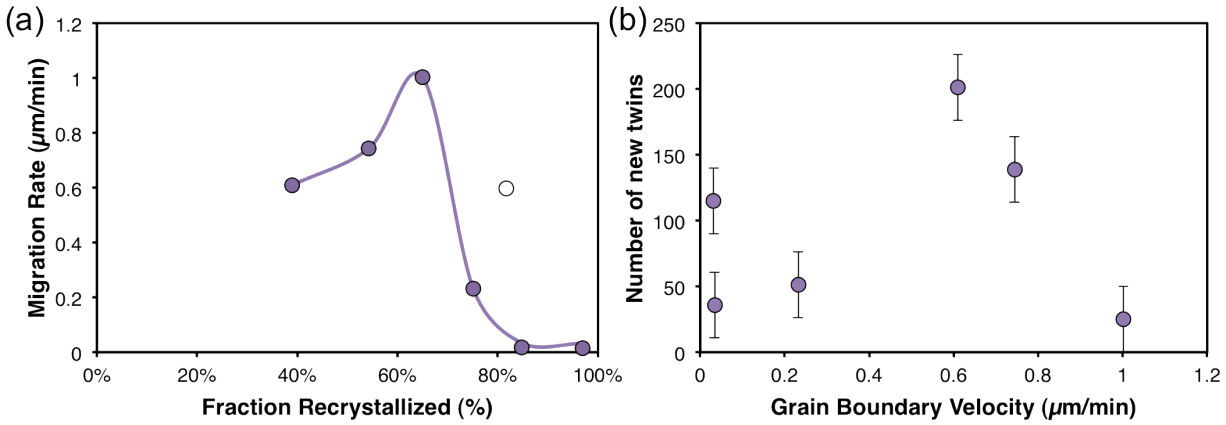

Figure 4.14. The average migration rate of grain boundaries against recrystallization is shown in (a) with a line showing the trend with the fraction recrystallized. The number of new twins against the grain boundary velocity is shown in (b), which reveals a large scatter. This suggests that the twin formation rate does not depend on the boundary velocity.

The change in grain area is calculated from the change in the average grain area during recrystallization in only the recrystallized fraction of material and is shown in Fig 4.15a. While grain boundary area swept exhibited a linear increase with time, it also does not correlate well with the number of new twins introduced into the microstructure, as shown in Fig. 4.15b. The increase in grain area does indeed lead to the formation of new twins in agreement with the previous statements that new twins are introduced in the recrystallization volume as the front migrates into the deformed matrix. However this relationship is not linear nor clear.

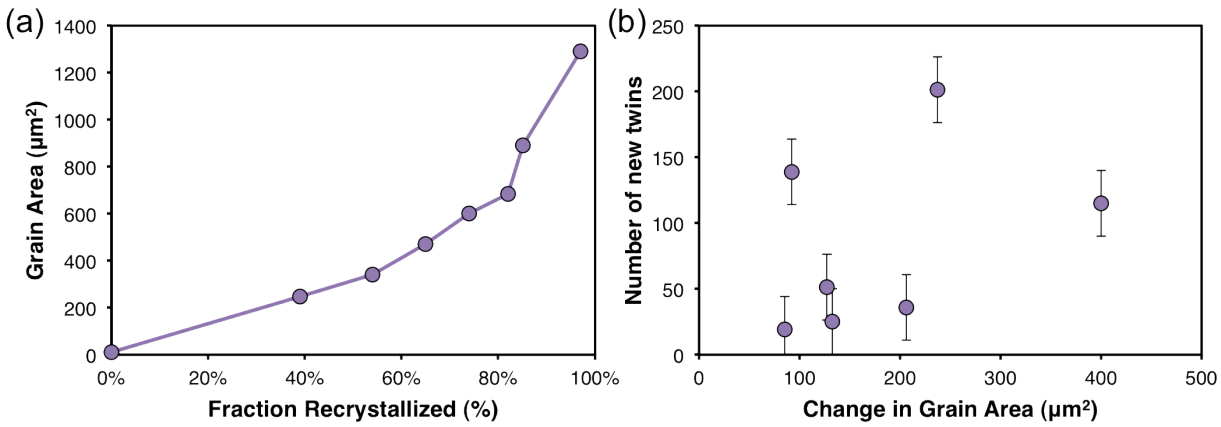

Figure 4.15. (a)The average grain area as a function of recrystallization where the grain area increases with the fraction recrystallized. (b) The number of new twins versus the change in grain area shows no strong correlation between the two variables.

The last investigated microstructure property was the change in the length per unit area of the recrystallizing interface. The change in specific length varies with recrystallization fraction similarly to the velocity, where at the start it increases, but past 50 % recrystallization begins to decrease as observed in Fig 4.16a. By using the absolute change in grain boundary length, a reasonable correlation between the number of new twins and change in interface length is observed. An increasing change in grain boundary length correlates to an increase in the number of new twinned grains introduced into the microstructure as shown in Fig. 4.16b. Or, expressed another way, the rate of formation of twins is proportional to the area of the recrystallization front.

While the recrystallized length front and average recrystallized grain area should be both related, this is only in the case of isolated, growing nuclei. As the growing nuclei impinge, the relationship between area to the length is lost then. Furthermore, the stronger correlation to length emphasizes that it is the number of planes that across the recrystallization front that are important.

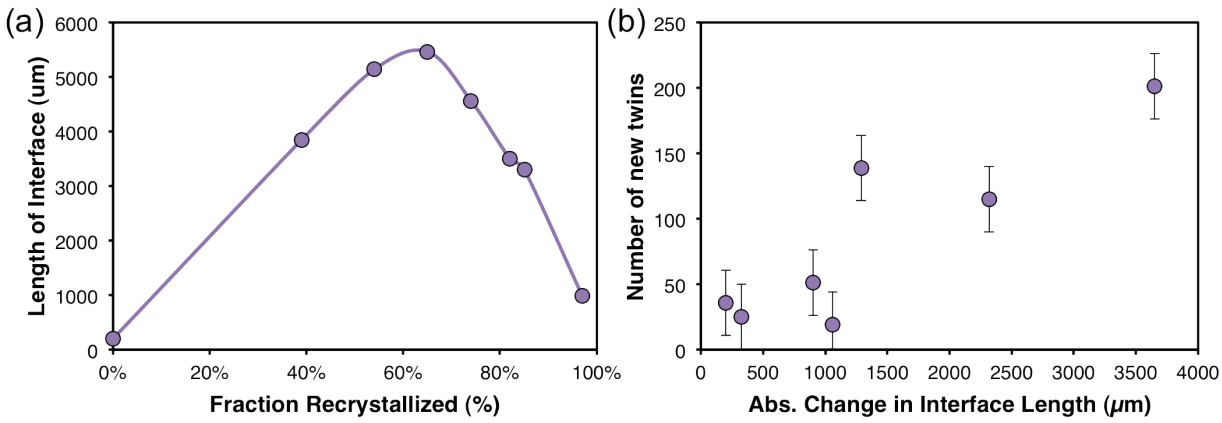

Figure 4.16. (a) The length of the recrystallized interface with fraction recrystallized with a line to show the increase then decrease with the recrystallization fraction. (b) The number of new twins increases as a function of the absolute change in grain boundary length.

4.4 Discussion

Based on the evidence presented, we conclude that annealing twins form on migrating {111} planes. Not only are there more {111} planes than other planes at the recrystallizing interface, as shown in Fig. 4.8, but these {111} planes are selectively chosen for annealing twin formation based on histogram in Fig. 4.13. Previous models had simply suggested that twins nucleate on {111} ledges [22]. Here we have shown that there is a strong correlation with the formation of a twin boundary with respect to the inclination of the boundary based on a stereological analysis. To further reinforce this, an additional, albeit weaker correlation was found between the absolute change in grain boundary length and the number of new twins introduced into the microstructure. This suggests that annealing twin formation is dependent on the number of planes close to the {111} available in the microstructure at a given time.

This agrees with the trends observed for increasing prior strain resulting in increasing twin density [79][80]. The increased deformation would increase the number of recrystallizing nuclei. Assuming a spherical nucleus, then each nucleus would have all possible {111} planes to

generate an annealing twin. Similarly, because the number of possible {111} planes is dependent on the number of nuclei, then temperature, which does not alter the number of recrystallizing nuclei in a given volume [111], has no effect on the twin content in the microstructure.

This conclusion is also in agreement with tortuosity measurements made on the recrystallizing interface by Jin *et al.* [79], where it was proposed that increasing the tortuosity provided additional {111} planes on the recrystallization front for twinning. Although at first this seems contradictory, with our suggestion that flat, recrystallizing {111} grain boundary surfaces are responsible for. However, for a front close to {111}, increasing tortuosity provides additional sites on the recrystallization front where an annealing twin can nucleate, as previously shown in Fig. 2.13.

The observed bias of forming twins on boundaries with the {111} orientated recrystallization front provides support for the growth accident model [22] over what is presented by Mahajan *et al.* [70]. The fact that the entire interface is {111} also means that there are a number of nucleation sites for the formation of a twin across the entire plane. If nucleation sites are not generated on the exactly the same plane however, then incoherent segments are formed to join the twin nuclei as shown in Fig. 4.17a-b. Additionally if the nature of the growth front is uneven, possibly due to residual orientation gradients, then incoherent segments can be generated if the new twinned grain does not have a higher velocity than the original parent grain shown in Fig. 4.18a-b.

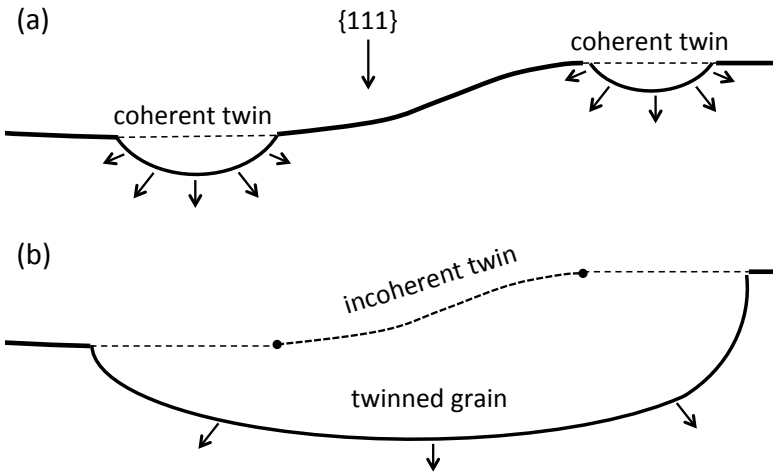

Figure 4.17. Schematic for annealing twin formation resulting in incoherent segments from the generation of multiple twin nuclei across the recrystallizing interface. Two independent nuclei of the same twin variant are formed at the interface in (a). In (b), if the nuclei grow and join together, the original recrystallizing interface can result in an incoherent twin boundary.

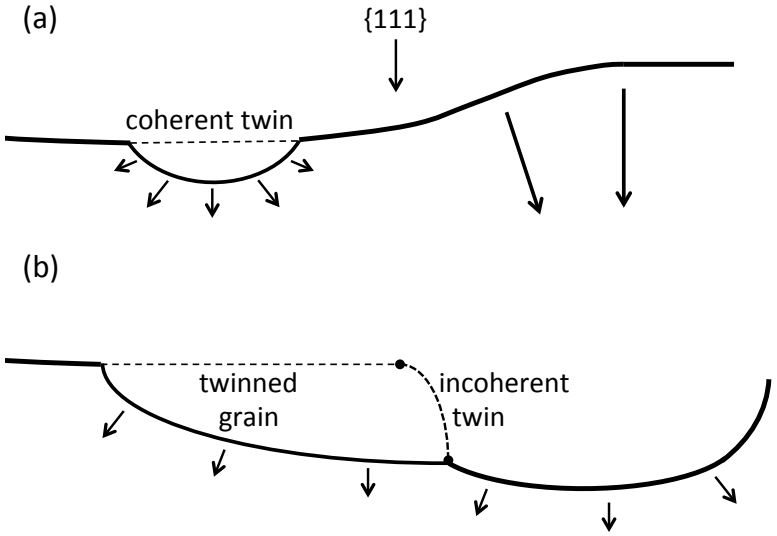

Figure 4.18. Schematic for the generation of incoherent twin boundaries in the recrystallizing volume resulting from uneven migration rates on the recrystallization front. In (a) the formation of a twin occurs on the recrystallizing interface on a plane close to the {111}. In (b) the twin continues to grow into the deformed region, but so does the original grain as a faster rate than the twin, creating an incoherent twin boundary despite starting as a coherent twin boundary.

The formation of other special boundaries, such as Σ9s, can come about from intersecting twin boundaries that arise from independent annealing twin formation events on different {111} planes of the recrystallizing grain. The evolution of a Σ9 from two separate annealing twin events can be visualized by the sequence of Fig. 4.19a-b.

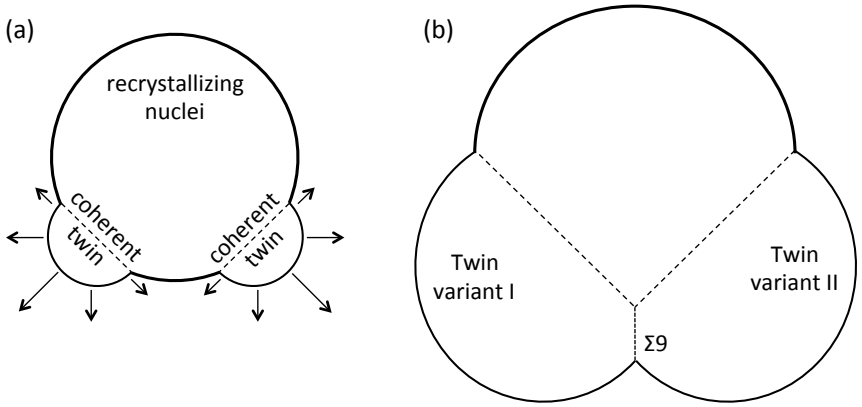

Figure 4.19. Schematic for two independent annealing twin formation events that results in the formation of a Σ9 boundary. In (a), the two different {111} planes of the recrystallizing nuclei are selected for nucleation and consequently leave the twin boundary behind. As these twins grow, shown in (b), the twin boundaries of the two twin variants are extended and the geometric constraints at the triple junction between the two results in a Σ9 relationship.

4.5 Summary

From the interval annealing recrystallization experiment, the change in the concentration of annealing twins with recrystallized fraction was studied. It was determined that annealing twins form primarily during recrystallization, and in particular form on the recrystallizing interface. On the recrystallizing interface, twins form on interfaces that are close to a {111} plane and the formation correlates well to the length of grain boundary available.

5 Annealing twin formation selection during recrystallization

From the interval heating experiments, we observe that annealing twins form primarily during recrystallization. At times we also see that multiple twin variants are introduced during recrystallization that are responsible for the development of other special boundaries. In this chapter we investigate the connectivity of these twin-related grains after recrystallization and undergone a small amount of grain growth in a 3D microstructure. The data is obtained by a novel technique known as near-field high energy x-ray diffraction to monitor the microstructure evolution of Ni annealed at 800°C over several anneals. The concept of twin-related domains is introduced in this chapter and an analysis of the twin variant selection in twin-related domains is investigated.

5.1 Experimental Details

5.1.1 Near-Field High Energy X-ray Diffraction

C.M. Hefferan prepared the sample, collected the data, and reconstructed the microstructure using methods detailed in his thesis [115]. A short summary is provided here. A 1 mm diameter high purity (99.999 %) nickel wire was obtained from Alfa Aesar. The initial sample was first homogenized for two hours at 750 °C to obtain a reasonable grain size for the nf-HEDM characterization. The same volume of microstructure was characterized in multiple anneals at 800°C in a 3 % H_2 / 97 % N_2 environment detailed in Table 5.1. While a total of five microstructure states were collected, only anneal states 1, 2, and 3 are analyzed in this and the following Chapter.

Table 5.1. Annealing conditions of nf-HEDM Ni grain growth experiment

State	Time (min)	Temperature	Environment	Z-Layers
1	23	800°C	97% N_2, 3% H_2	70
2	30			89
3	25			86

The reconstructed and cleaned microstructures, provided by Hefferan, are on a rectilinear grid where the final resolution of each microstructure was 600 by 600 voxels and by the number of z layers for each anneal state. Each voxel had a dimension of 2 μm by 2 μm by 4 μm. The data

was not meshed and smoothed, and the discrete microstructure images of the same observed volume are shown in Fig. 5.1.

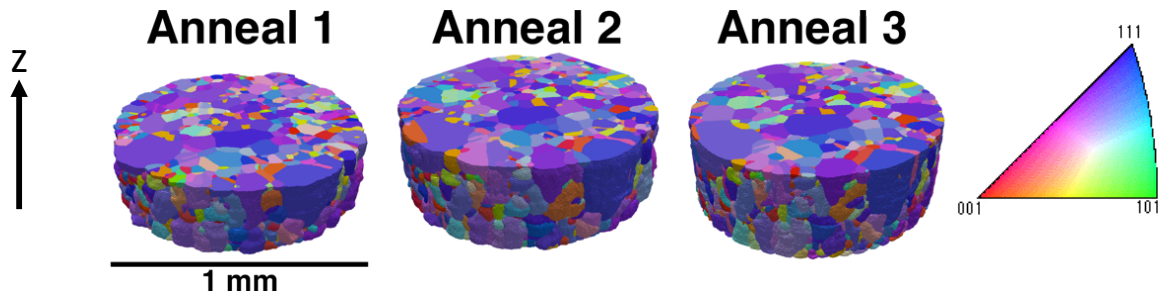

Figure 5.1. Reconstructions of the 3D microstructure colored by IPFz (where the z-axis points up) showing some texture. Although the volume at each time step differs (with the objective of bracketing the first volume measured), qualitative differences appear between anneals as a result of grain growth.

5.1.2 HEDM Ni Microstructure Statistics

Between the three microstructure states, the average grain size increases from 68 to 72 μm, as shown in Fig. 5.2. Similarly, by considering the number of grains per unit volume, the change is "small", thus indicating that grain growth has occurred, but not so much that most of the features from previous anneals are lost. Also the overall texture, which has weak fibers with {100} and {111} // ND, consistent with wire drawing, is unchanged with annealing. This texture is reflected in the IPFz microstructure images shown previously in Fig. 5.1.

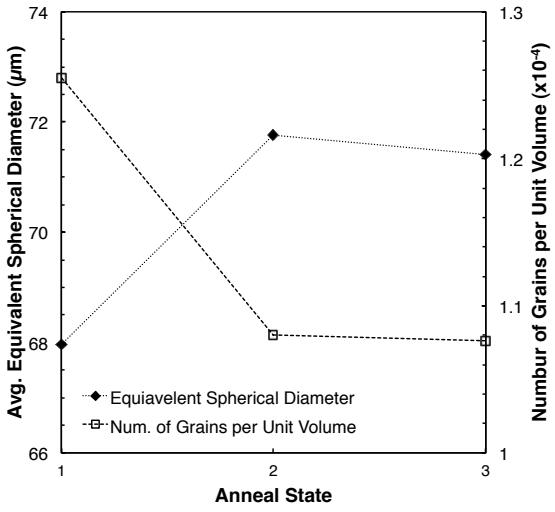

Figure 5.2. Change in average grain diameter and number of grains per unit volume. Although the change in diameter fluctuates as a result of the reconstruction, the number of grains per unit volume decreases as expected.

The misorientation distribution is shown in Fig. 5.3 where the overall behavior follows a random distribution with the exception of the peak at 60° indicating the presence of twin boundaries in the material and 39° from the presence of twin-related (i.e. Σ9) boundaries. The lower length fraction of twins (between 25-30 %) observed here is consistent with typical values found in Ni [87][88], where as the previous microstructure shown in Chapter 4 reflects values found in GBE Ni that have a length fraction of twins typically over 50 %. For the overall misorientation distribution, there is little change with annealing, except for a minor increase at the 60° peak and decrease at 39°.

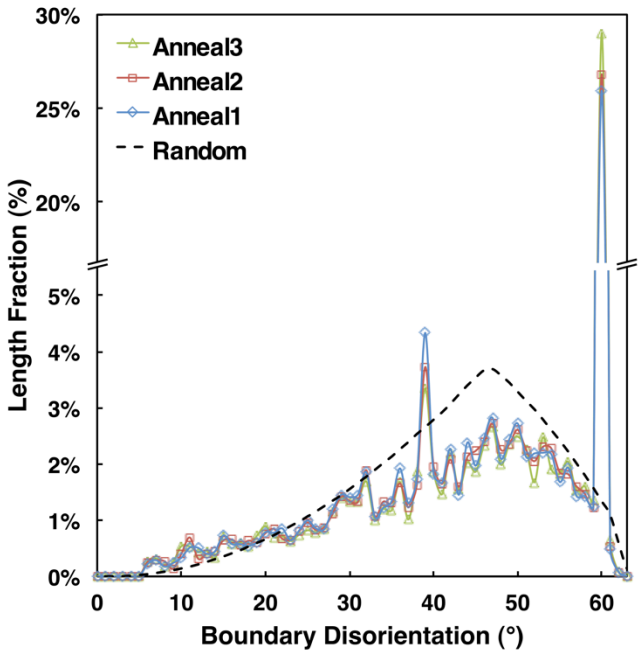

Figure 5.3. The misorientation distribution shows little change with annealing except for a slight increase at 60° which is presumably due to the preferential elimination of HAGBs in favor of low energy boundaries such as twins.

5.1.3 Definition of a twin-related domain

Twin-related grains were classified into twin-related domains (TRDs). The twin-related domain is a measure of the twin connectivity by counting the number of neighboring grains that share a twin misorientation relationship with one another [116]. This has often been used as a 2D analysis of grain boundary engineered microstructures to evaluate the degree of twinning [117], where longer twin-related domains correspond to improved integranular properties [118][119].

To avoid confusion, the number of "grains" in a TRD will be referred to as the number of "crystallites". One may interpret these as chains or clusters of crystallites misoriented by the twin relation. The assumption made here is that every new crystallite in a TRD is a result of a single annealing twin formation mechanism such as a growth accident [22]. The importance of analyzing a 3D microstructure is shown in Fig. 5.4. The cross sectional slices in 2D, shown in

Fig. 5.4b, may overestimate the number of crystallites in the TRD in comparison to 3D configuration of grains in Fig. 5.4a. In this specific example, from the 3D analysis we only have two twin-related features, but from the 2D cross sectional slice through the middle suggests that there are four, which are actually just different sections of the same two twins. Therefore a 3D microstructure is necessary to resolve this discrepancy and quantify the TRD structures.

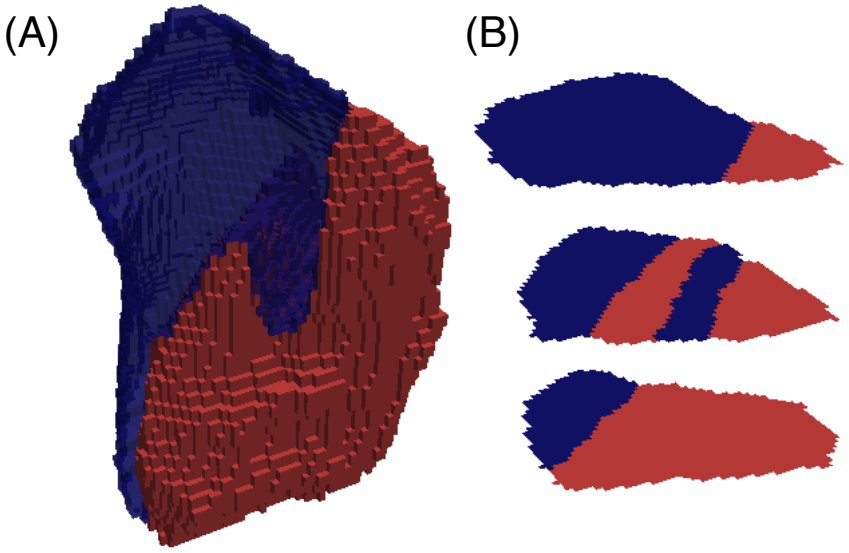

Figure 5.4. 3D observation of (a) two twin-related grains, but when only observing a 2D cross section of the grains in (b), there is a discrepancy in the number of twins that would be identified. Colors are arbitrary.

A TRD of two refers to two crystallites that are twin-related, which in terms of morphology is often the edge twin [120] such as that shown in Fig. 5.5a. Moving up the scale, TRDs of size 3 then may refer to complete lamellar twins [120] that bisect the parent grain thereby generating three different features like shown in Fig. 5.5b, but also a parent grain with two different twin-related crystallites shown in Fig, 5.5c (which have a Σ9 misorientation relationship between them).

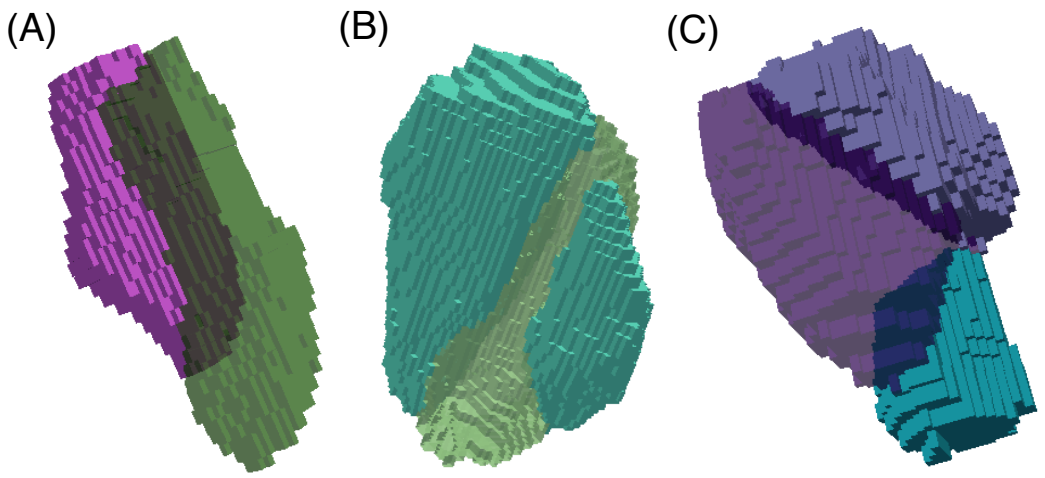

Figure 5.5. 3D observations of a (a) twin-related domain of size 2 show an edge-pair relationship, (b) a twin-related domain of size three showing a lamellar relationship, and (c) a TRD of size 3 of two different twin variants with respect to the transparent, purple grain in the middle. Colors are based on a Rodrigues-Frank orientation coloring scheme.

For analysis of the twin-related domains, only twin misorientation relationships, 60°<111>, within a 2° tolerance are considered. This is due to the high angular resolution of the nf-HEDM technique, which leads to a high degree of certainty in the calculated misorientation. Moreover using the Brandon Criterion (8.66°) resulted in much larger TRD sizes as a result of random grain encounters [25]. Due to the lack of meshing, there was no constraint placed on the grain boundary normal.

5.2 Results

5.2.1 Twin-related domain distributions

Converting the number of grains to twin-related domains reduced the number of features from more than 2200 grains to just approximately 400 twin-related domains. Approximately 80 % of all the grains in the initial state have a twin-related neighbor. The majority of TRDs across

anneal states consisted of single digit domain sizes shown by the distributions in Fig. 5.6a. For the given resolution and clean-up applied, the largest TRD was found to consist of 20 crystallites. Across anneals, there are increases and decreases in the relative percentage of each TRD population as observed in Fig. 5.6b, where no obvious trends are apparent. The TRD populations vary slightly because of the observed volume increases between each anneal (in order to ensure that the original volume is fully contained with each subsequent one), which can account for some of the increases. However it was also directly observed that TRDs could increase in size by forming a new crystallite, which is the focus of the next chapter.

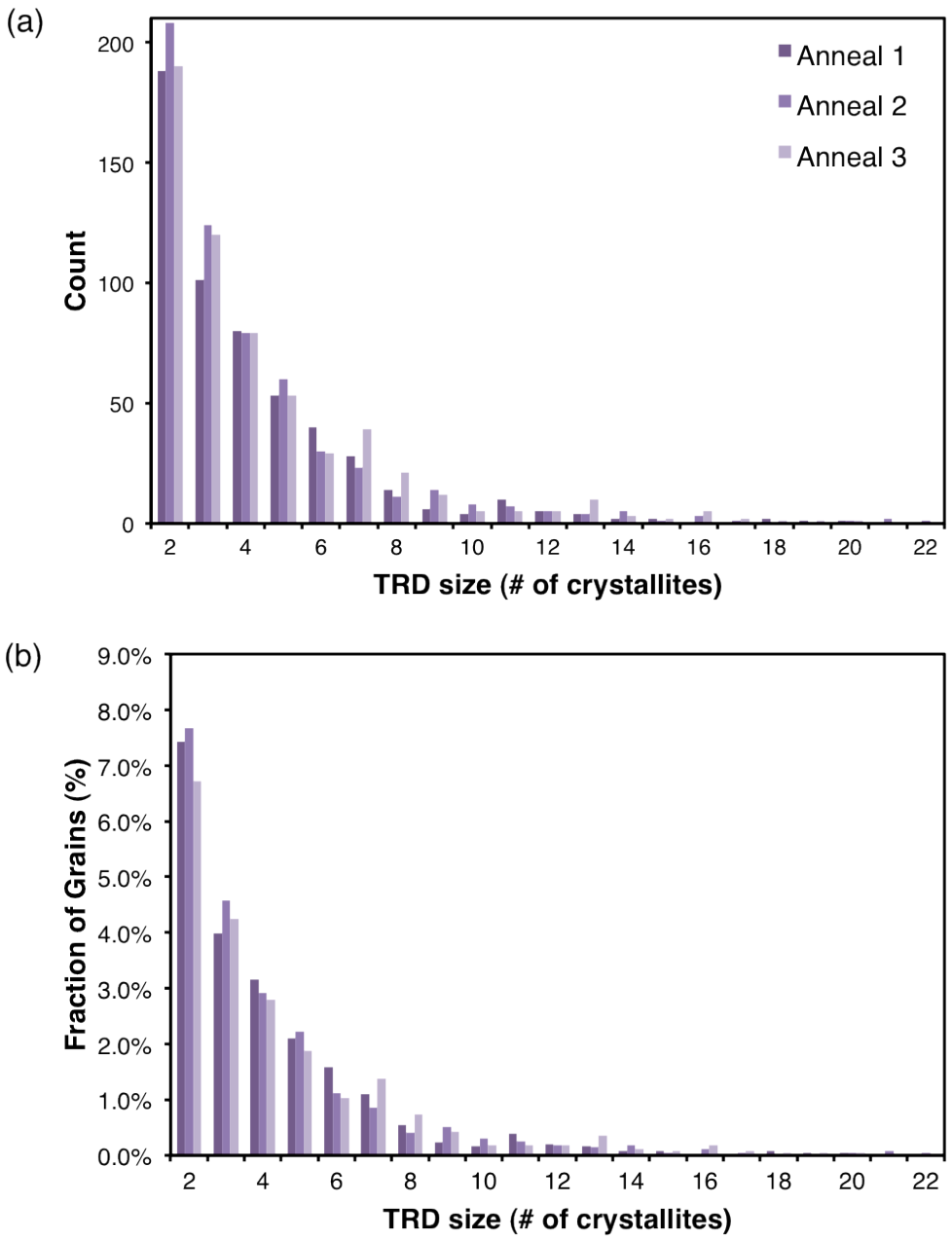

Figure 5.6. Distribution of twin-related domain sizes across all three anneals based on (a) the absolute number of counts and (b) the fraction of grains from the original microstructure. The distributions are mostly similar in that here are many small domains and fewer large domains.

5.2.2 Number of orientation repeats per twin-related domain

The frequency of orientation repeats, such that at least two crystallites had the same orientation, in a given TRD was characterized. In the growth accident model, for creating a TRD of size three, then two independent twinning events must occur. To create lamellar twin, it is assumed that the two twinning events are necessary and that the two events must select exactly the same twin variant from the four possibilities. Thus for a pre-existing TRDs with 2 crystallites, there is a 25 % probability that the correct variant will be selected that is necessary to create the ideal lamellar twin as seen in Fig. 5.5b, otherwise the result is two different twins as in Fig 5.5c. The TRDs from the previous analysis are classified by whether they contained a minimum of two identically orientated grains or not. The condition for identical orientations was done converting the Euler angles of each crystallite into integers and giving a +/- 1° for all of the phi1, PHI, phi2 that the two orientations are identical with symmetry considered.

The results of the partitioning for each of the three microstructure states are shown in Fig. 5.7a-c. The x-axis starts with a TRD size of 3 crystallites since the orientation of two crystallites will always differ. From the bar graph, the fraction of TRDs with two identical orientations increases with increasing TRD size. Across all three microstructure states, past a TRD size of 10 crystallites, then all TRDs feature at least two identical orientations. Furthermore, from Fig. 5.7, approximately 25% of the population of TRDs of size 3 features two identical orientations in all anneal states. This agrees with the previous statement that evolving from 2 to 3 crystallites, there is a 25 % probability of selecting the prior twin-relationship to produce two identical orientations in the TRD. The next step is to see if these behaviors can be predicted.

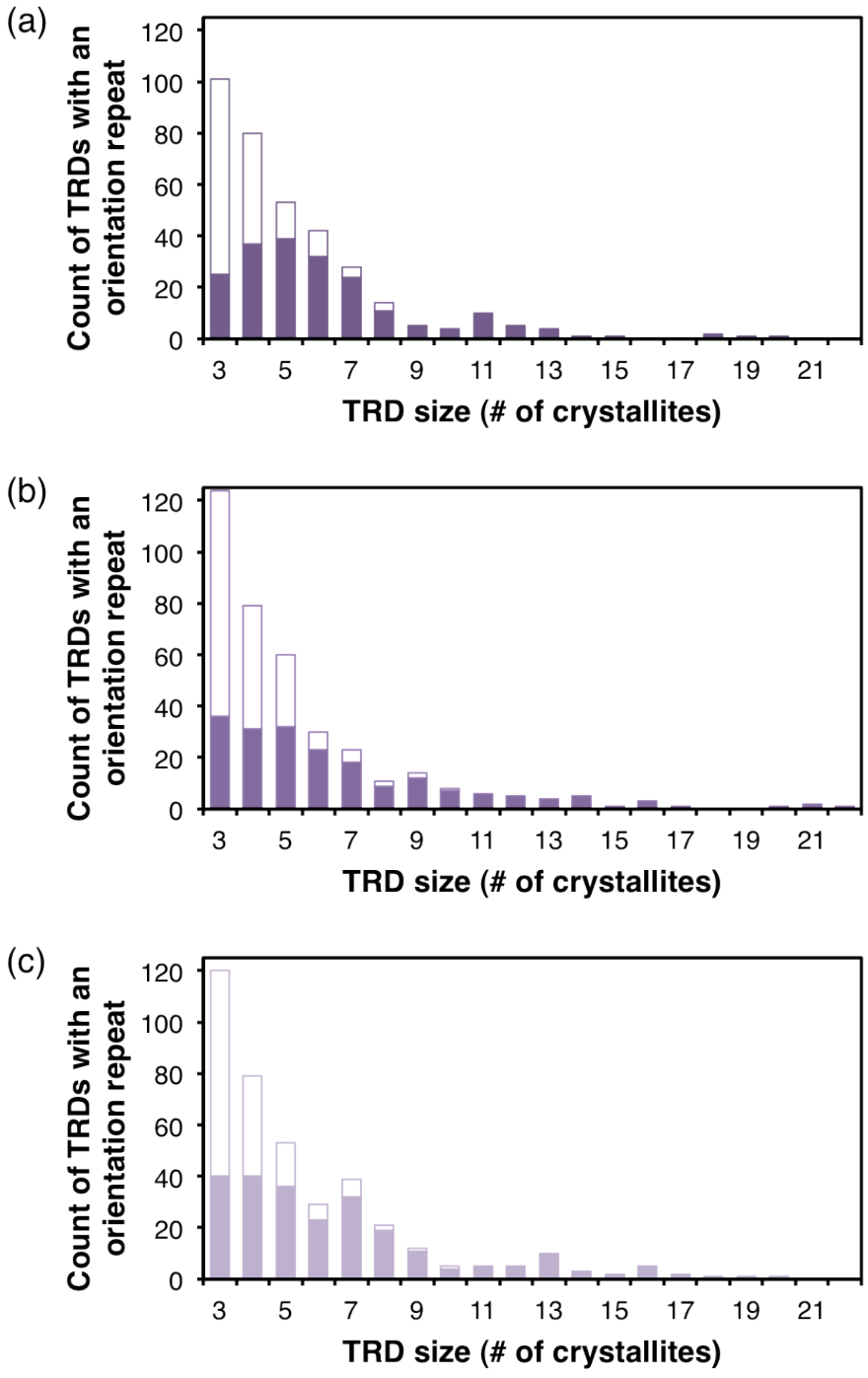

Figure 5.7. Distribution of twin-related domains within each size that feature at least two identical orientations colored in in (a) anneal state 1, (b) anneal state 2, and (c) anneal state 3. Past a certain TRD size of 9, the domains will always feature two identical orientations.

5.2.3 Modeling of twin related domains

Two models are introduced to account for the statistical probability of the growth accident model across all TRD sizes. Note that this does not take into account any of the geometric considerations, such as on which plane the annealing twin nucleates. The first model is a linear model, where the addition of a twin-related crystallite is considered from a previously nucleated crystallite. Essentially this treats the formation of annealing twins as a chain of one event after another, as illustrated in Fig. 5.8.

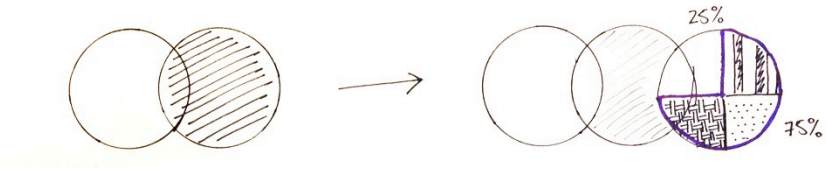

Figure 5.8. Linear model of twin variant selection, where new crystallites are only added on to the last added crystallite. The probability of returning back to the same twin variant is 25%.

In the linear model, the there is a 25 % probability that the twin variant selection of the previously nucleated crystallite will return back to an original orientation. Therefore the total probability for a given TRD size is one-fourth times the probability that the TRD currently has no two identical orientations in the chain. This is expressed in Eq. 5.1.

$$Probability\ of\ an\ Orientation\ Repeat\ = \sum_n \frac{1}{4} \times (1 - P_{n-1}) \qquad \text{(Eq. 5.1)}$$

The second model proposed is a branching model. The new crystallite can form on any of the pre-existing crystallites, thus at larger domain sizes the evolution is more similar to a cluster. The schematic of a TRD evolving from 3 to 4 is shown in Fig. 5.9, which emphasizes that there are two orientations that the new crystallite can twin from. Note that at the very first step of going from 2 to 3, the probabilities for both models are identical.

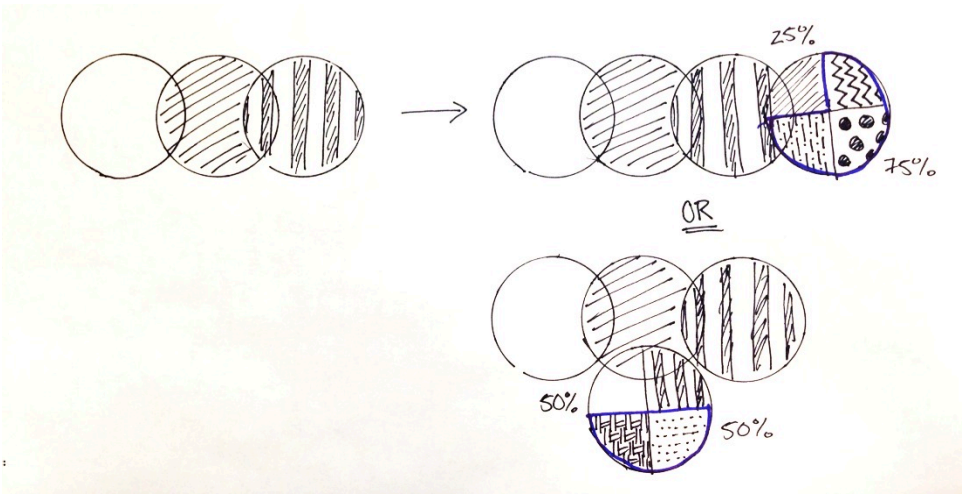

Figure 5.9. Branching model of twin variant selection, where new crystallites can be added on any of the previously nucleated crystallites.

The key difference is whereas as at the ends of the chain there is still a 75 % probability to form a new orientation, in the middle of the cluster there is only a 50 % probability to form a new orientation. The resulting probability distribution based on this approach is a negative binomial distribution as shown in Eq. 5.2.

$$Probability\ of\ an\ Orientation\ Repeat = 1 - \frac{n}{2^{n-1}} \quad \text{(Eq. 5.2)}$$

The results from the two models are shown in Table 5.2. In the two models, because the branching model has a lower probability of nucleating a new, independent orientation in the TRD, it is more likely to feature a TRD at smaller sizes with at least two identical orientations. In the branching model, at a TRD size of 12 there is a 99 % probability that the domain will feature two like-orientated crystallites. In contrast, in the linear model until the TRD size reaches 18, then there is a 99 % probability that the domain will feature two like-oriented crystallites.

Table 5.2. Expected fraction of TRDs that should exhibit two identical orientations.

	Probability of two identical orientations	
TRD Size	Linear Model	Branching Model
3	0.250	0.250
4	0.438	0.500
5	0.578	0.688
6	0.684	0.812
7	0.763	0.891
8	0.822	0.937
9	0.867	0.964
10	0.899	0.980
11	0.925	0.989
12	0.944	0.994
13	0.958	0.997
14	0.968	0.998
15	0.976	0.999
16	0.982	0.999
17	0.987	0.999
18	0.989	0.999
19	0.992	0.999
20	0.994	0.999

5.3 Discussion

5.3.1 Comparison of twin-related domain models to experimental values

The average fraction of twin-related domains that feature at least two identical orientations in experimental data is plotted against the two proposed models in Fig. 5.10. The average value is the calculated from all three microstructure states, and the lower and upper bounds determined by the highest and lowest values observed from the three anneal states. There is a general agreement for both models and the experimental data with the trend that the fraction of domains featuring an orientation repeat increases with increasing domain size, shown in Fig. 5.11, where the experimental data lies somewhere between the behavior of the linear and branching model.

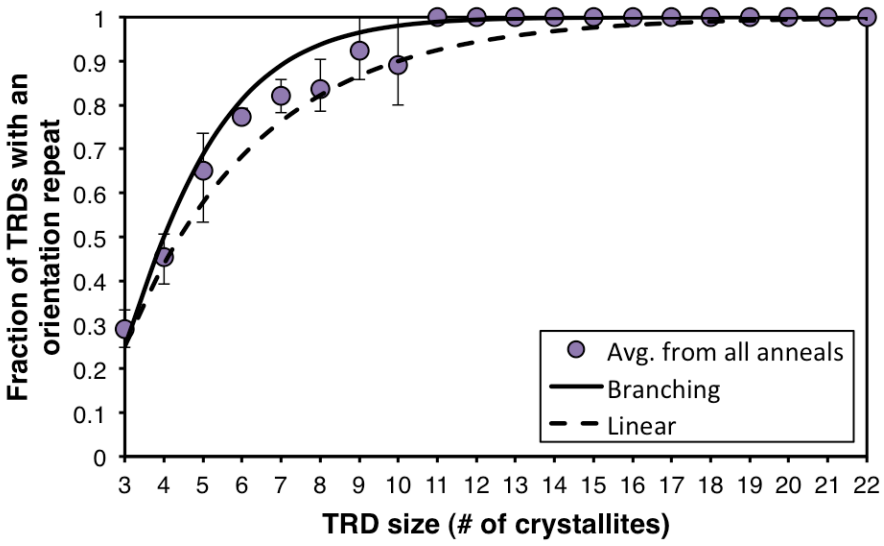

Figure 5.10. A comparison between experimental data and the two models for the fraction of twin-related domains that feature two identical orientations. The experimental data lies between the two models, suggesting that a possible mix of the two behaviors are present.

In the experimental data, past a TRD size of 10, all TRDs will feature two identical orientations. This convergence occurs sooner than both models predict. However past a TRD size of 10, the statistics are also weak and only a few twin-related domains per given size, typically one, are being sampled in the experimental data. Therefore the true experimental fraction at higher TRDs is difficult to capture due to the statistics necessary.

In general, the experimental data appears bounded by the two models presented. This can be qualitatively justified by the behavior of growth through recrystallization. In the initial stages of recrystallization, the recrystallizing grains are free to grow. Therefore their growth branches out in all directions, and all possible {111} directions are viable for nucleating an annealing twin similar to the branching model. However, as the recrystallizing grains gradually to impinge upon one another, then the remaining areas of deformed matrix that the recrystallizing grains can grow into are limited in direction, where the linear model would becomes more appropriate. Therefore

a better model in the future should take into consideration both the linear and non-linear nature of growth during recrystallization.

5.3.2 Results in comparison to Gleiter's growth accident model and other theories

For the given assumption, that a single twin formation event is responsible for producing a single twin boundary, the agreement in the results of TRDs that feature two identical orientations between the models presented and the experimental data reinforces the probability aspect of Gleiter's growth accident model. However, by only dealing with the connectivity, it is important to realize that this model does not take into account shape or morphology of crystallites [70][120].

For example, a partial lamellar twin in the growth accident theory requires two annealing twin formation events to occur. However, because it has only a TRD size of 2, this is still treated as single annealing twin formation event. If the partial lamellar twins were treated as complete twins separating the parent grain, this would be seen as a TRD of size 3 with the same twin variant selection. This implies that by considering the morphology the TRD crystallites and how many annealing twin formation events would be necessary for the observed partial lamellar features, then the statistics of the resulting TRDs will be different.

5.4 Summary

A high purity nickel specimen undergoing grain growth was observed by nf-HEDM. Twin-related domains were used to measure the connectivity of twinned grains in the microstructure. The orientations within different TRD sizes were analyzed and compared to two mathematical models of variant selections of annealing twins. It was found that the behavior of the experimental data was neither fully captured by linear nor branching mode presented, but did lie within the bounds of both models. The findings also show how the characterization of TRDs might be correlated to the annealing twin formation mechanism of the growth accident model.

6 Annealing twin formation during grain growth

In Chapter 4, it was shown that annealing twin formation primarily occurs during recrystallization. Furthermore, other authors have observed a decrease in twin density with additional grain growth [85]. However, these observations are drawn from 2D cross-sections. This suggests two possible conclusions, that (a) either annealing twins do not nucleate during grain growth and hence the decrease in twin density, or (b) annealing twins do nucleate during grain growth, but the elimination of twins consequently also drives down the twin density. This chapter will present the first observed annealing formation observations in a 3D microstructure of Ni undergoing grain growth. The energetic and geometric conditions behind annealing twin formation during grain growth are examined in detail and compared to that observed in recrystallization.

6.1 Experimental Details

6.1.1 nf-HEDM experiment of Ni and relevant statistics

This chapter examines the same high purity nickel 3D microstructure undergoing grain growth obtained by nf-HEDM used in chapter 5 [115]. The importance of studying a 3D microstructure in time intervals is that, within its spatial resolution, the formation of a twin can be observed. The appearance of a new twin on a planar surface, as reported in Chapter 4, may simply be a growth extension of a grain from the bulk to the surface. The same consecutive anneal states of the Ni microstructure considered in Chapter 5 are analyzed starting from Anneal 1 to Anneal 3.

In the interest of examining the grain boundary character and grain boundary energy, it was necessary to determine the normals of individual grain boundaries. This was achieved by dividing the 3D microstructure along the z-axis into two-dimensional xy-slices. The trace of each grain boundary was identified as were the triple junctions based on the intersection of three grain boundary traces. The triple junctions on adjacent layers with the same grain orientations were

identified and connected by a triple line. The grain boundary normal was calculated by taking the cross product of the triple line and the grain boundary trace segment.

6.1.2 Qualifications for annealing twin formation

The identification of a new twinned grains in the microstructure was achieved by searching between different anneal states. The process was sped up by identifying twin-related domain between anneals followed by identifying which of the TRDs exhibited an increase in the number of crystallites. A variety of TRD sizes, by both the number of voxels and the number of crystallites, were found to form a new twinned feature. The event of an annealing twin formation is considered when the following conditions are satisfied:

1. The feature is above 10 voxels and is not touching the surface or edge
2. The feature has a twin relationship, 60°<111>, with one of the prior grains
3. The feature did not spatially exist or was less than 10 voxels in the previous anneal
4. The feature continued to exist in the following anneal

6.1.3 Relative grain boundary energy measurements

The change in relative grain boundary energy associated with the formation of annealing twins was determined by the dihedral angles from the grain boundary normals measured at the triple line. This change in the triple junction with a formation of an annealing twin shown in Fig. 6.1, where the grain boundary energies per area (γ_{ij}), dihedral angles (θ_{ij}), and areas (A_{ij}), are labeled with subscripts that denote the relevant crystals. If a part of grain 2 adjacent to the triple line is replaced by a new grain with the twin disorientation, then a twin boundary is introduced and assumed to be on a (111) plane. The formation of this new grain reduces the energy if the following condition is met:

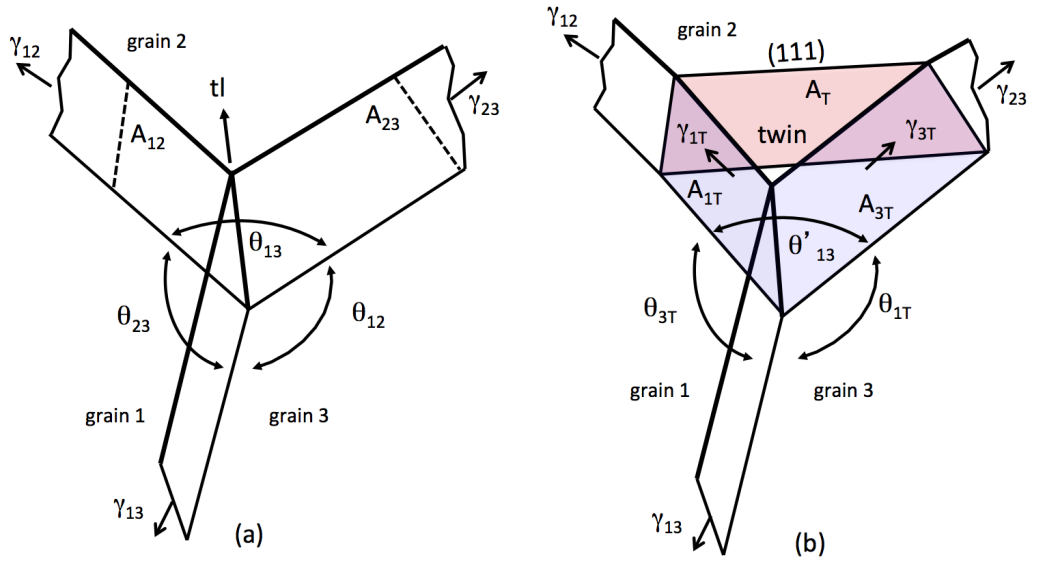

Figure 6.1. A schematic illustration of a triple junction before (a) and after (b) a new grain, twinned with respect to grain 2 and labeled 'twin', is inserted. Three grain boundaries separating grains 1, 2, and 3, meet along the triple line labeled *tl*. The schematic defines all of the parameters referred to throughout this paper. Adapted from [Murr 1968].

Assuming that local equilibrium at the triple lines of the microstructure is achieved and assuming that the torque terms at the triple line are negligible, the Herring condition [34] can be reduced to the Young equations as shown in Eq. 6.1, with the variables corresponding to the those in Fig. 6.2.

$$\frac{\gamma_{12}}{\sin\theta_{12}} = \frac{\gamma_{23}}{\sin\theta_{23}} = \frac{\gamma_{13}}{\sin\theta_{13}} \qquad \text{(Eq. 6.1)}$$

Equation 6.1 can be rearranged into Eq. 6.2, providing the summation of two the grain boundary energies as a function of the last boundary. This provides a method of comparing relative grain boundary energies if the characteristic of the last boundary does not change.

$$\gamma_{12} + \gamma_{23} = \gamma_{13}\left(\frac{\sin\theta_{23}+\sin\theta_{12}}{\sin\theta_{13}}\right) \qquad \text{(Eq. 6.2)}$$

6.2 Results

6.2.1 Local Observation of Annealing Twin Formation

Ten and nine new annealing twins can be identified from anneal one to anneal two and from anneal two to anneal three respectively. These annealing twins are noted to form along the triple lines of the microstructures. Although some events were identified to occur close to the proximity of quadruple points, the nucleation presumably occurred off one of the triple lines approaching the quadruple point. The most important point is that no observed cases occurred on a single grain boundary in the microstructure as literature has mostly suggested [22][70][71].

The formation of a new twinned grain is shown in the sequence of 3D and 2D images in Fig. 6.2. In the initial state, no feature is detected at the triple line. In the following anneal, the appearance of a new feature that is twin-related to the larger blue grain in the background appears at the triple line. This feature continued to exist and grew larger in the following anneal. The change in the dihedral angles is visibly apparent from the planar sections, implying a change in the grain boundary energy, which will be examined later.

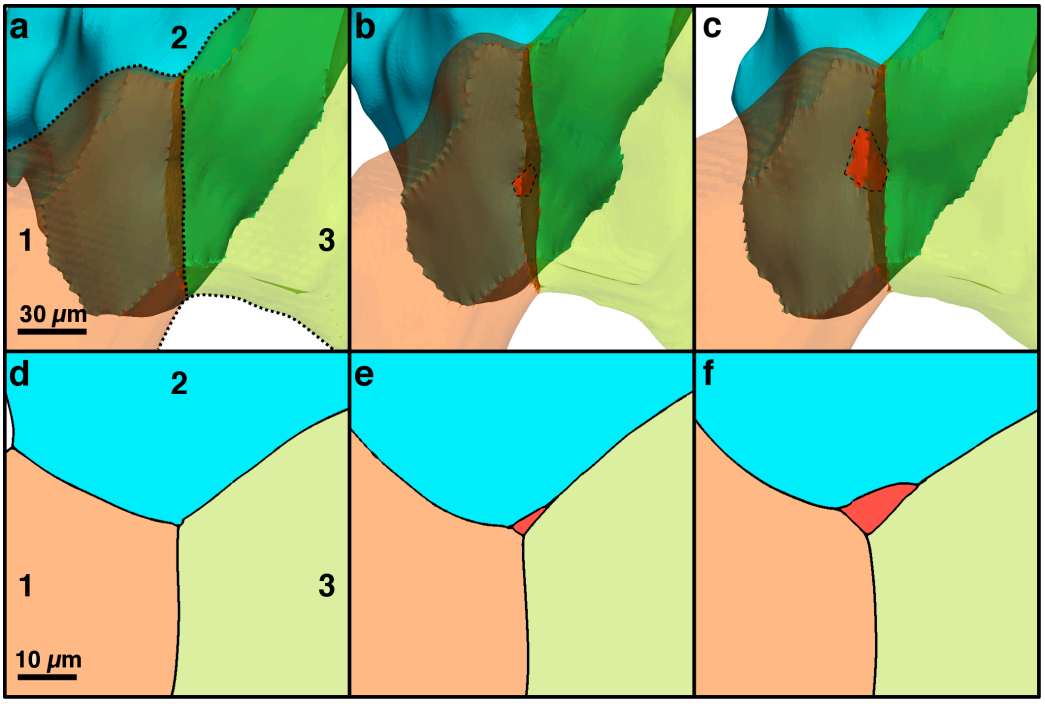

Figure 6.2. Illustration of three grains that meet at a triple line where a new twinned grain appears. (a-c) three-dimensional representations of the three grains. The peach (1) and olive (3) colored grains are semi-transparent to show the blue (2) grain in the rear and their line of intersection. The viewing direction is close to the plane of the boundary between the peach and olive colored grains. (a) Microstructure after 23 min at 800 °C, (b) after an additional 30 min at 800 °C, and (c) after an additional 25 min at 800 °C. The red grain that appears in (b) is at the line of intersection between the three grains and is twin related to the blue grain. (d-e) Plane sections of the same three grains through the triple line where the twin forms.

The growth rate of the annealing twins from when the new grain first appeared to the next measurement was monitored. The growth rate was calculated as the change in the number of voxels between annealing steps. In nine of the cases, no distinct trend appears in Fig. 6.3, as there are annealing twins that grow substantially and other cases where the size does not change much. However these are long annealing times where the growth of a twin might have occurred early on and then terminated later in time. The takeaway however is that all annealing twins increase in size with time and the dashed arrow denotes the average increase. Without taking into

account the energetics associated with annealing twin formation, the formation of new, growing grains with just three neighbors goes counter to the physics of isotropic grain growth.

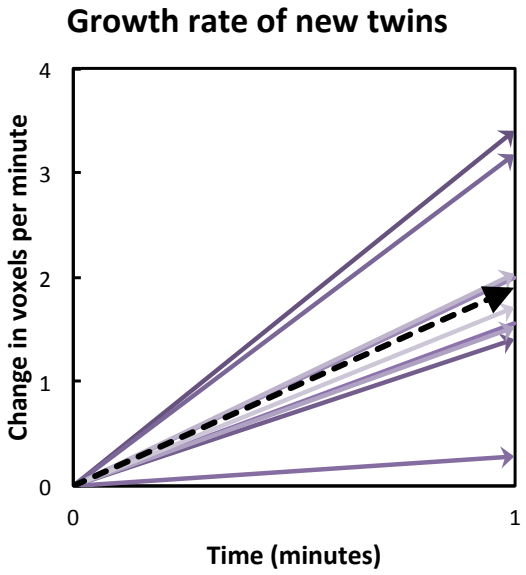

Figure 6.3. Growth rates of new annealing twins that identified in the first anneal and tracked in the next anneal. The growth rate is determined by taking the change in the number of voxels between the two anneals and dividing by the anneal time. A range of growth rates are observed, with dashed arrow representing the average, all indicated an increase in size with annealing.

6.2.2 Change in energy associated with annealing twin formation

In the interest of understanding the microstructure conditions resulting in the formation of annealing twins, only a total of nine cases from the consecutive anneals were examined. The complications that reduced the number of cases that could be analyzed were the twin and its resulting triple junctions must exist on multiple (at least two) layers to generate an appropriate mesh or linear interpolation. However, the uncertainty in the grain boundary inclination was taken account based on the size of the voxel.

The dihedral angles of the two boundaries of interest in the nine cases are plotted in Fig. 6.4a. In 17 of the boundaries, the dihedral angle increases with the formation of the annealing

twin. Even for the grain boundary that featured a decrease in the dihedral angle, the hollow data point, was within the range of uncertainty. However, recall that it is not necessary for every grain boundary to reduce its energy, only the sum of the energies. The relative grain boundary energy is determined assuming that the nature of the 1,3 grain boundary in Fig. 6.1 remains identical. By doing so and using Eq. 6.2, the change in relative grain boundary energy before and after twin formation at the triple line could be compared. For all nine triple junctions, the annealing twin formation decreases the relative energy within the estimated uncertainty as all points lie under the dashed line as shown in Fig. 6.4b. This implies that based on the interfacial energy only, annealing twin formation is energetically favorable.

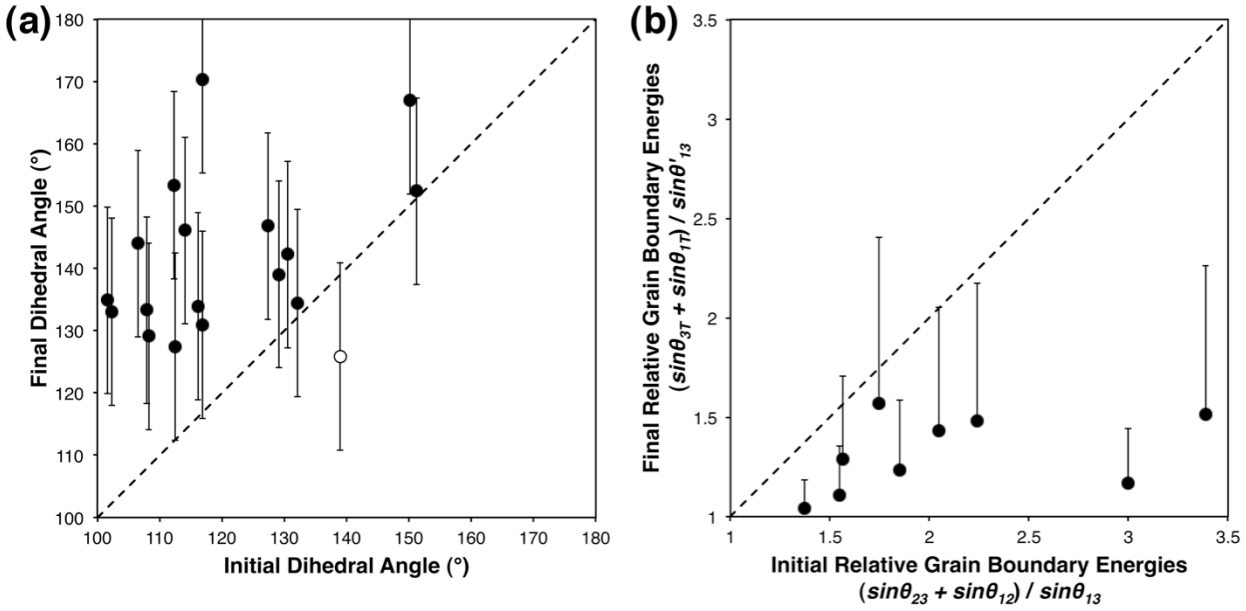

Figure 6.4. (a) The final dihedral angles (θ_{1T} and θ_{3T}) after twin formation (two per new grain) plotted against the angles before the twin formed (θ_{12} and θ_{23}). (b) The relative grain boundary energy after each twin formation event is compared to the relative energy before twin formation. In both plots, the dashed line marks the positions where the two quantities are equal. In (a) the vertical line through each data point marks the estimated uncertainty and in (b) it marks the uncertainty that would maximize the final energy; the uncertainty in the other direction is similar.

The grain boundary energy of the 1,3 interface can be matched to an experimental value. This was not done for the other boundaries of interest because of the difficulty of fitting a grain boundary normal on the new interfaces that the annealing twin forms due to the limited resolution. The 1,3 interface on the other hand is quite large and the grain boundary normal associated has less uncertainty. The grain boundary energy in this case was determined by the GBED experimentally measured by Li *et al.*, also in high purity nickel [35].

The modified change in relative grain boundary energy based on the GBED of Ni is shown in Fig. 6.5, where the in relative energy gain from the initial to the twinned configuration of the nine cases are sorted in ascending order. The average and standard deviation are across all nine cases is 0.639 a.u. and 0.511 a.u. respectively. This is skewed due to the two cases where the change in energy is over 1.0. Excluding these two cases, the average and standard deviation decreases to 0.389 a.u. and 0.139 a.u. The two cases that are excluded form slightly different annealing twin morphology than what has been previously presented. The two cases both feature an incoherent segment rather than just being a triangular wedge as shown in Fig. 6.5. The growth rates measured in Fig. 6.3 did not correlate to the change in energies.

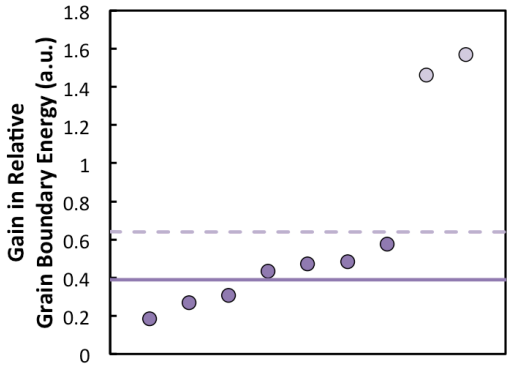

Figure 6.5. Gain in relative grain boundary energy based on experimental values (in arbitrary units) in ascending order for all nine cases. The average value, the dashed line, is 0.639 due to the large anomaly of the last two points. Not considering the two points brings the average (solid line) down to 0.389 with a standard deviation of 0.139 between the remaining 7 points.

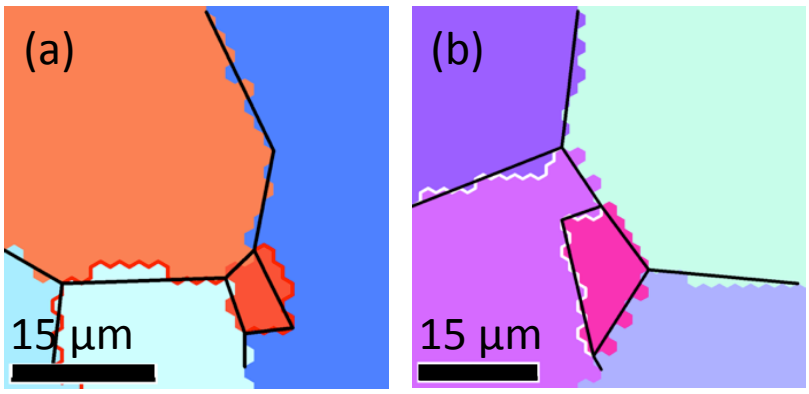

Figure 6.6. Plane section views of the two annealing twin formation cases where the change in relative grain boundary energy was exceptionally high. In these two cases the twin is not a wedge or triangle, but forms an incoherent segment as well.

6.2.3 Relationship of grain boundary inclination to triple line

The geometric relationship between the triple line directions during the formation of twins was investigated. The triple line vectors are transformed from the sample frame into the crystal frame of each of the three grains at the triple line. More specifically, the triple line vector in the crystal frame was compared to the closest {111} plane normal as illustrated in Fig 6.7a.

The triple line directions in the crystal frame are reduced to the fundamental zone of the crystal frame as shown in Fig. 6.7b, where the larger markers correspond to the parent grains. The (1-11) trace has is illustrated by the dashed line in the fundamental zone. Three of the parent grains of annealing twins lie close to the (1-11) trace and another five of the parent grains lie within 15° of the (1-11) trace. Only one parent grain, the point to the lying farthest left and closest to (001) is more than 15° away.

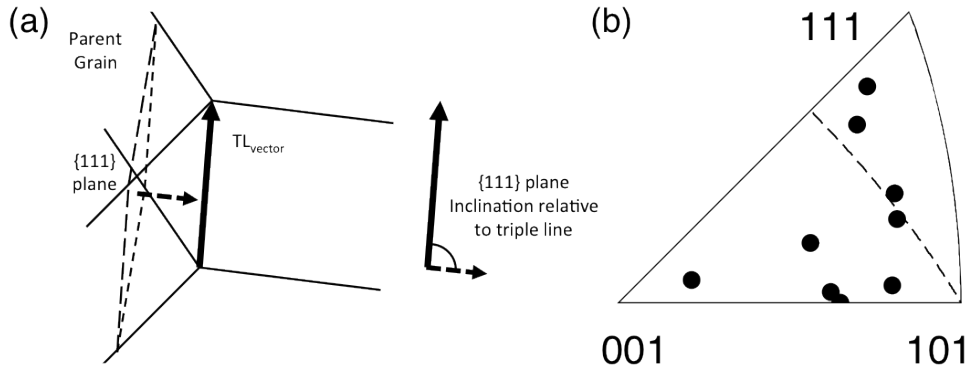

Figure 6.7. (a) Illustration of the triple line vector in the parent grain as well as position of a possible {111} type plane. In (b) The directions of triple lines, in crystal space, plotted in stereographic projection, for the nine triple lines where a twin was detected. The directions of each triple line in the reference frame of each of the three crystals are plotted; the larger circles are the direction in the parent grain. The dashed line corresponds to the (1-11) trace.

The average of the 8 angles (excluding the anomaly) between the triple line and the [1-11] direction was 90.2°. This suggests that for the triple line to form an annealing twin, there is possibly a crystallographic selection criterion where the triple line should lie within 15° of the {111} plane of the parent grain in addition to an energetic requirement as shown in the previous section. For transparency, the anomaly point laid within 27° away of a possible {111} plane.

6.3 Discussion

6.3.1 Nucleation at the triple lines in comparison to current theory

The majority of annealing twin formation theories discusses the formation of an annealing twin at a grain boundary. However, using a classical approach for heterogeneous nucleation, the activation energy for grain boundary is greater than a triple line [121], such that observing an event at a triple line is not unreasonable. The relevant theory to what is experimentally observed is Fullman and Fisher's proposition of the growth accident model, applied to triple junctions.

This was tested by thermal etching measurements of grain boundaries [21] and comparing the original widths of the parent grain boundaries to the widths of the corner twin boundaries, where some boundaries did show a reduction in width, but not always. Additionally Murr observed similar triple junction configurations in TEM with and without a twin to find the change in dihedral angles indicating a reduction in interfacial energy when a twin was present. Our results show complete and consistent agreement with the theory, but furthermore we know with certainty that a new grain is being formed at the triple line. We conclude that every annealing twin formation event leads to an overall reduction in grain boundary energy despite the increase in grain boundary area.

Fullman and Fisher's theory primarily dealt with the energetics of annealing twin formation, with no explicit regards to the geometric considerations of the microstructure. The new finding here is that the majority of triple lines that nucleate a twin lie within 15° of the {111} plane of the parent grain. This again suggests that the inclination of the {111} plays an important role as was previously observed in recrystallization. The close proximity can influence the diffusion necessary for atoms to migrate from either the grain boundary or the triple line to form a stacking fault sequence. Unlike the recrystallization study however, no migration study was made. Presumably because the twin does grow, and the coherent twin interface itself is known to be highly immobile, then the migration direction must be away from where the twin forms. Due to the challenges of tracking the grain boundary motion between anneals, this remains an area of open investigation.

It is also worth discussing that the observed annealing twin formation mechanism only generates a corner or edge twin. In order for a lamellar twin, a second annealing twin must form. From the same triple junction configuration of three grains, this is unlikely as the backwards

configuration is unfavorable in terms of energy. Only when the 1,3 boundary is completely consumed, then the new set of the neighbors might produce lower energetic triple junction configuration by twinning. The change in grain size in these anneals however was not enough to observe such an event.

6.3.2 Why are there still so few annealing twin nucleation events?

For all triple lines in the microstructure, we can calculate the energy reduction that would be achieved by introducing a twin-related grain in one of the three prior existing grains. It is assumed the new twinned grain would form a coherent twin interface with the parent grain. However this calculation does not take into account the change in inclination that was experimentally observed. Therefore the change in energy associated with this prediction is based solely on the change in misorientation characteristics. The change in grain boundary energy is based on the experimental values measured by Li et al. [34]. The additional condition that the triple line of the parent grain should lay within a certain number of degrees from the {111} plane can also be implemented. The steps to calculate the change in energy and inclination by inserting a twin is listed below:

1. Identify a triple junction in the microstructure
2. Calculate grain boundary energies based on misorientation and inclination
3. Pick on of the three grains at the triple junction and insert a twin misorientation
4. Calculate the new grain boundary energy based on the new twin misorientation
5. Compare to the initial grain boundary energy configuration
6. Calculate the angle between the triple line vector and the{111} plane normal for the specific twin variant selected
7. Repeat steps 4 to 6 for the other three possible twin variants

8. Repeat steps 3 to 7 for the other two possible grains at the triple junction
9. Repeats steps 1 to 8 for all other triple junctions in the microstructure

The result is the fraction of triple lines that could nucleate a twin as a function of the change in energy and inclination of the twin plane relative to the triple line. These results are plotted as a 3D map as shown in Fig. 6.8. There are two trends apparent from the calculations. First, as the change in energy necessary for the twin formation increases, then the number of triple lines that can nucleate a twin decreases. Second, as the tolerance restriction on the {111} plane to the triple line is reduced, the number of triple lines that can nucleate a twin also decreases.

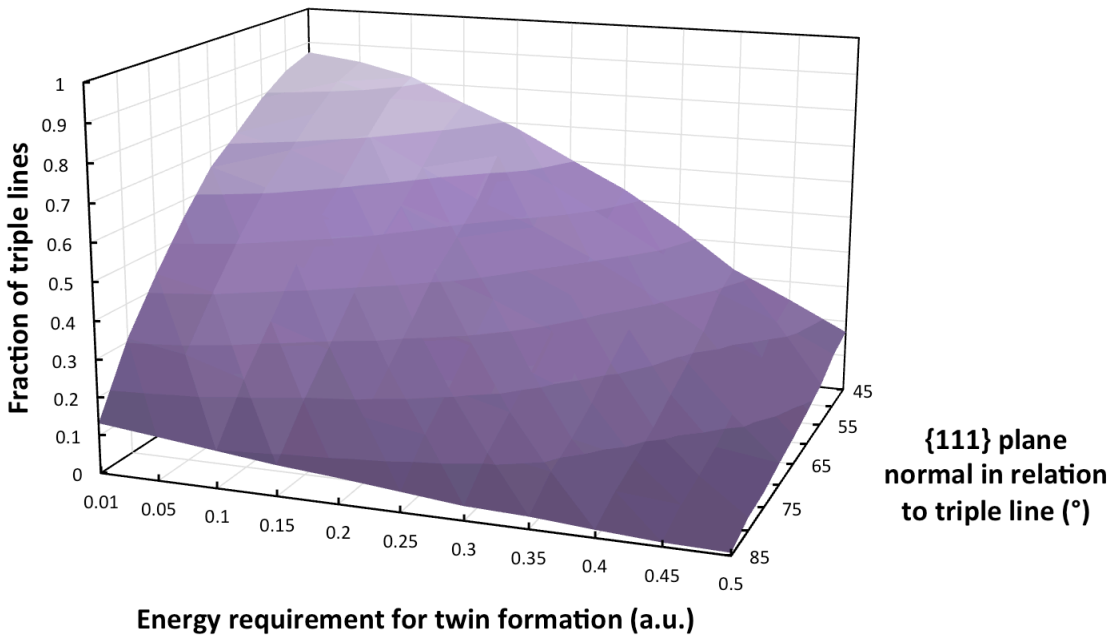

Figure 6.8. Estimated fraction of triple junctions that can form an annealing twin based on the change in energy by introducing a twinned grain and the inclination of the twin plane relative to the triple line.

When considering the range of energies observed in the 7 cases (excluding the two anomalies and rounded to 0.4) and the average tolerance of the 8 cases of the inclination (15°), the calculations suggest that only a small percentage, 8.4 %, are viable candidates for forming an annealing twin. Out of some 20,000 triple lines, this computes to roughly 2,000 triple lines, which is orders of magnitude greater than the 10 cases observed. The discrepancy suggests that perhaps the conditions are too relaxed, that is, maybe a smaller tolerance than 15° should be used, or that the change in energy values should be greater than 0.4.

Additionally, we have focused only on the "thermodynamics" for an annealing twin to form and have not considered the kinetics or the rate of transformation. If grain boundary migration is a necessary requirement as in recrystallization, there are two motions for triple lines. Either the triple line moves towards the center of mass of the parent grain (parent grain shrinking), or the triple line moves away from the center of mass of the parent grain (parent grain growing). Assuming that approximately half of the cases grow and the other half shrink, then this reduces our number of cases by a factor of 2. Nonetheless, this is still significantly larger than the number of observed case and is open to investigation.

6.3.3 Formation of new grains in relation to grain growth theory

The formation of new grains during grain growth comes as a surprise. The conventional idea of grain growth is that big grains grow at the expense of small grains. This is achieved by curvature driven growth [60][61][62] such that both the interfacial area and interfacial energy are reduced. Additionally the high energy grain boundaries are preferentially eliminated during grain growth resulting in an anisotropic distribution of grain boundary energies [123][124]. In that sense, the twinning mechanism observed here is behaving in the same manner by replacing higher energy

grain boundaries with lower energy grain boundaries to create an anisotropic grain boundary energy distribution.

The implication of this is that the formation of a new grain, twin-related or not, can occur by an energetic balance. For new grains that do not include twin boundaries, this is unlikely simply because the coherent twin boundary energy in low-medium stacking fault FCC materials is so much lower than all others. The formation of any other special or randomly orientated grain presumably never leads to a reduction of grain boundary energy and has so far not been reported. In that regards, the annealing twin is indeed special due to the very low energy of the coherent twin boundary.

6.4 Summary

In FCC nickel, new grains with a twin misorientation with one of the three prior grains at the triple line were observed to form during grain growth. Despite the increase in the interfacial area with introducing a new grain the, overall interfacial energy is reduced still by replacing higher energy grain boundaries with lower energy grain boundaries. Additionally for this twinning mechanism, it was found that the twin plane relative to the triple line may play a role as eight of the nine triple line directions of the parent grain lie within 15° of the twin plane. By taking into account both the necessary change in energy and triple line direction, it was found that only a fraction of triple lines are potential sites for forming a twin. However the discrepancy between this fraction to the actual number of observed events still requires more investigation.

7 Effect of temperature on annealing twin content

The results of the previous chapters emphasized the role of the {111} plane on annealing twin formation. Furthermore, in the Chapter 6, we showed that there is a possible selectivity to triple junctions that can nucleate twins. However, we still observe that only a fraction of the triple junctions result in annealing twin formation event. In this chapter, we focus on the effect of temperature on annealing twin formation in both recrystallization and grain growth to determine if thermal fluctuations may play a role in achieving the appropriate activation energy and critical nuclei for annealing twin formation.

7.1 Experimental Details

7.1.1 Varying temperature of recrystallization

A sample of high purity nickel (99.999 %) was obtained from Alfa Aesar and first homogenized similar to Chapter 4. The initial deformation however was 30 % by compression instead of 25% by cold-rolling. Specimens were sectioned from the 30 % sample with a low speed saw, where it is assumed that the additional damage from sectioning is negligible. Specimens were polished in cross section following the same procedure presented in Section 3.1. The starting microstructure is shown in Fig. 7.1a with a relatively fine grain size average of 15.7 µm and the cross section of the deformed specimen is shown in Fig 7.1b.

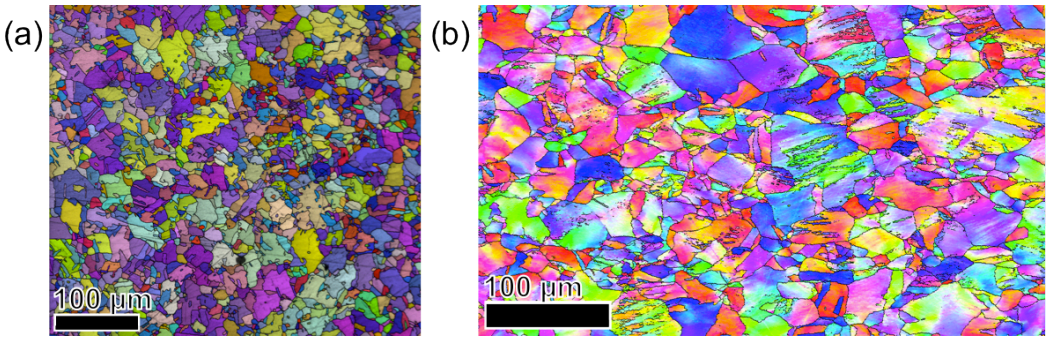

Figure 7.1. EBSD IPFz of (a) the normal to compression of the initial starting microstructure and (b) of the axial view to the compression axis of the microstructure deformed to 30 % reduction.

Three specimens were annealed at the following temperatures: 350 °C, 450°C, and 550°C. 100°C intervals were selected to ensure there would be a large enough difference in the kinetics. While this implies that the 350 °C sample will undergo more recovery prior to recrystallization than the 550 °C sample, this effect was not quantified nor considered. The specimens are repeatedly annealed until full recrystallization. While full recrystallization was nearly achieved in the first anneal of 550°C, it was assumed that minimal grain growth occurred. The fraction of recrystallization was observed by using EBSD again based on the grain orientation spread threshold of < 1°. The resulting kinetics of the recrystallization experiments is shown in Fig. 7.2 and recrystallized microstructures at various stages in Fig. 7.3a-c.

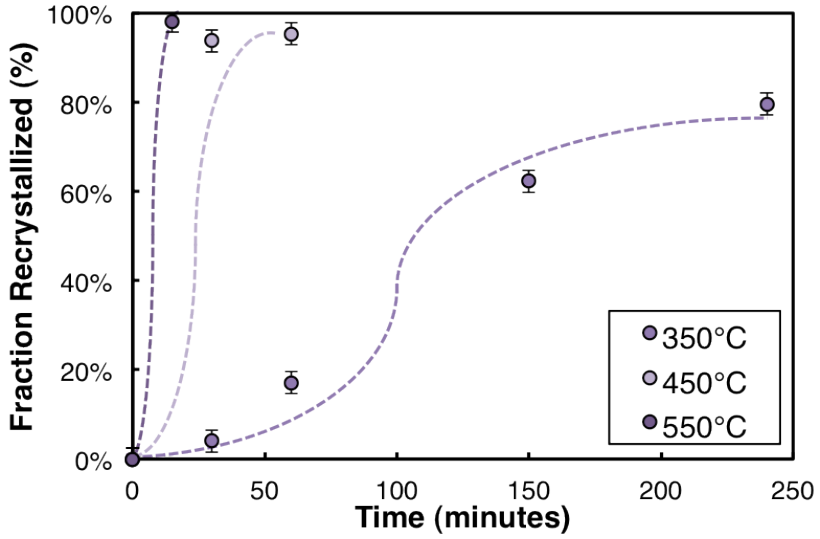

Figure 7.2. Fraction recrystallized as a function of time using a GOS threshold < 1°. The three different annealing temperatures of 350, 450, and 550°C show different kinetics as expected.

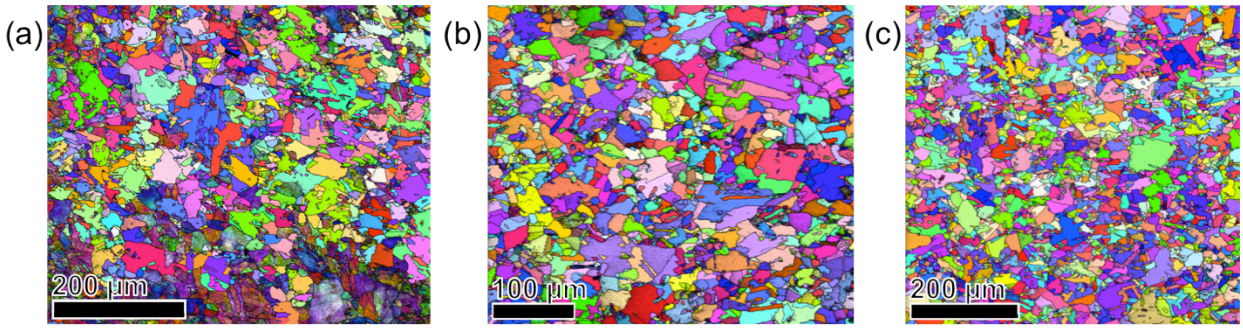

Figure 7.3. (a) EBSD IPFz of the microstructure annealed at 350 °C for 150 minutes, at approximately 62 % recrystallized. (b) EBSD IPFz of the microstructure annealed at 450 °C for 60 minutes, at approximately 94% recrystallized. And lastly, (c) EBSD IPFz of the microstructure annealed at 550 °C for 15 minutes, at approximately 98 % recrystallized.

7.1.2 Varying temperature of grain growth

A high purity nickel (99.999 %) sample was obtained from Alfa Aesar. The starting sample was homogenized and after heat treatment had a starting grain size of 10 µm with a twin length fraction of the 50 ± 2 %. The samples were annealed at five temperatures of 550 °C, 650 °C, 750 °C, 850 °C, 950 °C to ensure a wide range kinetics. The other requirement was that the change in grain size for all examples is equal. Using the normal grain growth equation shown in Eq. 7.1 and an activation energy of 115 kJ/mol, the appropriate annealing times were calculated and summarized in Table 7.1.

$$d^2 - d_0^2 = kt \qquad \text{(Eq. 7.1)}$$

Table 7.1. Grain growth annealing times in FCC Ni

Temperature (°C)	Time (hr:min:sec)
950	1:00
850	2:36
750	8:40
650	37:30
550	3:51:45

The resulting microstructures of each annealing temperature are shown in Fig. 7.4a-f. The original microstructure is obviously replaced with larger grains, where the average grain size has increased from 15 μm to almost 100 μm. Doing so ensures that we reduce the effects of the prior microstructure to negligible levels.

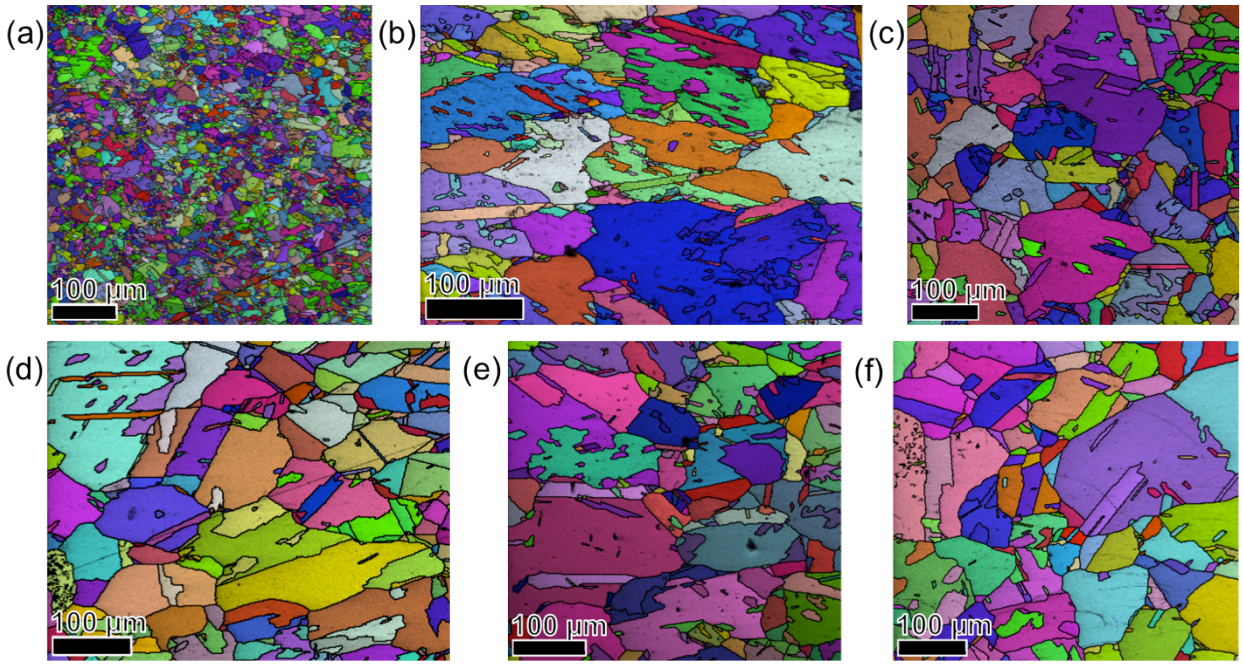

Figure 7.4 EBSD IPFz maps of the microstructure in the (a) initial state, (b) 550 °C, (c) 650 °C, (d) 750 °C, (e) 850 °C, (f) 950 °C annealed for the times reported in Table 7.1. Qualitatively the five anneals produced similar grain sizes with a large fraction of twin boundaries.

7.2 Results

7.2.1 Effect of temperature on recrystallization

Although temperature increases the rate of recrystallization (and consequently the grain boundary velocity), it did little to change the final grain size after recrystallization. The final grain size across the three anneals is approximately 19.2 μm as shown in Fig. 7.5a. Consequently, the final annealing twin density after recrystallization was also similar with an average of 64 mm^{-1}. The relationship between the twin density and grain size is shown in Fig.

7.5b, where the difference in grain size is presumably responsible for the minor difference in twin density. Similarly, the length fraction as a function of temperature, as well as the number of twins per grain are plotted in Fig. 7.5c and 7.5d respectively. The differences in the length fraction of annealing twins and number of twins per grain are within the statistical uncertainty, where the average is 53.2 % and 4.9 respectively. The lack of differences between the twin content as a function of recrystallization temperature indicates that temperature plays a minor role beyond providing the necessary kinetics for grain boundary migration.

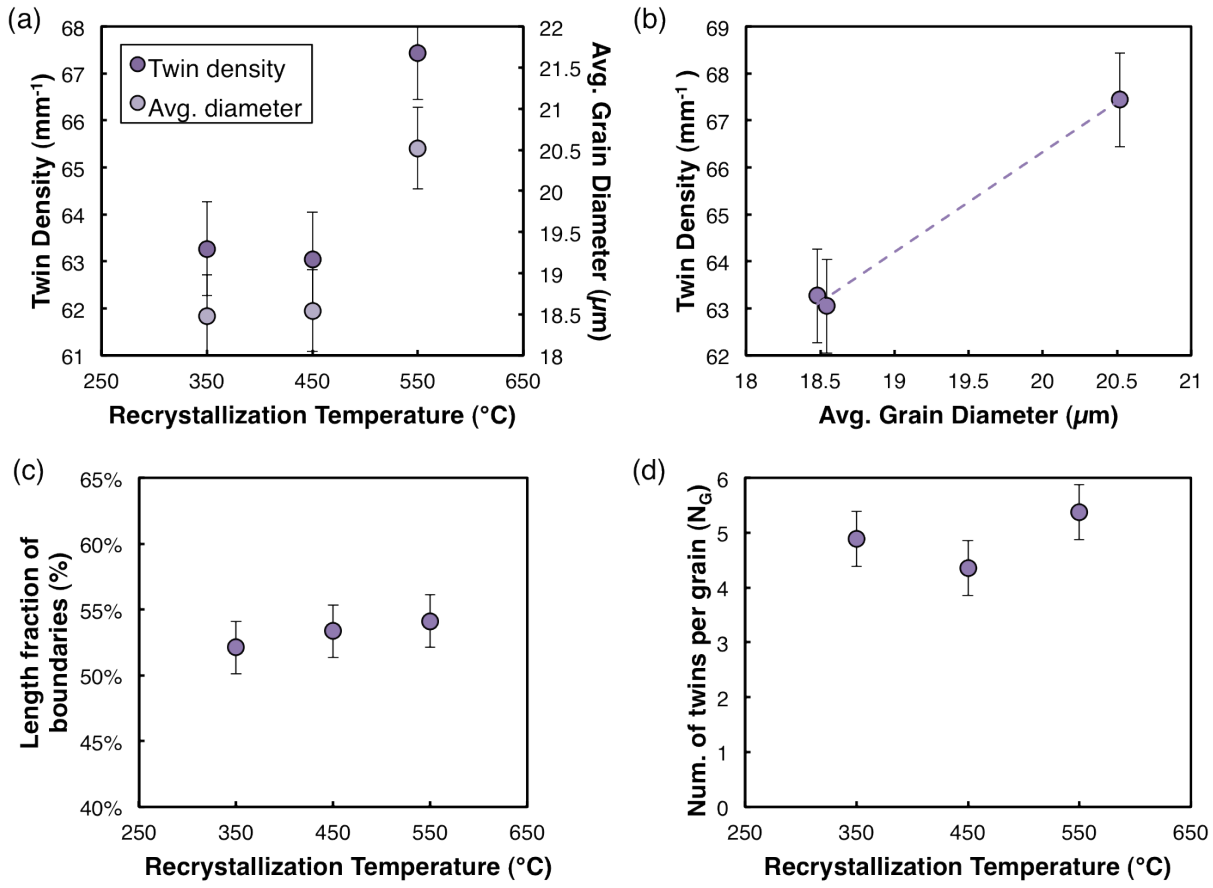

Figure 7.5. (a) Twin density and average grain diameter, (c) length fraction of boundaries, and (d) number of twins per grain in the final recrystallized microstructure are plotted as a function of recrystallization temperature. Additionally the twin density as a function of recrystallized grain diameter is plotted in (b). No distinct trend is apparent with temperature, thus suggesting negligible effect.

7.2.2 Effect of temperature on grain growth

Although the intent was to achieve the same change in grain size, the final average grain size varied from 75 μm to 110 μm as shown in Fig. 7.6a. The twin content was measured a function of temperature for the different annealing temperatures. The twin density is shown Fig. 7.6a, length fraction of twins in Fig. 7.6c, and the number of twins per grain in Fig. 7.6d. The twin density as a function of grain size from the starting microstructure is shown in Fig. 7.6b, where the trend seems to suggest that the decrease in twin density is most likely attributed with the average grain size (ignoring the 750 °C anomaly).

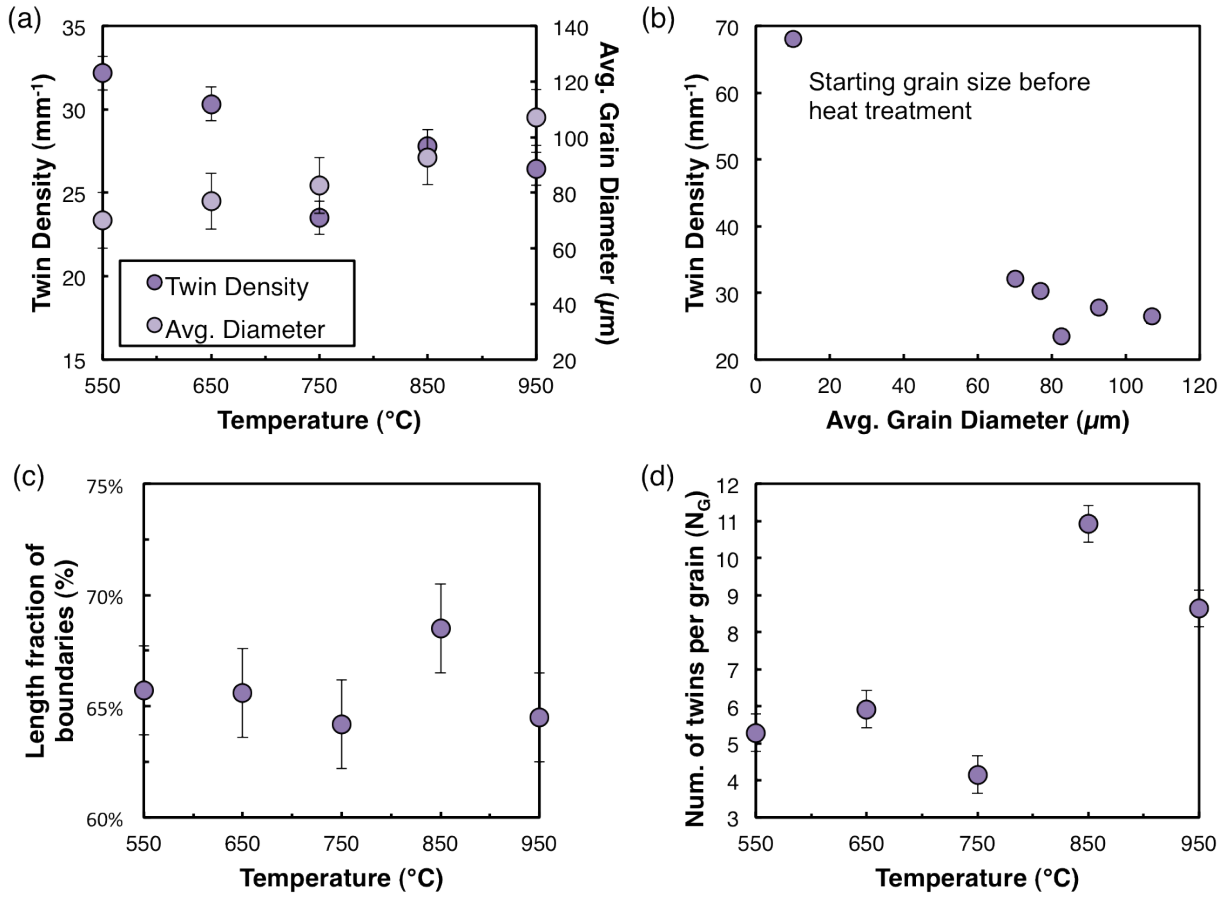

Figure 7.6. (a) Twin density and average grain diameter, (c) length fraction of boundaries, and (d) number of twins per grains in the final recrystallized microstructure are plotted as a function of grain growth temperature. Additionally the twin density as a function of grain diameter is plotted

in (b) starting from the initial grain diameter. Again there are no distinct trends that are apparent with temperature, thus suggesting negligible influence of temperature.

One curious anomaly that did appear was in the twin "morphology" and connectivity. At 550 °C, there were a number of island twin grains in the microstructure. The fraction of grains with a number of neighbors equal to one (thus implying an island grain) is shown in Fig. 7.7. One plausible explanation is that at 550 °C, a temperature necessary for the migration of incoherent twin boundaries is not achieved. Therefore island grains that are eliminated at high temperatures remain at 550 °C.

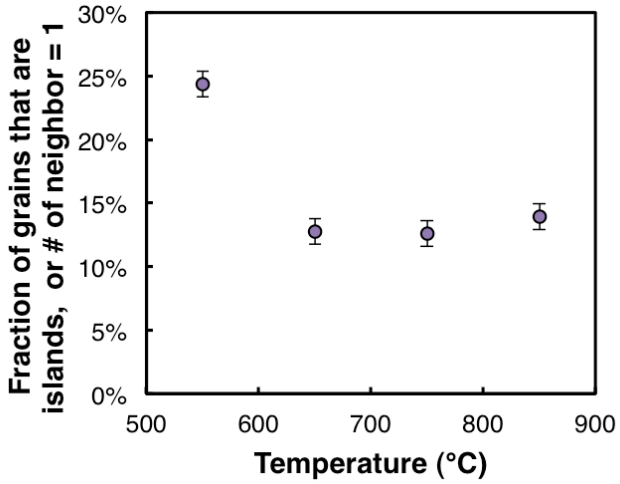

Figure 7.7. Fraction of grains that are island grains (grains with their number of neighbors equal to one) as a function of temperature shows that at 550 °C there are more island grains than any other grain growth temperature.

7.3 Discussion

For approximately the same change in grain size at different temperatures for recrystallization and grain growth, we observe a negligible effect on the annealing twin content despite the different growth kinetics. There was no systematic change identified in the twin content as a function of temperature. The grain growth findings agree with those presented by Pande *et al.*

[71], in which twin content depended primarily on grain size despite Gleiter's model using a classical nucleation approach which would have suggested otherwise. Additionally, Cahoon *et al.* asserts that, in the recrystallization regime, the stored energy term will primarily eliminate any influence of temperature [68], which is in effect observed in the recrystallization findings. However, Rath *et al.* has also suggested that the twin content might depend on the grain boundary velocity [76] and has shown some correlation as well [114]. This is not observed here as the different kinetics for recrystallization and growth resulted in the overall same twin content. This suggests that neither the temperature nor the kinetics of grain boundary migration play a strong role in annealing twin formation in either regime.

A lack of influence of temperature, in particular in the grain growth regime, has two possible explanations. Assuming a lack of influence in the kinetics, then annealing twin formation might be justified by a diffusion-less, or martensitic-type, transformation. The other explanation is annealing twin formation is a heterogeneous nucleation event in which the driving forces negate any effect of temperature, similar to what is observed in recrystallization.

A diffusionless transformation [125] similar to a martensitic-type transformation provides an explanation for how the crystal lattice would transform from a FCC to HCP stacking sequence to generate a stacking fault. The diffusion-less transformation could either be driven by the interfacial energy (like that observed in grain growth) or stored energy (in which we treat recrystallization similar to a phase transformation). The troubling part with this idea is where does the strain necessary for a diffusion-less transformation come from? While there may be some small surface tractions during annealing and recrystallization, this is mostly unclear.

The second proposition is a heterogeneous nucleation event. The experimental results suggest that there is a crystallographic importance of the {111} plane of the grain that will

exhibit twinning relative to the microstructural features. Based on the proximity of the {111} to the grain boundary in recrystallization or the triple line in grain growth, this appears to influence the formation of nucleation. Therefore in the microstructure, there are only a fraction, and not all, grain boundaries or triple lines that can nucleate an annealing twin. Coupled with grain growth, the absolute number of grain boundaries and triple lines decrease with time in a given volume of material. Furthermore increasing temperature increases the rate of decrease of these microstructural features. This may be a justification that although increasing temperature should increase the number of nuclei, the physical number of microstructural features from which these nuclei form are disappearing, and hence no observable effect on the twin content is made.

An experimental design would be a random, polycrystalline microstructure compared to a textured, polycrystalline microstructure with the same starting grain size. Depending on the texture, microstructure could have either statistically greater number of potential triple line nucleation sites than the random microstructure and therefore produce more twins. Both samples should be annealed to the same change in grain size and the twin content observed afterwards. At least within recrystallization where there are some obvious differences in twin content based presumably based on orientation [86], we might observe a similar effect here also.

7.4 Summary

For the temperatures of interest, it was observed that the twin content did not vary significantly either during grain growth or recrystallization in nickel. This not only suggests that annealing twin formation is insensitive to temperature fluctuations and also the grain boundary velocity. Based on results from previous chapters, we conclude that the number of microstructural features available for nucleation influences annealing twin formation. The conditions of nucleation are those detailed from the earlier chapters with regards to the geometric configuration of either the grain boundary plane (during recrystallization) or triple line direction (during grain growth) relative to the twin plane.

8 Discussion

The following hypothesis was presented:

> *"…It is hypothesized that certain microstructural geometries will promote annealing twin formation. More specifically, it is hypothesized that migrating {111} interfaces during recrystallization and grain growth create favorable conditions for twin formation…"*

In the recrystallization regime this is deemed to be true. Although the migration behavior was not studied in the grain growth regime, we conclude that there is a measurable influence of the twin plane in relation to the triple line. In this sense, the hypothesis is only true for grain boundaries in recrystallization, whereas for grain growth it is incorrect because annealing twin formation only occurred at triple lines. However, we see that there is a relationship between the triple line direction and the {111} plane in the parent grain for nucleating the twin. This implies that some geometric relationship may still influence annealing twin nucleation in grain growth. These findings provide some useful discussion points.

8.1 Role of the {111} plane geometry and energy

The position of the {111} plane relative to either the grain boundary or triple junction may play a role due to the ease of formation of a stacking fault. Stacking faults on the {111} plane cost the least amount of energy in comparison to other low-index crystal planes (and hence are never observed on other planes) [126][127]. Thus during grain boundary migration, forming a {111} stacking fault is not necessarily the lowest energy state, but nor is it overly expensive as diagramed in Fig. 8.1a. In nickel, the gap between the twin and the original grain boundary would only be 0.06 J/m^2, the energy of a twin boundary, assuming the interface formed was a coherent {111} interface. In contrast, across a non-{111} index plane, an incoherent twin boundary will be formed, which will increase the overall energy of the interface. This causes the

twin stacking fault sequence in a less favorable condition as demonstrated by Fig. 8.1b. The reason why the lowest energetic state is not ultimately achieved is due to non-equilibrium thermodynamics. The kinetics of atomic motion is presumably limiting the migration of atoms into the proper stacking sequence.

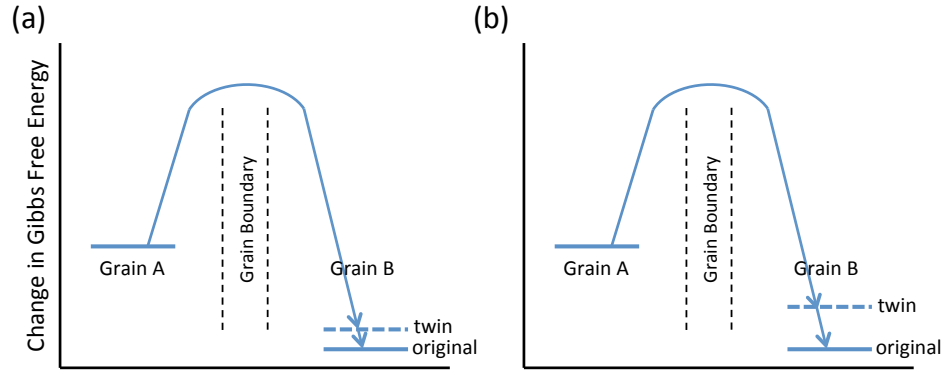

Figure 8.1. The proposed thermodynamics of grain boundary motion for Grain B growing at the expense of Grain A is shown for an interface (a) close to the {111} and (b) away from the {111}. The formation of a twin on (a) {111} interface is energetically cheap due to the low energy of the coherent twin boundary and stacking fault energy, which overall makes the possibility of creating a stacking fault sequence more likely on a {111} plane over other migrating planes.

To address the need to form a critical nucleus with an appropriate size, the {111} plane also has the highest number of nucleation sites to form an improper stacking sequence. In the ABC stacking schematic, the atomically flat {111} A plane has an equal number of proper, B, and improper, C, adsorption sites for atoms moving from one grain to the other. Some atoms will diffuse across the boundary into the improper stacking sequence, while other atoms at the surface can shift from a proper to an improper site and vice versa. The combined atomic motions are presumably what might lead to the formation of the necessary nuclei. In contrast, a non-{111} plane would have steps and ledges. These steps and ledges can promote the placement of atoms in the proper stacking sequence, which would eliminate the interfacial energy of what would otherwise have been an incoherent twin segment.

Although aluminum also features a large population of {111} planes, the lack of twins is excused by the high SFE, 160-200 mJ/m^2 [128]. Earlier literature presented in the background chapter has shown that higher SFE results in lower twin content in the microstructure [71][75]. Although annealing twins are governed by the SFE, the SFE is an intrinsic material property at the atomistic level. Therefore identifying a relationship at the microstructure level may provide a more appropriate link for predicting the annealing twin content as demonstrated in Fig 8.2. This should imply that for materials with low SFE but with growth that is governed by planes distant from {111} planes, the microstructure should exhibit a lack of twins.

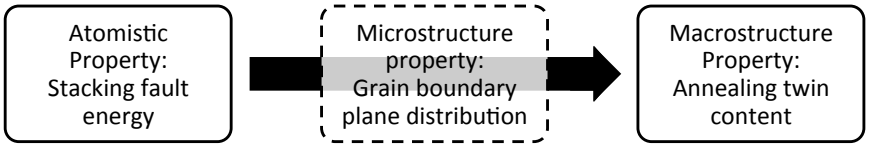

Figure 8.2. Flow-chart of current, stacking fault energy, and proposed, grain boundary plane distribution, factors for predicting annealing twin content. While stacking fault energy does influence annealing twin content, because of the length-scale difference the two might not always correlate well together. Therefore it is proposed by also by taking account the grain boundary plane distribution, one can achieve better predictions of the annealing twin content.

This is the case with late-stage abnormal grain growth (LS-AGG) in electrodeposited nanocrystalline nickel [129]. While it is unclear exactly how abnormal grain growth proceeds, the abnormal grains grow as facetted grains shown in Fig. 8.3a that are several times larger than the original matrix. Despite the abnormal grains substantial size difference, which would suggest that several twinning events should have occurred, the abnormal grains show a relatively low twin density in comparison to recrystallized nickel. For relatively the same average grain size of 50-60 μm, the twin content in this material compared to recrystallized Ni is one twin per grain vs. the four to five twins per grain respectively. One plausible explanation is that the facets on the abnormal grains are {100} [130], as shown in the GBPD in Fig. 8.3b, and therefore do not

promote the formation of annealing twins unlike the GBPD of the recrystallization interface observed in high-purity nickel from Chapter 4. Additional details on the behavior of LS-AGG are provided in Appendix 11B.

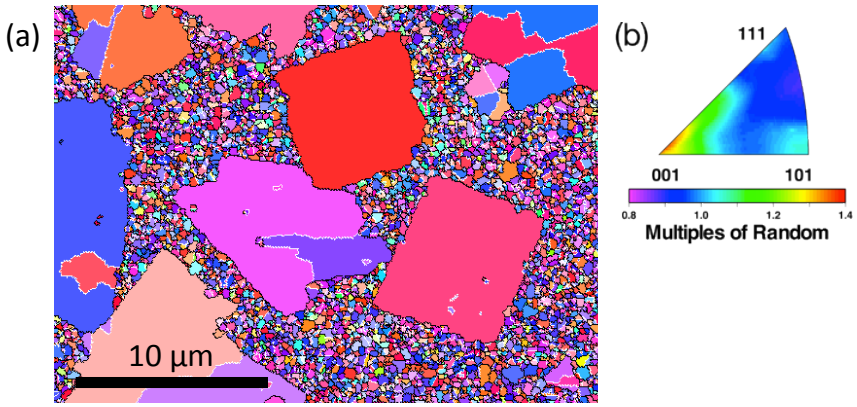

Figure 8.3. EBSD of LS-AGG in electrodeposited nanocrystalline nickel of (a) a sample annealed for 30 minutes at 500°C in a flowing H_2/Ar environment and (b) the grain boundary plane distribution of the facets of the abnormal grains. The abnormal grains show relatively few twins which is presumably due to the fact that the facets are primarily {100} and therefore far from the annealing twin condition.

It would be interesting to derive relationships to test for the correlation between the grain boundary plane distribution or triple junction line distribution to annealing twin formation. The challenge however is that both distributions are in discretely binned space and its units of multiples of random are not readily calculated into a function. Also it is worth investigating if lower stacking fault materials provide a "wider" distribution of migration directions for annealing twin formation. In silver, where the stacking fault energy is 20-30 mJ/m^2 [131], annealing twins are readily formed, but in a much larger abundance and not the typical lamellar appearance [96]. The larger fraction of incoherent segments of annealing twins can be achieved by the nucleation of more twins that are close to, but not necessarily the {111} plane. While in

high purity nickel we have found this range to be 10° from a stereological analysis, whereas in silver the deviation tolerated from the {111} might be greater.

8.2 {111} plane and the formation of lamellar twins and other morphologies

By showing a directional relationship between the {111} plane and the formation of a twin, it becomes easier to explain the formation of a lamellar twin. Assuming that the migration direction remains unchanged (although the relative environment in terms of triple line configuration or stored energy does), then the twinning event will preferentially select the identical twin plane. Therefore the two twinning events will create a lamellar twin. This is schematically shown in Fig. 8.4. The same idea also applies to grain growth as well, except at a triple line versus a grain boundary, and there is an increased selectivity with regard to the interfacial energy requirement. This would all suggest that if the direction of migration was constant, then all twins observed would usually be of this lamellar morphology. This is qualitatively consistent with the indentation in a Cu single-crystal presented in Fig. 2.14 [86] as well as in directionally annealed cold-rolled Cu rods by Baker *et al.* [132]

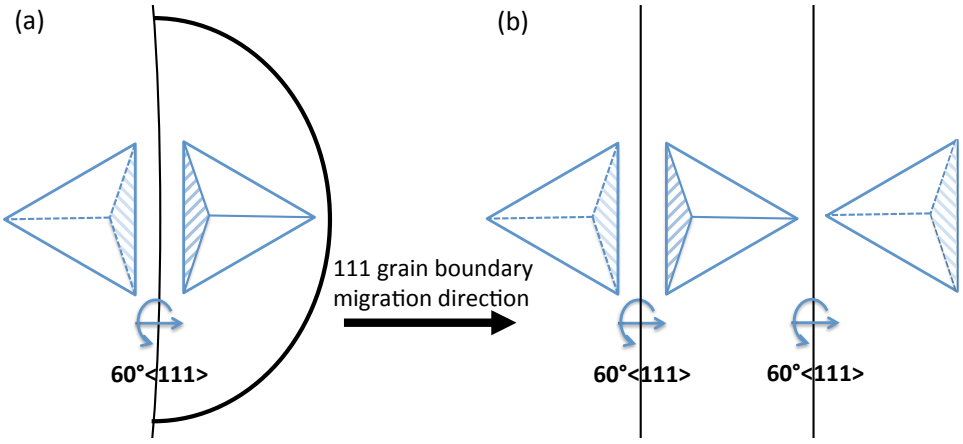

Figure 8.4. The formation of a twin on a migrating {111} interface shown in (a) would continue to preferentially select the same {111} twin variant that would produce the same twin misorientation

relationship shown in (b). This geometric factor provides better reasoning behind the formation of a lamellar twin that is typically observed in FCC metals.

The formation of incoherent twin segments arising from migrating {111} planes was previously discussed in Chapter 4. The shape of "v-twins" can best be explained when the migration direction is not constant, and therefore another {111} plane is the more optimal for nucleating the twin plane. An illustration of this is shown in Fig. 8.5, where taking the same starting configuration as before, selecting another twin variant produces a very different morphology. A Σ9 boundary would separate the original and later nucleated twin as previously discussed in the orientation repeat study of Chapter 5. This occurs when the migration direction is not constant and varies with time. This has been presented and discussed by [133] in the formation of annealing twins in gold particles that show these types of morphologies.

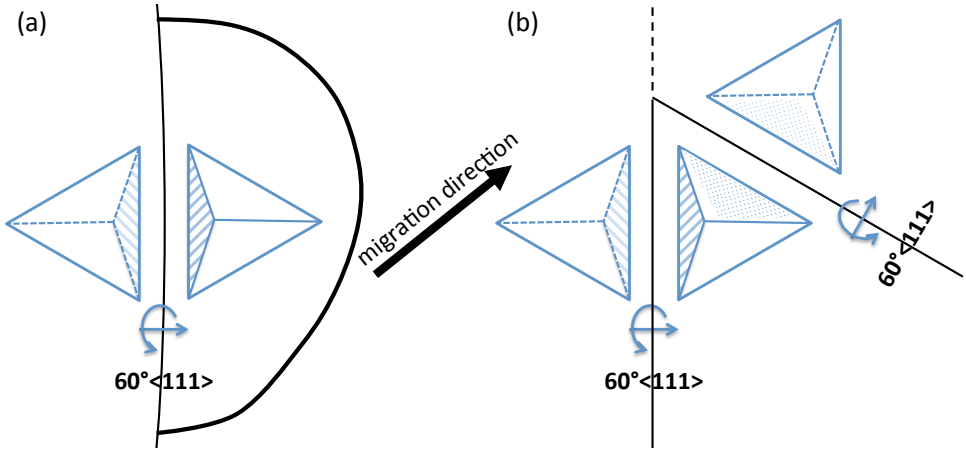

Figure 8.5. The formation of a twin on a migrating {111} interface shown in (a) would select the another {111} twin variant closer to the migration direction that would produce the a different twin misorientation relationship shown in (b). This geometric factor provides better reasoning behind the formation of v-twins that is observed in FCC metals.

The ideas presented are obvious, but emphasize the geometric role of the {111} plane and how it can influence the typically observed twin morphologies. It was not studied here, but the

proposed ideas suggest that there could be a systematic difference in twin morphologies based on recrystallization conditions such as prior strain, prior grain size and shape, and temperature. This is because the migration directions during recrystallization can be dependent on the underlying deformed microstructure. For example, by increasing the deformation, the orientation gradients in the deformed microstructure become larger and influence the growth behavior of new grains. At higher deformations, the recrystallizing grains are inclined to grow along shear bands and prior grain boundaries [111][134]. Hence these microstructures might be expected to produce more lamellar twins, while lower deformations promote the varying twin variant selections and network of twin boundaries that is often observed in and necessary for grain boundary engineering.

8.3 Potential areas of investigation for grain boundary engineering

The geometric relationship found between annealing twin formation to the {111} plane suggests that by controlling the grain boundary character or triple junction character, then the twin content in the microstructure can be manipulated. This would be of interest in strain-recrystallization methods of grain boundary engineering involving medium strains and the occurrence of recrystallization. In FCC metals, the goal would be to increase the number of {111} planes on the recrystallization interface to favorably induce the twinning mechanism.

The challenge is that the {111} planes in FCC metals are typically favored to begin with as they are the low energy plane. This was observed in the grain boundary plane distribution in Ni with a peak at the {111} presented in Fig. 4.8 but also in α-brass [135], aluminum [136], copper [137], and stainless steel [138]. While higher deformations would increase the number of recrystallizing nuclei and therefore the physical number of {111} planes for a given volume, this limits the grain size as well as the number of twins per grain. Lower deformations would limit

the number of recrystallizing nuclei, which would induce more twinning to replace the deformed matrix. To increase the amount of twinning, one might manipulate the tortuosity of the recrystallization front that has shown a positive correlation with the twin density [79]. The tortuosity appears dependent on the starting microstructure, so this could be accomplished by controlling the heterogeneity of the initial deformation, or the starting grain size and shape.

Additionally, annealing twin formation might hold promise for other material systems if one can regulate the planes of interest. That is, by increasing the number of twinning planes present in either crystal structures one might be able to increase the number of special boundaries. In BCC metals, in which the Σ3 boundaries are also often low in energy, this might be achieved by increasing the {110} planes in the material system (which is typically weakly biased to the {100} [96]. For HCP metals this would be the $\{11\bar{2}1\}$ plane. While a solution is not immediately obvious, this might be possible by methods mentioned above but also by controlling the recrystallization texture in these materials.

The same concept should be extendable to grain growth as well. During grain growth, controlling the triple junction distribution (coupled with the grain boundary planes) could induce more twinning. This level of microstructure control is not readily feasible in a bulk, polycrystalline sample, but may be more readily implemented in columnar microstructures. Through control the texture of the columnar microstructure, the types grain boundary planes and also the triple lines can be manipulated. For example, in a recent experiment by Rohrer *et al.*, an aluminum thin film exhibited a 20 % length fraction of twins after annealing [139], where as in bulk Al are twins are rarely found [74]. The nature of these twins are mostly corner type, akin to what was observed in the grain growth of Ni and twin formation at triple lines, but distinctly unique from nano-laminate twins that have been reported from deposition in Al [140]. While the

starting microstructure conditions are unknown, having a perfect {111} texture would provide a large number of {111} tilt boundaries that are high in energy to promote twin formation.

8.4 Summary Remarks

The results indicate that at the microstructure level geometric factors play a role in annealing twin formation. Taking into account the geometric role of the {111} provides a better link between the atomistic level occurrences to the microstructure level occurrences of annealing twin formation in FCC materials. The possible geometric role that a {111} plane would play on nucleating an annealing twin is discussed as well as how it would be responsible for the twin morphologies observed. Furthermore we propose it may be possible to control annealing twin nucleation events in materials through control of the grain boundary planes and triple junction characteristics. While we have not provided a definitive mechanism behind annealing twin formation, we have expanded the knowledge on factors that will influence twin formation.

9 Conclusion

The crystallographic factor involved with annealing twin formation in FCC nickel was studied in both recrystallization and grain growth. This was achieved by ex-situ studies of the microstructure evolution captured by electron backscatter diffraction and near-field high energy x-ray diffraction microscopy. Both techniques provide the spatial orientation mapping necessary for studying the grain boundary character of the microstructure. EBSD provided a 2D map where stereological techniques were used to study the orientation of the grain boundary plane of the recrystallization front in nickel. nf-HEDM provided a 3D Ni microstructure in which the full five-parameter grain boundary information was readily available during grain growth.

In recrystallization it was determined that annealing twins form on {111} planes at the recrystallization interface growing into the deformed region. Furthermore, studying the twin-related domains in the 3D microstructure showed that the twin variant selection is a random process. In contrast, we identified the first, true annealing twin formation events in grain growth in a polycrystalline sample and found that annealing twins do not form on grain boundaries. Instead, annealing twins are formed at triple lines through reducing the overall interfacial energy and these triple lines lie in the {111} plane of the parent grain. Testing the effect of temperature in recrystallization and grain growth showed little change in the twin content when the change in grain size is constant. This suggests that annealing twin formation is a heterogeneous nucleation event that is dependent on the prior microstructure, where crystallographic factors, such as the positioning of the {111} plane, plays a major role.

This new understanding should provide new leads to ideas about grain boundary engineering in FCC materials as well as materials of other crystal structures. For example, it is proposed by controlling the population of planes that exhibit twinning, is that feasible to regulate

the population of special boundaries. This was shown in late-stage abnormal grain growth in electrodeposited nanocrystalline nickel, where the migration of {100} planes produced fewer annealing twins in the final microstructure.

Ultimately, these findings have provided much needed insight into annealing twin formation mechanisms. They stress the importance of looking at the grain boundary character for dictating behaviors in microstructure evolution. In doing so, we have found a better link from the atomistic scale to the mescoscopic, and from the mesoscopic to the macroscopic. The relationships between these length-scales require development, but will come with time.

9.1 Future Directions

There are three areas of immediate investigation based on the findings of this work:

- Characterizing the grain boundary migration direction during recrystallization relative to the coherent twin plane in a 3D microstructure
- Studying the grain boundary migration behavior at triple line that form annealing twins during grain growth in the present 3D Ni microstructure
- Testing the effect of texture on the annealing twin content for the same change of grain size in both recrystallization and grain growth

The other primary area of interest will be the microstructure simulation of annealing twin formation during recrystallization and grain growth. In fact annealing twins have already been observed to form during grain growth in molecular dynamic simulations [141], but not extensively to clarify the atomistic behaviors and mechanisms involved. Meanwhile mesoscopic simulations, similar to [142], provide us with more accurate models of microstructure evolution and enable the understanding of the microstructure control needed to design and introduce new, grain boundary engineered materials to society.

10 References

1. Kocks, U. Fred, Carlos Norberto Tomé, and H-R. Wenk. *Texture and anisotropy: preferred orientations in polycrystals and their effect on materials properties*. Cambridge university press, 2000.
2. Turnbull, D., and R. E. Hoffman. "The effect of relative crystal and boundary orientations on grain boundary diffusion rates." *Acta metallurgica* 2, no. 3 (1954): 419-426.
3. Watanabe, Tadao, and Sadahiro Tsurekawa. "The control of brittleness and development of desirable mechanical properties in polycrystalline systems by grain boundary engineering." *Acta Materialia* 47, no. 15 (1999): 4171-4185.
4. Hoffman, RE. "Anisotropy of grain boundary self-diffusion." *Acta Metallurgica* 4, no. 1 (1956): 97-98.
5. Viswanathan, R., and C. L. Bauer. "Kinetics of grain boundary migration in copper bicrystals with [001] rotation axes." *Acta Metallurgica* 21, no. 8 (1973): 1099-1109.
6. Peterson, N. L. "Grain-boundary diffusion in metals." *International metals reviews* 28, no. 1 (1983): 65-91.
7. Aust, K. T. "Grain boundary engineering." *Canadian metallurgical quarterly* 33, no. 4 (1994): 265-274.
8. Kumar, Mukul, Adam J. Schwartz, and Wayne E. King. "Microstructural evolution during grain boundary engineering of low to medium stacking fault energy fcc materials." *Acta materialia* 50, no. 10 (2002): 2599-2612.
9. Randle, V. "Grain boundary engineering: an overview after 25 years." *Materials Science and Technology* 26, no. 3 (2010): 253-261.
10. Watanabe, Tadao. "Grain boundary engineering: historical perspective and future prospects." *Journal of materials science* 46, no. 12 (2011): 4095-4115.
11. Watanabe, Tadao. "An approach to grain boundary design for strong and ductile polycrystals." *Res Mechanica* 11, no. 1 (1984): 47-84.
12. Randle, V. "Mechanism of twinning-induced grain boundary engineering in low stacking-fault energy materials." *Acta materialia* 47, no. 15 (1999): 4187-4196.
13. Randle, Valerie. "Twinning-related grain boundary engineering." *Acta materialia*52, no. 14 (2004): 4067-4081.
14. Randle, Valerie, and Gregory Owen. "Mechanisms of grain boundary engineering." *Acta materialia* 54, no. 7 (2006): 1777-1783.
15. Schuh, Christopher A., Mukul Kumar, and Wayne E. King. "Analysis of grain boundary networks and their evolution during grain boundary engineering." *Acta Materialia* 51, no. 3 (2003): 687-700.
16. Lin, P., G. Palumbo, U. Erb, and K. T. Aust. "Influence of grain boundary character distribution on sensitization and intergranular corrosion of alloy 600."*Scripta Metallurgica et materialia* 33, no. 9 (1995): 1387-1392.
17. Lehockey, E. M., D. Limoges, G. Palumbo, J. Sklarchuk, K. Tomantschger, and A. Vincze. "On improving the corrosion and growth resistance of positive Pb-acid battery grids by grain boundary engineering." *Journal of power sources* 78, no. 1 (1999): 79-83.

18. Zelinski, Jeffrey A. "An evaluation of grain boundary engineering technology and processing scale-up." PhD diss., Massachusetts Institute of Technology, 2005.
19. Carpenter, H. C. H., and S. Tamura. "The formation of twinned metallic crystals." *Proceedings of the Royal Society of London. Series A, Containing Papers of a Mathematical and Physical Character* (1926): 161-182.
20. 1 (1940). 6 J. E. Burke, Trans. Am. Inst. Mining Engrs. 188, 1324 (1950). 1350
21. Fullman, R. L., and J. C. Fisher. "Formation of annealing twins during grain growth." *Journal of Applied Physics* 22, no. 11 (1951): 1350-1355.
22. Gleiter, H. "The formation of annealing twins." *Acta metallurgica* 17, no. 12 (1969): 1421-1428.
23. Meyers, Marc A., and Lawrence E. Murr. "A model for the formation of annealing twins in FCC metals and alloys." *Acta metallurgica* 26, no. 6 (1978): 951-962.
24. Goodhew, P. J. "Annealing twin formation by boundary dissociation." *Metal Science* 13, no. 3-4 (1979): 108-112.
25. Burgers, W. G., J. C. Meijs, and T. J. Tiedema. "Frequency of annealing twins in copper crystals grown by recrystallization." *Acta Metallurgica* 1, no. 1 (1953): 75-78.
26. Nielsen, John P. "The origin of annealing twins." *Acta Metallurgica* 15, no. 6 (1967): 1083-1085.
27. Dash, S., and N. Brown. "An investigation of the origin and growth of annealing twins." *Acta Metallurgica* 11, no. 9 (1963): 1067-1075.
28. Hall, E. O. "The deformation and ageing of mild steel: III discussion of results."*Proceedings of the Physical Society. Section B* 64, no. 9 (1951): 747.
29. Petch, N. J. "The cleavage strength of polycrystals." *J. Iron Steel Inst.* 174 (1953): 25-28.
30. Saylor, David M., Adam Morawiec, and Gregory S. Rohrer. "Distribution of grain boundaries in magnesia as a function of five macroscopic parameters." *Acta Materialia* 51, no. 13 (2003): 3663-3674.
31. Brandon, D. G. "The structure of high-angle grain boundaries." *Acta metallurgica* 14, no. 11 (1966): 1479-1484.
32. Gottstein, G., and L. S. Shvindlerman. "Grain Boundary Migration in Metals: Thermodynamics." *Kinetics, Applications (FL: CRC)* (1999).
33. Read, W. T., and W. Shockley. "Dislocation models of crystal grain boundaries."*Physical review* 78, no. 3 (1950): 275.
34. Herring, Conyers. “Some theorems on the free energies of crystal srfaces.” Phyiscal Review 82, no. 1 (1951): 87.
35. Li, Jia, Shen J. Dillon, and Gregory S. Rohrer. "Relative grain boundary area and energy distributions in nickel." *Acta Materialia* 57, no. 14 (2009): 4304-4311.
36. Rohrer, Gregory S. "Grain boundary energy anisotropy: a review." *Journal of materials science* 46, no. 18 (2011): 5881-5895.
37. Mullins, William W. "Theory of thermal grooving." *Journal of Applied Physics* 28, no. 3 (1957): 333-339.

38. Olmsted, David L., Stephen M. Foiles, and Elizabeth A. Holm. "Survey of computed grain boundary properties in face-centered cubic metals: I. Grain boundary energy." *Acta Materialia* 57, no. 13 (2009): 3694-3703.
39. Rohrer, Gregory S., Elizabeth A. Holm, Anthony D. Rollett, Stephen M. Foiles, Jia Li, and David L. Olmsted. "Comparing calculated and measured grain boundary energies in nickel." *Acta Materialia* 58, no. 15 (2010): 5063-5069.
40. Holm, Elizabeth A., Gregory S. Rohrer, Stephen M. Foiles, Anthony D. Rollett, Herbert M. Miller, and David L. Olmsted. "Validating computed grain boundary energies in fcc metals using the grain boundary character distribution." *Acta Materialia* 59, no. 13 (2011): 5250-5256.
41. Bulatov, Vasily V., Bryan W. Reed, and Mukul Kumar. "Grain boundary energy function for fcc metals." *Acta Materialia* 65 (2014): 161-175.
42. Zehetbauer, M., and V. Seumer. "Cold work hardening in stages IV and V of FCC metals—I. Experiments and interpretation." *Acta metallurgica et materialia* 41, no. 2 (1993): 577-588.
43. Zehetbauer, M. "Cold work hardening in stages IV and V of FCC metals—II. Model fits and physical results." *Acta metallurgica et materialia* 41, no. 2 (1993): 589-599.
44. Schafler, E., M. Zehetbauer, A. Borbely, and T. Ungar. "Dislocation densities and internal stresses in large strain cold worked pure iron." *Materials Science and Engineering: A* 234 (1997): 445-448.
45. Nes, Erik. "Modelling of work hardening and stress saturation in FCC metals." *Progress in Materials Science* 41, no. 3 (1997): 129-193.
46. Nes, E., and K. Marthinsen. "Modeling the evolution in microstructure and properties during plastic deformation of fcc-metals and alloys–an approach towards a unified model." *Materials Science and Engineering: A* 322, no. 1 (2002): 176-193.
47. Dillamore, I. L., P. L. Morris, C. J. E. Smith, and W. B. Hutchinson. "Transition bands and recrystallization in metals." In *Proceedings of the Royal Society of London A: Mathematical, Physical and Engineering Sciences*, vol. 329, no. 1579, pp. 405-420. The Royal Society, 1972.
48. Every, R. L., and M. Hatherly. "Oriented nucleation in low-carbon steels." In *Texture*, vol. 1, pp. 183-194. 1974.
49. Hurley, P. J., and F. J. Humphreys. "The application of EBSD to the study of substructural development in a cold rolled single-phase aluminium alloy." *Acta Materialia* 51, no. 4 (2003): 1087-1102.
50. Ørsund, R., J. Hjelen, and E. Nes. "Local lattice curvature and deformation heterogeneities in heavily deformed aluminium." *Scripta metallurgica* 23, no. 7 (1989): 1193-1197.
51. Beck, Paul A. "Annealing of cold worked metals." *Advances in Physics* 3, no. 11 (1954): 245-324.
52. Bever, M. B. "Creep and recovery." *Am. Soc. Met., Cleveland, Ohio* (1957): 22.
53. Titchener, Alan Lee, and Michael Berliner Bever. "The stored energy of cold work." *Progress in metal physics* 7 (1958): 247-338.

54. Holm, Elizabeth A., Mark A. Miodownik, and Anthony D. Rollett. "On abnormal subgrain growth and the origin of recrystallization nuclei." *Acta materialia* 51, no. 9 (2003): 2701-2716.
55. Wang, Sheng Yu, and Anthony D. Rollett. "Abnormal Subgrain Growth by Monte Carlo Simulation Based on Hot-Rolled AA5005 Aluminum Alloy Texture." In *Materials Science Forum*, vol. 558, pp. 377-382. 2007.
56. Hatch, J. E. "'Work Hardening, Recovery, Recrystallization, and Grain Growth." *Aluminum Properties and Physical Metallurgy, ASM, Ohio* (1984): 1057133.
57. Mehl, Robert F. "Recrystallization." In *Metals Handbook*, pp. 259-263. American Society for Metals Cleveland, Ohio, 1948.
58. Burke, J. E., and D. Turnbull. "Recrystallization and grain growth." *Progress in metal physics* 3 (1952): 220-292.
59. Jensen, D. Juul. "Growth rates and misorientation relationships between growing nuclei/grains and the surrounding deformed matrix during recrystallization." *Acta metallurgica et materialia* 43, no. 11 (1995): 4117-4129.
60. Neumann, J. von. "Curvature driven grain growth in two dimensions." *Metal Interfaces* (1952): 108-118.
61. Mullins, William W. "Two-Dimensional Motion of Idealized Grain Boundaries." *Journal of Applied Physics* 27, no. 8 (1956): 900-904.
62. Hillert, M. "On the theory of normal and abnormal grain growth." *Acta metallurgica* 13, no. 3 (1965): 227-238.
63. Schwartz, Adam J., Wayne E. King, and Mukul Kumar. "Influence of processing method on the network of grain boundaries." *Scripta materialia* 54, no. 6 (2006): 963-968.
64. Lehockey, E. M., and G. Palumbo. "On the creep behaviour of grain boundary engineered nickel 1." *Materials Science and Engineering: A* 237, no. 2 (1997): 168-172.
65. Cheung, C., U. Erb, and G. Palumbo. "Application of grain boundary engineering concepts to alleviate intergranular cracking in Alloys 600 and 690."*Materials Science and Engineering: A* 185, no. 1 (1994): 39-43.
66. Kopezky, Ch V., V. Yu Novikov, L. K. Fionova, and N. A. Bolshakova. "Investigation of annealing twins in fcc metals." *Acta Metallurgica* 33, no. 5 (1985): 873-879.
67. Kurzydłowski, K. J. "On the formation of twin grains as a result of grain encounters during the process of recrystallization and grain growth." *Scripta metallurgica et materialia* 25, no. 5 (1991): 1099-1102.
68. Cahoon, J. R., Qiangyong Li, and N. L. Richards. "Microstructural and processing factors influencing the formation of annealing twins." *Materials science and engineering: a* 526, no. 1 (2009): 56-61.
69. Haasen, Peter. "How are new orientations generated during primary recrystallization?." *Metallurgical and Materials Transactions A* 24, no. 5 (1993): 1001-1015.
70. Mahajan, S., C. S. Pande, M. A. Imam, and B. B. Rath. "Formation of annealing twins in fcc crystals." *Acta materialia* 45, no. 6 (1997): 2633-2638.

71. Pande, C. S., M. A. Imam, and B. B. Rath. "Study of annealing twins in fcc metals and alloys." *Metallurgical transactions A* 21, no. 11 (1990): 2891-2896.
72. Hu, Hsun, and Cyril Stanley Smith. "The formation of low-energy interfaces during grain growth in alpha and alpha-beta brasses." *Acta Metallurgica* 4, no. 6 (1956): 638-646.
73. Baro, G., and H. Gleiter. "Formation of Annealing Twins." *Z. Metallkunde* 63, no. 10 (1972): 661-663.
74. Charnock, W., and J. Nutting. "The factors determining the frequency of occurrence of annealing twins." *Metal Science* 1, no. 1 (1967): 78-83.
75. Charnock, W., and J. Nutting. "The effect of carbon and nickel upon the stacking-fault energy of iron." *Metal Science* 1, no. 1 (1967): 123-127.
76. Rath, B. B., M. A. Imam, and C. S. Pande. "Nucleation and growth of twin interfaces in Fcc metals and alloys." *Mater. Phys. Mech* 1 (2000): 61-66.
77. Pande, Chandra S., and M. Ashraf Imam. "Grain growth and twin formation in boron-doped nickel polycrystals." *Materials science and engineering: a* 512, no. 1 (2009): 82-86.
78. Li, Qiangyong, J. R. Cahoon, and N. L. Richards. "Effects of thermo-mechanical processing parameters on the special boundary configurations of commercially pure nickel." *Materials Science and Engineering: A* 527, no. 1 (2009): 263-271.
79. Y. Jin, B. Lin, G.S. Rohrer, A.D. Rollett, M. Bernacki, N. Bozzolo,, "Thermo-mechanical factors influencing annealing twin development in nickel during recrystallization," Journal of Materials Science, 50 (2015) 5191-5203.
80. Wang, W., F. Brisset, A. L. Helbert, D. Solas, I. Drouelle, M. H. Mathon, and T. Baudin. "Influence of stored energy on twin formation during primary recrystallization." *Materials Science and Engineering: A* 589 (2014): 112-118.
81. Field, D. P., L. T. Bradford, M. M. Nowell, and T. M. Lillo. "The role of annealing twins during recrystallization of Cu." *Acta materialia* 55, no. 12 (2007): 4233-4241.
82. Gastaldi, J., and C. Jourdan. "Observation of the annealing twin growth by synchrotron radiation X-ray topography." *physica status solidi (a)* 52, no. 1 (1979): 139-148.
83. Song, Kook-Hyun, Y. B. Chun, and Sun-Kuen Hwang. "Direct observation of annealing twin formation in a Pb-base alloy." *Materials Science and Engineering: A* 454 (2007): 629-636.
84. Viswanathan, R., and C. L. Bauer. "Formation of annealing twins, faceting, and grain boundary pinning in copper bicrystals." *Metallurgical Transactions* 4, no. 11 (1973): 2645-2650.
85. Jin, Yuan, Brian Lin, Marc Bernacki, Gregory S. Rohrer, A. D. Rollett, and Nathalie Bozzolo. "Annealing twin development during recrystallization and grain growth in pure nickel." *Materials Science and Engineering: A* 597 (2014): 295-303.
86. M.F. Ashby and E. Harper: Harvard Report, Harvard University, Cambridge, MA, 1967.

87. Horton, D., C. B. Thomson, and V. Randle. "Aspects of twinning and grain growth in high purity and commercially pure nickel." *Materials Science and Engineering: A* 203, no. 1 (1995): 408-414.
88. Thomson, C. B., and V. Randle. "A study of twinning in nickel." *Scripta materialia* 35, no. 3 (1996): 385-390.
89. Thomson, C. B., and V. Randle. "The effects of strain annealing on grain boundaries and secure triple junctions in Nickel 200." *Journal of materials science* 32, no. 7 (1997): 1909-1914.
90. Randle, V., P. R. Rios, and Y. Hu. "Grain growth and twinning in nickel." *Scripta Materialia* 58, no. 2 (2008): 130-133.
91. Lee, S-L., and N. L. Richards. "The effect of single-step low strain and annealing of nickel on grain boundary character." *Materials Science and Engineering: A* 390, no. 1 (2005): 81-87.
92. Miller, Herbert M. *Influences of processing and composition on the grain boundary character distribution*. ProQuest, 2009.
93. Miller, Herbert M., Chang Soo Kim, Jason Gruber, Valerie Randle, and Gregory S. Rohrer. "Orientation Distribution of Σ3 Grain Boundary Planes in Ni Before and After Grain Boundary Engineering." In *Materials Science Forum*, vol. 558, pp. 641-647. 2007.
94. Lehockey, E. M., G. Palumbo, and P. Lin. "Improving the weldability and service performance of nickel-and iron-based superalloys by grain boundary engineering." Metallurgical and Materials Transactions A 29, no. 12 (1998): 3069-3079.
95. Souaï, Nadia, Nathalie Bozzolo, Loic Nazé, Yvan Chastel, and R. Logé. "About the possibility of grain boundary engineering via hot-working in a nickel-base superalloy." *Scripta materialia* 62, no. 11 (2010): 851-854.
96. Ratanaphan, Sutatch. "Grain Boundary Character Distributions In Isostructural Materials." (2013).
97. KIKUCHI, Seishi. "Diffraction of cathode rays by mica." *Proceedings of the Imperial Academy* 4, no. 6 (1928): 271-274.
98. Schwartz, Adam J., Mukul Kumar, Brent L. Adams, and David P. Field, eds. *Electron backscatter diffraction in materials science*. Vol. 2. New York: Springer, 2009.
99. Wright, S. I., and R. J. Larsen. "Extracting twins from orientation imaging microscopy scan data." Journal of microscopy 205, no. 3 (2002): 245-252.
100. Rohrer, Gregory S., David M. Saylor, Bassem El Dasher, Brent L. Adams, Anthony D. Rollett, and Paul Wynblatt. "The distribution of internal interfaces in polycrystals." *Zeitschrift für Metallkunde* 95, no. 4 (2004): 197-214.
101. Saylor, David M., Bassem S. El-Dasher, Brent L. Adams, and Gregory S. Rohrer. "Measuring the five-parameter grain-boundary distribution from observations of planar sections." *Metallurgical and Materials Transactions A* 35, no. 7 (2004): 1981-1989.
102. Lienert, Ulrich, Jonathan Almer, Bo Jakobsen, Wolfgang Pantleon, Henning Friis Poulsen, D. Hennessy, C. Xiao, and R. M. Suter. "3-dimensional characterization of polycrystalline bulk materials using high-energy

synchrotron radiation." In *Materials science forum*, vol. 539, pp. 2353-2358. (2007).

103. Suter, R. M., D. Hennessy, C. Xiao, and U. Lienert. "Forward modeling method for microstructure reconstruction using x-ray diffraction microscopy: Single-crystal verification." *Review of Scientific Instruments* 77, no. 12 (2006): 123905.
104. Li, S. F., and R. M. Suter. "Adaptive reconstruction method for three-dimensional orientation imaging." *Journal of Applied Crystallography* 46, no. 2 (2013): 512-524.
105. Hefferan, Christopher M., Jonathan Lind, Shiu Fai Li, Ulrich Lienert, Anthony D. Rollett, and Robert M. Suter. "Observation of recovery and recrystallization in high-purity aluminum measured with forward modeling analysis of high-energy diffraction microscopy." *Acta Materialia* 60, no. 10 (2012): 4311-4318.
106. Lind, J., S. F. Li, R. Pokharel, U. Lienert, A. D. Rollett, and R. M. Suter. "Tensile twin nucleation events coupled to neighboring slip observed in three dimensions." *Acta Materialia* 76 (2014): 213-220.
107. Stein, Clayton A., Albert Cerrone, Tugce Ozturk, Sukbin Lee, Peter Kenesei, Harris Tucker, Reeju Pokharel et al. "Fatigue crack initiation, slip localization and twin boundaries in a nickel-based superalloy." *Current Opinion in Solid State and Materials Science* 18, no. 4 (2014): 244-252.
108. Pokharel, Reeju, Jonathan Lind, Shiu Fai Li, Peter Kenesei, Ricardo A. Lebensohn, Robert M. Suter, and Anthony D. Rollett. "In-situ observation of bulk 3D grain evolution during plastic deformation in polycrystalline Cu." *International Journal of Plasticity* 67 (2015): 217-234.
109. Alvi, Mohammed H., Soon Wuk Cheong, Hasso Weiland, and Anthony D. Rollett. "Recrystallization and texture development in hot rolled 1050 aluminum." In *Materials Science Forum*, vol. 467, pp. 357-362. 2004.
110. Cheong, Soon Wuk, and Hasso Weiland. "Understanding a microstructure using GOS (grain orientation spread) and its application to recrystallization study of hot deformed al-cu-mg alloys." In *Materials Science Forum*, vol. 558, pp. 153-158. 2007.
111. Rollett, Anthony, F. J. Humphreys, Gregory S. Rohrer, and M. Hatherly. *Recrystallization and related annealing phenomena*. Elsevier, 2004.
112. Randle, Valerie. "The coincidence site lattice and the 'sigma enigma'." *Materials Characterization* 47, no. 5 (2001): 411-416.
113. Kim, Chang-Soo, Ted R. Massa, and Gregory S. Rohrer. "Interface character distributions in WC–Co composites." *Journal of the American Ceramic Society* 91, no. 3 (2008): 996-1001.
114. Jin, Yuan, Marc Bernacki, Gregory S. Rohrer, Anthony D. Rollett, Brian Lin, and Nathalie Bozzolo. "Formation of annealing twins during recrystallization and grain growth in 304L austenitic stainless steel." In *Materials Science Forum*, vol. 753, pp. 113-116. 2013.
115. Hefferan, Christopher M. "Measurement of annealing phenomena in high purity metals with near-field high energy x-ray diffraction microscopy." PhD diss., CARNEGIE MELLON UNIVERSITY, 2012.

116. Reed, Bryan Walter, and Mukul Kumar. "Mathematical methods for analyzing highly-twinned grain boundary networks." *Scripta materialia* 54, no. 6 (2006): 1029-1033.
117. Cayron, C. "Quantification of multiple twinning in face centred cubic materials." *Acta Materialia* 59, no. 1 (2011): 252-262.
118. Xia, Shuang, Bangxin Zhou, and Wenjue Chen. "Grain cluster microstructure and grain boundary character distribution in Alloy 690." *Metallurgical and Materials Transactions A* 40, no. 12 (2009): 3016-3030.
119. Xia, Shuang, Hui Li, Ting Guang Liu, and Bang Xin Zhou. "Appling grain boundary engineering to Alloy 690 tube for enhancing intergranular corrosion resistance." *Journal of Nuclear Materials* 416, no. 3 (2011): 303-310.
120. Bystrzycki, J., and W. Przetakiewicz. "3-dimensional reconstruction of annealing twins shape in FCC metals by serial sectioning." *Scripta metallurgica et materialia* 27, no. 7 (1992): 893-896.
121. Christian, John Wyrill. *The theory of transformations in metals and alloys*. Newnes, 2002.
122. Murr, L.E. Energetics of grain-boundary triple juncitons and corner-twinned junctions – transmission electron microscope studies. *J. Appl. Phys.* 39(12), 5557-& (1968).
123. Gruber, Jason, Denise C. George, Andrew P. Kuprat, Gregory S. Rohrer, and Anthony D. Rollett. "Effect of anisotropic grain boundary properties on grain boundary plane distributions during grain growth." *Scripta materialia* 53, no. 3 (2005): 351-355.
124. Dillon, Shen J., and Gregory S. Rohrer. "Mechanism for the development of anisotropic grain boundary character distributions during normal grain growth." *Acta Materialia* 57, no. 1 (2009): 1-7.
125. Porter, David A., Kenneth E. Easterling, and Mohamed Sherif. *Phase Transformations in Metals and Alloys, (Revised Reprint)*. CRC press, 2009.
126. Dillamore, I. L., R. E. Smallman, and W. T. Roberts. "A determination of the stacking-fault energy of some pure FCC metals." *Philosophical Magazine* 9, no. 99 (1964): 517-526.
127. Dillamore, I. L., and R. E. Smallman. "The stacking-fault energy of fcc metals." *Philosophical Magazine* 12, no. 115 (1965): 191-193.
128. Murr, Lawrence Eugene. "Interfacial phenomena in metals and alloys." (1975).
129. Hibbard, G. D., J. L. McCrea, G. Palumbo, K. T. Aust, and U. Erb. "An initial analysis of mechanisms leading to late stage abnormal grain growth in nanocrystalline Ni." *Scripta Materialia* 47, no. 2 (2002): 83-87.
130. Cheng, L., and G. D. Hibbard. "Abnormal grain growth via the migration of planar growth interfaces." *Materials Science and Engineering: A* 492, no. 1 (2008): 128-133.
131. Howie, A., and P. R. Swann. "Direct measurements of stacking-fault energies from observations of dislocation nodes." *Philosophical Magazine* 6, no. 70 (1961): 1215-1226.
132. Baker, I., and J. Li. "Directional annealing of cold-rolled copper single crystals." *Acta materialia* 50, no. 4 (2002): 805-813.

133. McGinn, Joseph T., Victor A. Greenhut, Thomas Tsakalakos, and Joseph Blanc. "Formation of fault structures during coalescence and growth of gold particles in a fused silica matrix—I." *Acta Metallurgica* 30, no. 12 (1982): 2093-2102.
134. Miszczyk, M., H. Paul, J. H. Driver, and C. Maurice. "New orientation formation and growth during primary recrystallization in stable single crystals of three face-centred cubic metals." *Acta Materialia* 83 (2015): 120-136.
135. Rohrer, Gregory S., Valerie Randle, Chang-Soo Kim, and Yan Hu. "Changes in the five-parameter grain boundary character distribution in α-brass brought about by iterative thermomechanical processing." *Acta materialia* 54, no. 17 (2006): 4489-4502.
136. Saylor, David M., Bassem S. El Dasher, Anthony D. Rollett, and Gregory S. Rohrer. "Distribution of grain boundaries in aluminum as a function of five macroscopic parameters." *Acta Materialia* 52, no. 12 (2004): 3649-3655.
137. Randle, V., G. S. Rohrer, H. M. Miller, M. Coleman, and G. T. Owen. "Five-parameter grain boundary distribution of commercially grain boundary engineered nickel and copper." *Acta materialia* 56, no. 10 (2008): 2363-2373.
138. Downey II, Steven T., Nicholas Bembridge, Peter N. Kalu, Herbert M. Miller, Gregory S. Rohrer, and Ke Han. "Grain boundary plane distributions in modified 316 LN steel exposed at elevated and cryogenic temperatures." *Journal of Materials Science* 42, no. 23 (2007): 9543-9547.
139. Rohrer, Gregory S. "The grain boundary character distribution of a highly twinned nanocrystalline aluminum thin film compared to bulk microcrystalline aluminum." In preparation.
140. Bufford, D., Y. Liu, Y. Zhu, Z. Bi, Q. X. Jia, H. Wang, and X. Zhang. "Formation mechanisms of high-density growth twins in aluminum with high stacking-fault energy." *Materials Research Letters* 1, no. 1 (2013): 51-60.
141. Farkas, Diana, Eduardo Bringa, and Alfredo Caro. "Annealing twins in nanocrystalline fcc metals: A molecular dynamics simulation." *Physical Review B* 75, no. 18 (2007): 184111.
142. Wang, W., A. L. Helbert, F. Brisset, M. H. Mathon, and T. Baudin. "Monte Carlo simulation of primary recrystallization and annealing twinning." *Acta Materialia* 81 (2014): 457-468.

11 APPENDICES

11.A Development of Σ9 and Σ27 boundaries with recrystallization

The behaviors in the length fraction of Σ9 and Σ27 boundaries were observed similar to the analysis of Σ3 boundaries in Chapter 4. Grain orientation spread was used to measure the area fraction recrystallized and partition the microstructure into the recrystallized area and deformed area. The behaviors of the Σ9 and Σ27 boundaries were observed both across the entire area observed by EBSD and by just the recrystallized area. The behaviors are shown in Fig. 11.1a-b respectively.

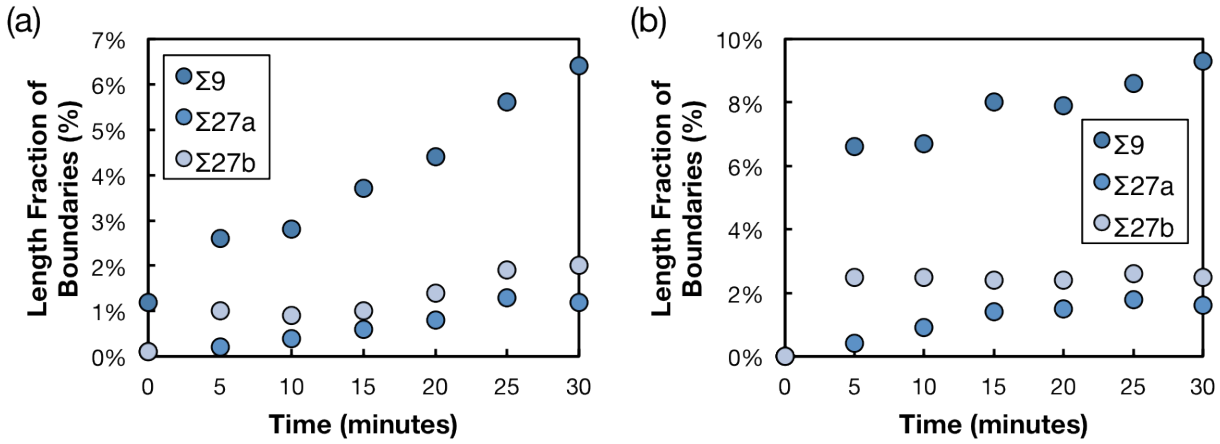

Figure 11.1. Length fraction of special boundaries of interest as a function of time corresponding to the recrystallization progress in (a) the entire area observed and (b) only the recrystallized fraction. In both cases, the length fraction of special boundaries are observed to increase with time.

In contrast to the behavior of Σ3 boundaries, the length fraction of Σ9 and Σ27 boundaries increased regardless of considering entire area or just the recrystallized area. The Σ9 length fraction approaches 9%. The Σ27 length fraction behavior has been divided to considered both Σ27a and Σ27b boundaries. The Σ27a boundaries increase in length fraction to approximately 2%, while the Σ27b length fraction stays constant at approximately 2.5%. While the overall increase in Σ9 and Σ27 boundaries is explained by the geometric interaction of Σ3 boundaries that are formed from various twin nuclei during recrystallization, which is reflected in the triple junction distribution in Fig. 11.2.

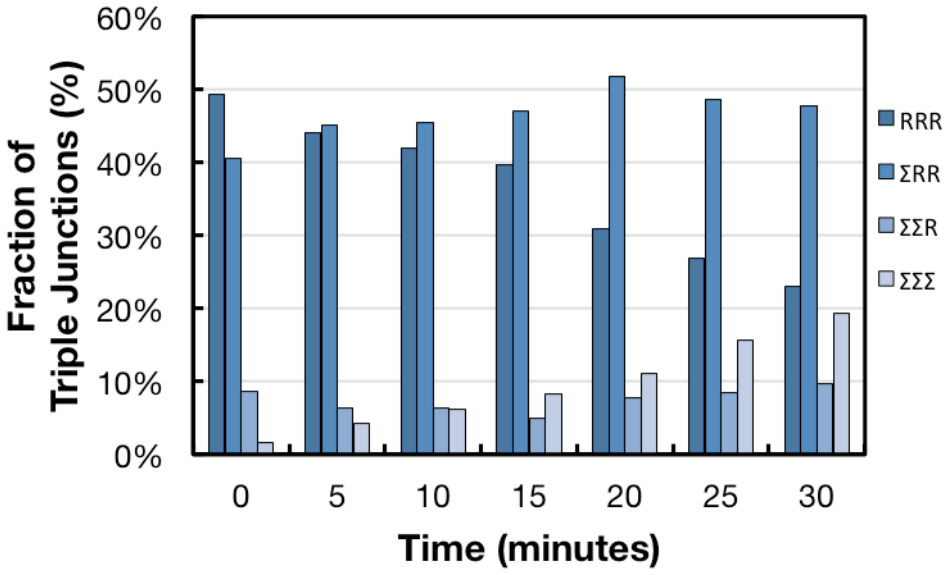

Figure 11.2. Triple junction type distribution as a function of time corresponding to the recrystallization progress. The most notable changes with time are the decrease in RRR triple junctions and the increase in ΣΣΣ triple junctions with recrystallization

The decrease in the RRR triple junctions is expected along with a pronounced increase of ΣΣΣ types of triple junctions. This is associated with both the increase of special boundary fractions and the increasing connectivity as recrystallizing regions impinge on each other. Specifically, the rise in ΣΣΣ triple junctions is attributed to mostly the increase of 3 / 3 / 9 boundaries. This is shown in Table 11.1, where the values of the ΣΣΣ increase are those from Fig. AI.2, the fraction of 3 / 3 / 9 boundaries as a fraction of all the triple junctions is also increasing and accounts for the majority of the ΣΣΣ. This behavior is expected as two Σ3 boundaries that meet must form Σ9 at the triple junction. Again, this behavior correlates with the increasing fraction of Σ9 boundaries as observed in Fig. 11.1.

Table 11.1. ΣΣΣ type triple junction with time plus 3 / 3 / 9 type triple junctions

Boundary Type	**Time (minutes)**						
	0	**5**	**10**	**15**	**20**	**25**	**30**
ΣΣΣ	1.6%	4.3%	6.2%	8.2%	11.1%	15.7%	19.3%
→ 3/3/9	1.5%	3.9%	5.3%	6.7%	8.9%	11.5%	14.7%

11.B Late-stage abnormal grain growth in nanocrsytalline-nickel

Late-stage abnormal grain growth in electrodeposited nanocrystalline-nickel has been characterized, with a special emphasis on the behavior and quantitative evolution of grain boundaries. Results for the initial state prior to the appearance of large, facetted abnormal grains, the bimodal state as a result of LS-AGG, and, lastly the subsequent unimodal microstructure after LS-AGG are presented. A detailed comparison on the grain boundary character is made among the three states. The nature of LS-AGG results in a high fraction of {100} grain boundary planes, which also features less twins per grain than conventional Ni.

An electro-deposited nanocrystalline nickel self-standing plate was provided by Integran Technologies Inc. (Canada). The as-received sample was quoted to have a nominal grain size from 10 – 20 nm. Samples with dimensions of approximately 5 mm × 5 mm × 1 mm were sectioned from the original plate and embedded in a epoxy resin and polished with the same procedure as detailed in Chapter 3.1. Samples were subjected to various heat treatments at 500 °C in a flowing Ar/H2 tube furnace to minimize the surface oxidation. Three heat treatments were performed : 10 minutes to achieve a sub-micron normal grain size distribution, 30 minutes to achieve a bimodal grain size distribution, and 90 minutes to obtain normal grain size distribution again. EBSD post-processing is similar to which has been presented in the thesis.

The EBSD scans of the three microstructures are detailed in Fig. 11.3. The unimodal grain size microstructure after 10 minutes of annealing is shown in Fig. 11.3a with an average grain size of 0.9 μm in agreement with previous reports of the microstructure after IS-AGG. The microstructure after 30 minutes of annealing is shown in Fig. 11.3b, where the highly faceted, abnormal grains are distinctly larger than the initial matrix grains. These abnormal grains are isolated from one another with an average grain size of 40-50 μm, but also occur as Σ3-related pairs of crystals. The final microstructure is shown in Fig. 11.3c after annealing the microstructure for 90 minutes such that all LS-AGG coarsen and consume the starting matrix. In the final appearance of the microstructure, the faceted grain boundaries seen in Fig. 1b are not as obvious due to the impingement of the LS-AGG. The final microstructure achieves a unimodal grain size distribution with an average of grain size of 60-70 μm.

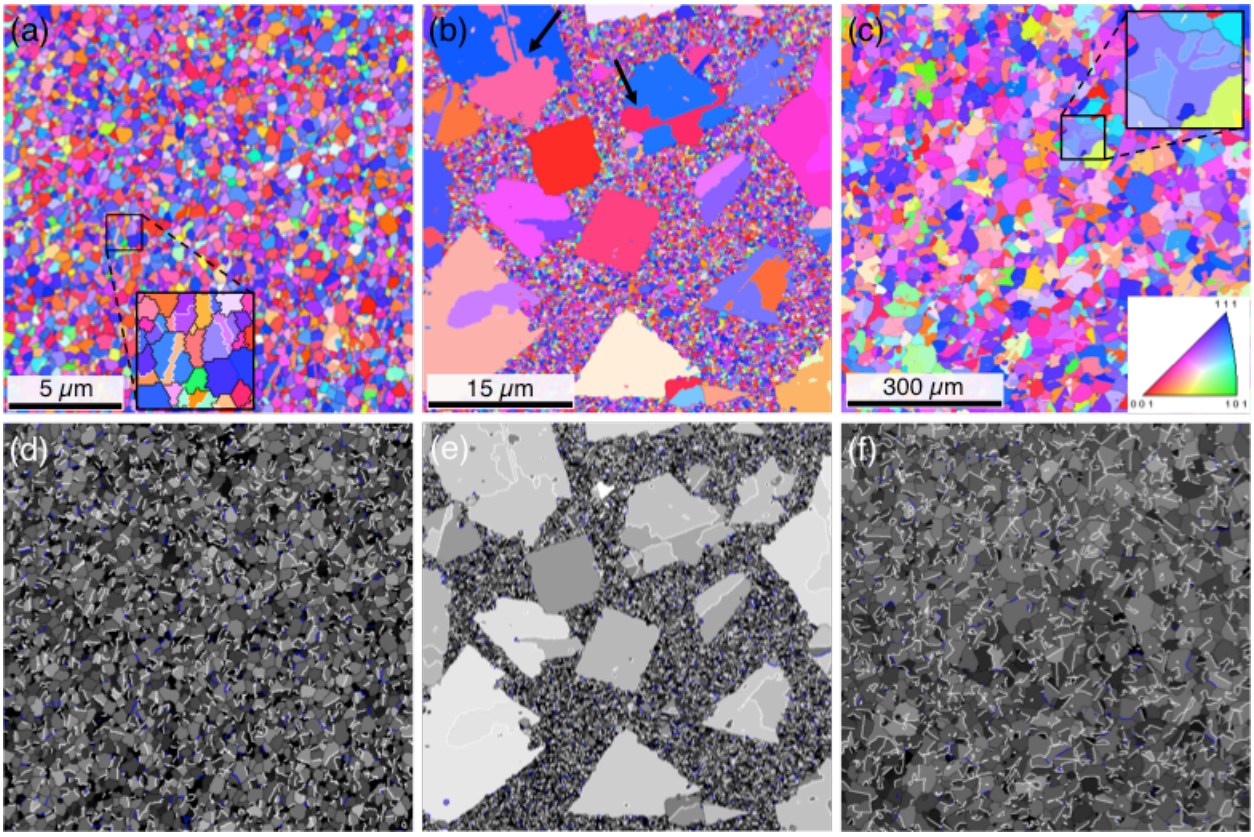

Figure 11.3. EBSD orientation maps of electrodeposited nanocrystalline nickel annealed after (a) 10 minutes, (b) 30 minutes, and (c) 90 minutes at 500°C in flowing Ar/H2. The color code, defined in the standard triangle, shows which crystallographic plane is parallel to the sample surface (normal to the deposition direction). The grain boundary maps after (d) 10 minutes, (e) 30 minutes, and (f) 90 minutes are color coded by HAGBs as black, Σ1 boundaries as blue, and Σ3 boundaries as white. The boxed in region in (a) shows the usual, straight Σ3 boundaries, while in (c) the boxed region shows the contorted Σ3 boundaries.

The misorientation character was analyzed at the interface between the abnormal grain and the matrix in the sample annealed for 30 min. On the abnormal grain, the interface borders anywhere from 30-50 matrix grains as shown in Fig. 11.4a. For the abnormal grains, the grain boundary plane distribution (GBPD) in Fig. 11.4b shows a bias towards the {001} within the fundamental zone. This supports the claim that the facets overall are close to {001}, based on the geometry of the LS-AGG [11]. Nevertheless, at higher resolutions, the interface exhibits significant local roughness as, for example, in the regions circled in Fig. 11.4a.

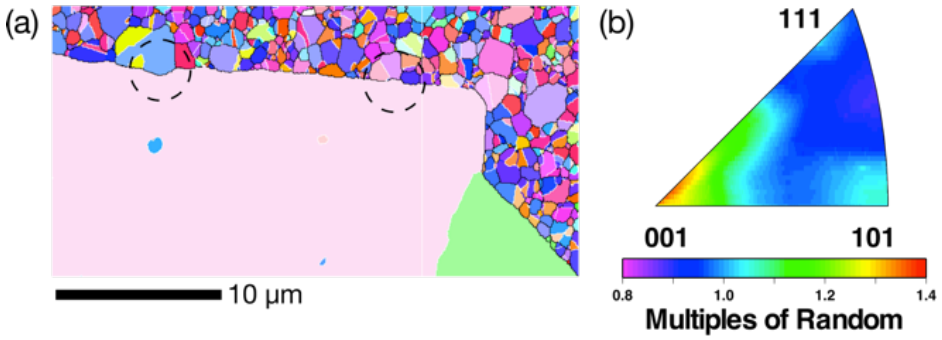

Figure 11.4. (a) EBSD orientation map of the AGG interfaces and (b) the grain boundary plane distribution of the abnormal grains. The interface is not perfectly flat and exhibits some local roughness and perturbations circled in (a), which spreads out the {001} peak in the GBPD.

A comparison of the GBPD of the initial microstructure compared to the final LS-AGG impinged microstructure further supports the previous observation. The starting GBPD shows a bias towards {111} planes as illustrated in Fig. 5a; this is due to the prevalence of coherent twin boundaries in the material. In final LS-AGG impinged state, the {111} planes remain, but increased intensity about the {100} also appears, Fig. 5b. Not only is the {100} grain boundary surface characteristic of LS-AGG, but this bias is retained within the microstructure even after the LS-AGG has terminated.

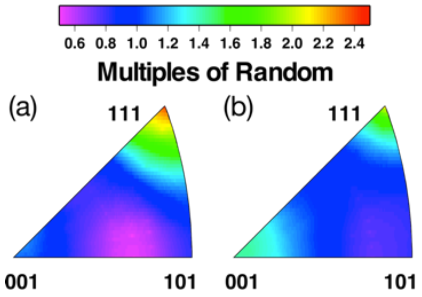

Figure 11.5. GBPD of the (a) initial microstructure compared to (b) the final LS-AGG impinged microstructure. Most notable difference is the {100} peak associated with the LS-AGG.

Although the LS-AGG results in a significant increase in length fraction of twin boundaries (increasing from 20 → 33%), the average number of twins per grain is approximately constant from the initial matrix to final microstructure at one twin per grain. Compared to conventional Ni that has an average of four twins per grain, this value is lower. The lower value is suggested to be a result of the lack of migrating {111}, but instead {100} that do not promote the favorable formation of annealing twin boundaries in the microstructure.